THE UNIVERSITY OF CALGARY

Neural Network Based Digital Differential Relay for Synchronous Generators

by

Ashraf Ibrahim Megahed

A DISSERTATION

SUBMITTED TO THE FACULTY OF GRADUATE STUDIES

IN PARTIAL FULFILLMENT OF THE REQUIREMENTS FOR THE

DEGREE OF DOCTOR OF PHILOSOPHY

DEPARTMENT OF ELECTRICAL AND COMPUTER ENGINEERING

CALGARY, ALBERTA

FEBRUARY, 1998

Abstract

Differential protection is the most common method used by electric utilities for generator stator winding protection. Digital relays, used in differential protection, take one cycle or more after fault inception to issue a trip signal. Minimizing the damage due to stator faults, by using high speed relays, is important. A new high speed neural network based digital differential relay for generator stator winding protection is proposed in this dissertation.

A direct 3-phase model that enables an exact study of synchronous machine performance is presented. This model is capable of simulating normal operation and various kinds of external faults. In this dissertation a new method for simulating internal faults in a synchronous generator, using the direct phase quantities, is developed. The internal faults algorithm is capable of simulating internal single phase to ground faults and internal two phase to ground faults in multi-path and single-path generators.

The relay uses two multi-layer feed-forward neural networks (FNNs). One FNN is used by the fault detector module and the other by the fault classifier module. The fault detector module is used to discriminate between three generator states, namely the normal operation, external fault and internal fault states. In the event of an internal fault the relay issues a trip signal and activates the fault classifier module, which identifies the faulted phase(s). In the case of an external fault the relay acts as a backup relay for

the main protection against external faults. Simulation results showing the performance of the protection scheme are presented and indicate that it is fast, robust and reliable. The relay tripping time, for the majority of internal faults, is well within half a cycle.

The laboratory experiments are divided in two parts. The first part provides experimental verification of the developed internal faults algorithm. In the second part implementation and real-time experimental verification of the proposed relay are described.

Acknowledgements

I would like to express my sincere gratitude to my supervisor, Dr. O.P. Malik, for his much appreciated support, valuable suggestions and constant guidance throughout the whole program.

I also wish to acknowledge the financial support which I received from the Egyptian Ministry of Higher Education and the University of Calgary.

Special thanks go to Mr. Pat Walsh and Mr. Garwin Hancock for their continuous assistance during my laboratory work. Also, I would like to thank my friends in our research group for their help during my study here.

I am greatly indebted to my family which has always been my source of inspiration, support and encouragement. I would like to thank my parents, my sister and my grandfather.

Contents

List of Tables

List of Figures

List of Symbols

A/D	analog to digital
$AVEF$	averaged output of EFS neuron
$AVFA$	averaged output of phase a neuron
$AVFB$	averaged output of phase b neuron
$AVFC$	averaged output of phase c neuron
$AVIF$	averaged output of IFS neuron
$AVNS$	averaged output of NOS neuron
CT	current transformer
DARAM	dual access RAM
DAS	data acquisition system
DMA	direct memory access
DSP	digital signal processing
$\Delta w_{kj}(x)$	correction applied to the weight $w_{kj}(x)$
EFS	external fault state
E_{bus}	peak value of the infinite bus phase voltage
$E(x)$	total squared error for pattern x
FI	fault inception time in samples
FIR	finite-duration impulse response
FNN	feed-forward neural network
$G_1, .., G_6$	generators 1 through 6 used in the simulation studies

H	inertia constant
$H(s)$	transfer function of the antialiasing low pass filter
IFS	internal fault state
I_{diff}	differential current
I_{pe}	current of protected equipment
I_{sum}	sum current
L	self-inductance of a machine winding
$\mathbf{L_1}, \mathbf{L_{11}}, \mathbf{L_{12}}$	inductance matrices during NOS or EFS
$\mathbf{L_2}, \mathbf{L_{21}}, \mathbf{L_{22}}$	inductance matrices during a single phase internal fault in phase a of a multi-path machine
$\mathbf{L_3}$	inductance matrix during a two phase internal fault in phases a, b of a multi-path machine
$\mathbf{L_4}, \mathbf{L_{41}}, \mathbf{L_{42}}$	inductance matrices during a single phase internal fault in phase a of a single-path machine
$\mathbf{L_5}$	inductance matrix during a two phase internal fault in phases a, b of a single-path machine
LMS	least-mean-square
L_{TL}	inductance of the TL
L_l	leakage inductance of a machine winding
L_{ma}	main inductance of a machine winding
L_{ma0}	constant part of the main inductance of a machine winding
L_{ma1}	variable part of the main inductance of a machine winding
$\mathbf{L_{mod}}$	modified inductance matrix
M	mutual inductance between any two windings
MFNN	multi-layer feed-forward neural network
M_{ad}	mutual inductance between armature and field winding
M_{aq}	mutual inductance between armature and quadrature

	axis damper winding
N	effective number of series turns of phase a
NN	neural network
NOS	normal operation state
N_m	effective number of turns of the m winding
N_n	effective number of turns of the n winding
N_r	effective number of turns of the r winding
N_s	effective number of turns of the s winding
OCC	open circuit characteristics
P	power in pu
PC	personal computer
$\mathbf{\Psi_1}$	flux linkage vector during NOS or EFS
$\mathbf{\Psi_2}$	flux linkage vector during a single phase internal fault in phase a of a multi-path machine
$\mathbf{\Psi_3}$	flux linkage vector during a two phase internal fault in phases a, b of a multi-path machine
$\mathbf{\Psi_4}$	flux linkage vector during a single phase internal fault in phase a of a single-path machine
$\mathbf{\Psi_5}$	flux linkage vector during a two phase internal fault in phases a, b of a single-path machine
R	resistance of a machine winding
$\mathbf{R_1}$	resistance matrix during NOS or EFS
$\mathbf{R_2}$	resistance matrix during a single phase internal fault in phase a of a multi-path machine
$\mathbf{R_3}$	resistance matrix during a two phase internal fault in phases a, b of a multi-path machine
$\mathbf{R_4}$	resistance matrix during a single phase internal fault in

	phase a of a single-path machine
$\mathbf{R_5}$	resistance matrix during a two phase internal fault in phases a, b of a single-path machine
RAM	random access memory
R_{TL}	resistance of the TL
R_{g1}	generator ground resistance
R_{g2}	infinite bus ground resistance
$\mathbf{R_{mod}}$	modified resistance matrix
Sen	sensitivity factor
TL	transmission line
TMS320C30	Texas Instruments DSP board
T_{elc1}	electrical torque during NOS or EFS
T_{elc2}	electrical torque during a single phase internal fault in phase a of a multi-path machine
T_{elc3}	electrical torque during a two phase internal fault in phases a, b of a multi-path machine
T_{elc4}	electrical torque during a single phase internal fault in phase a of a single-path machine
T_{mec}	prime-mover mechanical torque
$\mathbf{V}$	voltage vector
W_{fld}	energy stored in the generator coupling field
X	number of parallel paths
Y	setting for backup tripping for EFS
Z^{-1}	delay element
a, b, c	stator phases: phase a, phase b and phase c, respectively
ac	alternating current
α	momentum factor

an, aTL	faulty windings of phase a of a single-path machine
bn, bTL	faulty windings of phase b of a single-path machine
cn, cTL	faulty windings of phase c of a single-path machine
dc	direct current
δ	load angle with reference to the infinite bus
$\delta_k(x)$	local gradient of neuron k for pattern x
δ_{mo}	displacement angle of the m winding from the original axis of the a winding due to the fault
δ_{no}	displacement angle of the n winding from the original axis of the a winding due to the fault
δ_{ro}	displacement angle of the r winding from the original axis of the b winding due to the fault
δ_{so}	displacement angle of the s winding from the original axis of the b winding due to the fault
$d_k(x)$	desired output of neuron k for pattern x
e	instantaneous voltage of a machine winding
$\mathbf{e_1}$	machine voltage vector during NOS or EFS
$\mathbf{e_2}$	machine voltage vector during a single phase internal fault in phase a of a multi-path machine
$\mathbf{e_3}$	machine voltage vector during a two phase internal fault in phases a, b of a multi-path machine
$\mathbf{e_4}$	machine voltage vector during a single phase internal fault in phase a of a single-path machine
$\mathbf{e_5}$	machine voltage vector during a two phase internal fault in phases a, b of a single-path machine
η	learning rate
f	field winding

$g_1, g_2, ., g_q$	input signals to a NN
h_k	bias of neuron k
i	instantaneous current of a machine winding
$\mathbf{i_1}, \mathbf{i_{11}}, \mathbf{i_{12}}$	machine current vectors during NOS or EFS
$\mathbf{i_2}, \mathbf{i_{21}}, \mathbf{i_{22}}$	machine current vectors during a single phase internal fault in phase a of a multi-path machine
$\mathbf{i_3}$	machine current vector during a two phase internal fault in phases a, b of a multi-path machine
$\mathbf{i_4}, \mathbf{i_{41}}, \mathbf{i_{42}}$	machine current vectors during a single phase internal fault in phase a of a single-path machine
$\mathbf{i_5}$	machine current vector during a two phase internal fault in phases a, b of a single-path machine
kd	direct axis damper winding
kq	quadrature axis damper winding
n	indication of most recent sample
ν	generator instantaneous speed
ω	synchronous speed
pf	power factor
pg	single phase to ground fault
$\phi(.)$	activation function
p, m, n	faulty windings of phase a of a multi-path machine
pp	phase to phase fault
ppg	two phase to ground fault
ψ	instantaneous flux linkage of a machine winding
pu	per-unit
θ	instantaneous position of the rotor with reference to the axis of phase a

$\theta_m, \theta_n, \theta_r, \theta_s$	modification in rotor displacement angle relative to the faulty winding m, n, r or s, respectively
$\theta_{mn}, \theta_{mr}, \theta_{ms}$	modification in rotor displacement angle relative to two faulty windings mn, mr or ms, respectively
$\theta_{nr}, \theta_{ns}, \theta_{rs}$	modification in rotor displacement angle relative to two faulty windings nr, ns or rs, respectively
u_k	linear output of neuron k
v_k	total weighted sum of neuron k
$w_{k1}, w_{k2}, ., w_{kq}$	synaptic weights of neuron k
$w_{kj}(x)$	synaptic weight connecting the output of neuron j to the input of neuron k at iteration x
$y_k(x)$	actual output of neuron k for pattern x
z, r, s	faulty windings of phase b of a multi-path machine

Chapter 1

Introduction

1.1 Role of Protection

The extensive use of electric energy in all branches of the national economy has made the reliability of operation of electrical elements in power systems a problem of special importance. In an electric power system comprised of generators, motors, transformers, switchgears, transmission lines and other elements there is always a possibility for a fault to occur. Faults are generally caused by the breaking of conductors or failure of insulation. Other causes of faults include accidents, excessive internal or external stress.

It is fair to say that without discriminative protection it would be impossible to operate a modern power system. The function of the protective equipment is to isolate, as quickly as possible, any element of the power system in which a fault has developed. Protective schemes are required to possess the following properties in order to adequately perform their function:

- *Selectivity*

  The relay should isolate the faulty part only.

- *Speed*

Quick disconnection of the faulty part helps in maintaining the stability of the power system.

- *Stability*

  The relay should remain inoperative and stable under certain specified transients.

- *Reliability*

  The protective relay should not fail to operate in the event of a fault.

1.2 Generator Protection

Synchronous generators are an essential part of the power system. Loss of even a single unit seriously jeopardizes the operation of the power system to which it is connected. The collective function of all forms of protection applied to generators is, therefore, to reduce the outage period to a minimum by rapid discriminative clearance of all fault conditions associated with it. All faults associated with synchronous generators may be classified as either insulation failures or abnormal running conditions [1–3]. However, this dissertation focuses only on the protection of synchronous generators against stator winding insulation failures. This kind of protection is usually referred to as *generator stator winding protection* [4].

An insulation failure in the stator winding will result in either an interturn fault, a phase fault or a ground fault, but most commonly the latter since most insulation failures eventually bring the winding into direct contact with the core [1]. Generator stator faults are always considered to be serious because of the high currents encountered and the partial damage to the machine windings as well as to the shafts and couplings [3].

A high speed differential relay is normally used to detect three phase, phase to phase and double phase to ground faults. In the case of single

phase to ground faults, the differential relay can provide some ground fault protection for higher level of ground currents, i.e. for generators with low impedance stator grounding [3]. However, the differential relay will not provide ground fault protection for the entire stator winding. It is common practice to provide supplemental ground fault protection [2, 5–8]. Protection against interturn faults is not considered of prime importance, because breakdown of insulation points on the same phase winding will very rapidly change into a ground fault, and will be detected by either the stator differential protection or stator ground fault protection. Protection against interturn faults can be provided for generators with several paths per phase [1,3].

Early differential relays used electro-mechanical technology. They suffered from many problems like slowness, high burden on the current and voltage transformers, contact pitting and high maintenance cost. The next generation used static relays. In their early version they were built assuming pure sinusoidal waveforms as inputs. That is why many utilities did not accept these relays. Later, some modifications were done and their use increased gradually during the sixties and seventies. However, the rapid advances in digital technology enabled researchers and designers to make significant progress in developing microprocessor based protection algorithms [9–13].

1.3 Digital Protection

Digital protection essentially means using a digital computer to protect a certain part of the power system. Methods of using a digital computer for protecting all the equipment in an extra high voltage substation and the transmission lines emanating from it have been introduced in [14]. Though the concept of using a single computer along with its backup has since been discarded in favor of using individual relaying microprocessors for each major

protection function, reference [14] provided a comprehensive description of digital protection.

Besides the benefits of digital technology, properly designed microprocessor relays are superior to conventional electro-mechanical and static relays in several ways. Some of the benefits and advantages of digital relays are [9, 10, 13]:

- *Economics*

  The cost of hardware has been decreasing steadily. The cost of a digital relay is now less than the cost of a comparable analog relay.

- *Performance*

  The performance of the commercial digital relay is considered to be as good as the corresponding perfect analog relay. A digital relay has some inherent features, such as memory action and complex shaping of operational characteristics, which lead to better performance.

- *Reliability*

  A high level of diagnostic functions can be realized in a digital relay which makes the relay much more reliable. As an example, the digital relay can perform self checking at regular intervals.

- *Flexibility*

  The same hardware can be used for different functions by changing only the software program.

1.4 Neural Network Based Digital Protection

1.4.1 History of Neural Networks

A Neural Network (NN) is a parallel, distributed, information processing structure consisting of processing elements, which can possess a local memory

and carry out localized information processing operations. The processing elements are interconnected together with signal channels called connections. Each processing element has a single output connection that branches into as many collateral connections as desired. The processing element output signal can be of any desired mathematical type. All of the processing that goes on within each processing element is completely local; i.e. it depends only upon the current values of the input signals arriving at the processing element via impinging connections and upon values stored in the local memory of the processing element [15]. The structure of the NN is based on the present understanding of biological nervous systems.

In recent years, interest in studying the mechanism and structure of the brain has been increasing. Based on this biological background, recent work has led to the development of new computational models for solving problems such as pattern recognition, fast information processing and adaptation.

In the early 1940s, pioneers of this field studied the potential and capabilities of the adaptation laws involved in neural systems [16]. In the 1950s and 1960s, the perceptron architecture which has subsequently received much attention was developed and its properties and limitations were analyzed. In the 1970s and 1980s, the work reported on self organizing maps using competitive learning [17,18], the use of the energy function in recurrent networks [19] and the development of the back propagation algorithm [20,21] provided a strong impetus to the area and was the catalyst for much of the subsequent research in this field. Since then, much research on neural networks has been done and today there are several well defined architectures to apply to a variety of problems.

Neural networks enjoy a variety of advantages [15,22]:

- *Capability to synthesize complex mappings*

  Neural networks may be employed to synthesize complex and trans-

parent mappings which may be very difficult or even impossible to be expressed in mathematical form. Since a NN is trained by input-output data, a properly trained NN can perform highly non-linear mappings.

- *High speed*

  Due to the parallel mechanism, the NN has the potential to solve the mapping problem much faster than the conventional methods and other artificial intelligence methods, such as expert systems.

- *Robustness and fault tolerance*

  Neural networks are robust. Even if the input data is not complete or has some noise, the NN can still produce good results.

- *Adaptability*

  Neural networks can be trained on-line by using their error performance. This allows the NN to adjust to a new environment.

- *Capacity for generalization*

  Neural networks are able to respond properly to the inputs they have not come across in training. If NNs are trained properly they are able to generalize the input space.

1.4.2 Neural Network Applications in Power Systems

The advantages of the NNs have made them useful in solving several power system problems. Neural networks have been applied in the following fields of power engineering [23,24]:

- Load forecasting
- Dynamic security assessment
- Static security assessment

- System fault detection and classification
- Component fault detection and diagnosis
- Power system control
- Machine control
- Voltage security assessment
- Economic load dispatching
- Unit commitment

1.4.3 Why Neural Network Based Protection?

The current and voltage waveforms during a short circuit condition or a disturbance in a power system are distorted. To determine whether the power system is faulty or healthy using digital techniques, an extensive amount of filtering is performed to obtain phasors. Consequently, the majority of these digital techniques take at least one cycle after fault inception to issue a trip signal. On the other hand, NNs have the ability to learn nonlinear relationships and to acquire underlying knowledge from input-output examples. Inclusion of a NN in a protection scheme allows the direct use of transient waveform data to determine the state of the power system. In addition, the data window can be quite short and does not need to satisfy particular rules as in the case of digital techniques [11,23].

1.5 Dissertation Objectives

The main objective of this dissertation is to propose a new neural network based digital differential relay for synchronous generator stator winding protection. In order to achieve that objective, the following topics are investigated and developed in this dissertation:

- Investigation and selection of a suitable algorithm to simulate generator normal operation and external faults.

- Developing an algorithm for simulating internal faults at different percentages of the stator winding of a synchronous generator.

- Designing a NN based differential relay which is able to discriminate between three generator states, namely the normal operation state, external fault state and internal fault state. In the case of an internal fault the relay should trip the generator and identify the faulted phase or phases. In the case of an external fault the relay should act as a backup relay for the main protection against external faults.

- Simulation studies to evaluate the performance of the NN based relay.

- Experimental verification of the developed internal faults algorithm.

- Hardware implementation and real-time experimental verification of the proposed NN based relay.

1.6 Dissertation Organization

Chapter 2 serves as a brief review of the basic concepts and theories required for this dissertation. The principles of differential protection are first outlined and then the existing digital techniques used in generator differential protection are briefly described. The features that make the multi-layer feed-forward neural network suitable for power system protection applications are presented. A general description of the use of neural networks in protection schemes is given. A full description of a method to simulate the generator performance during normal operation and external faults in direct phase quantities is finally given.

In Chapter 3 the concepts behind the development of an internal faults algorithm are presented. The steps required to enable the simulation of internal single phase to ground faults and internal two phase to ground faults in multi-path per phase generators are described. A similar description for the case of single-path per phase generators follows. The modifications required to include a ground resistance for the generator, as a means of reducing the magnitude of the fault current, in the internal faults algorithm are presented at the end of the chapter.

Simulation results showing the generator currents during normal operation state, external fault state and internal fault state are presented in Chapter 4. Illustrative simulation results showing the normal operation state and external fault state are first presented and briefly discussed. Simulation results showing internal fault currents are then presented and discussed in detail. The effect of ground resistance is shown by comparing internal fault currents with and without a ground resistance. The effect of internal fault location is shown by presenting internal faults at different winding percentages.

The design of the NN based digital differential relay is presented in Chapter 5. The important modules needed for the proposed relay are presented and the function of each module is described. The relay uses two multi-layer feed-forward neural networks (FNNs), one FNN is used by the fault detector module and the other by the fault classifier module. The structure and training process of each FNN is described.

Chapter 6 gives the detailed simulation studies that are done to evaluate the performance of the proposed NN based relay. The relay proper operation is checked for all three states. In protection it is more important to ensure proper relay operation during transient conditions and light faults. Studies showing the performance of the relay during these conditions are also

presented.

The internal faults algorithm is developed in this dissertation and is used to provide the FNNs with training data. So, it is necessary to obtain experimental verification of the proposed algorithm. Simulation results showing the internal fault currents are compared with actual fault currents in Chapter 7. At first, the laboratory power system model is described, then results confirming the accuracy of the internal faults algorithm are presented. The effect of magnetic saturation on the performance of the algorithm is also discussed.

Laboratory implementation and experimental tests of the proposed NN based digital relay are described in Chapter 8. Details of the software written to enable the operation of the relay are described. Behavior of the NN based relay is observed and the experimental results are described in this chapter.

Finally conclusions and comments on further research topics in the area of generator internal fault simulation and neural network based protection are summarized in Chapter 9.

1.7 Dissertation Contribution

The work presented in this dissertation makes original contribution in the following respects:

- Development of an algorithm for simulating internal faults at different percentages of the stator winding of multi-path and single-path generators. The internal faults algorithm is capable of simulating internal single phase to ground faults and internal two phase to ground faults in these generators.

- Design of a NN based differential relay which is able to discriminate between three generator states, namely the normal operation state,

external fault state and internal fault state, through the help of a FNN based fault detector module. In the case of an internal fault the relay identifies the faulted phase or phases by means of a FNN based fault classifier module.

- Evaluation of the relay performance through simulation studies. The relay tripping time, for the majority of internal faults, is well within half a cycle. Fault classification is fast and accurate.

- Experimental verification of the developed internal faults algorithm and the use of the saturated values for the machine reactances in the case of internal two phase to ground faults.

- Laboratory implementation of the proposed NN based relay and experimental tests on a physical model.

Chapter 2

Generator Digital Protection, Neural Networks and Generator Representation in Direct Phase Quantities - An Overview

2.1 Introduction

Prior to attempting to develop a new neural network based digital differential relay for synchronous generators, it is necessary to study the following topics: Digital differential protection of generators, neural networks (NNs) and generator representation in direct phase quantities. This chapter covers the basics of these three areas, which are addressed in separate sections.

A brief review of the digital techniques used in generator protection will provide a knowledge of the latest developments in that field and their drawbacks. In Section 2.2 the principles of differential protection are explained,

then four different digital techniques are briefly discussed. The limitations of existing digital techniques are also pointed out.

Neural networks are based on a simplified model of the brain, with the processing tasks being distributed across many simple nodes. The power of a NN comes from the collective behavior of the simple nodes. In addition to the capability of learning and adaptation, this structure offers many other advantages including speed, robustness and fault tolerance. In Section 2.3 the reasons that the multi-layer feed-forward neural network (FNN) is currently receiving the most attention as a viable candidate for applications to power system protection are stated. As the back-propagation algorithm is usually used in training the multi-layer feed-forward neural networks, a brief description of it is given. Also, a general description of the use of neural networks in protection schemes is given in this section, together with a brief description of some NN based protection applications that were reported in the literature.

Analysis of faults in a power system is of major importance in all aspects of power engineering. Applications of fault analysis include protection system design, security analysis and contingency planning. All applications depend on accurate estimates of system voltages and currents when faults occur. In this dissertation accurate estimation of generator 3-phase currents during normal operation, external faults and internal faults is of primary importance. In Section 2.4 a direct 3-phase model that enables a more exact study of synchronous machine performance is presented. This model is capable of simulating the normal operation of a synchronous machine. The modifications required in the basic direct 3-phase model for the simulation of various kinds of external faults are also presented in this section.

2.2 Digital Differential Protection of Generators

2.2.1 Principles of Differential Protection

The differential principle used in differential protection can be illustrated by reference to Fig. 2.1. For normal operation or for a fault outside the two sets of current transformers (CTs), I_{pe} entering the machine equals I_{pe} leaving the machine in all phases [25]. On a per-unit (pu) basis, the secondary current is equal to the primary current. Hence, during normal operation and external faults, ideally, no current passes through the relay. If a fault occurs between the two sets of CTs, one or more of the left-hand currents will suddenly increase, while currents on the right side may either decrease or increase and flow in the reverse direction. Either way, the total fault current will now flow through the relay, causing it to operate.

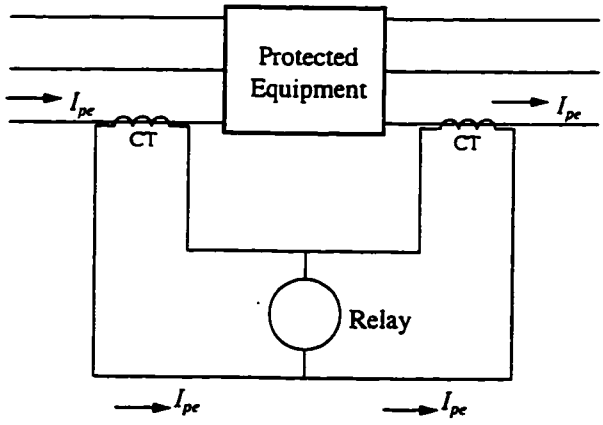

Figure 2.1: The basic differential connection.

If perfect CTs are available, the relay can be set to respond very sensitively and quickly. In practice, however, no two CTs will give exactly the same secondary current for the same primary current. Discrepancies can be traced to manufacturing variations and to differences in secondary loading.

As a result, the differential current produced flows through the relay. While normally small, the differential current can become appreciable when short circuit current flows to an external fault, causing the relay to maloperate.

The percentage differential relay, shown in Fig. 2.2, solves the above problem without sacrificing sensitivity. The restraining windings receive the transformer secondary current and desensitize the relay to high external fault currents. Hence, the current required for relay operation increases with the magnitude of the external fault current. The effect of the restraint windings on internal faults is negligible, because the operating winding has more ampere turns and receives the total secondary fault current.

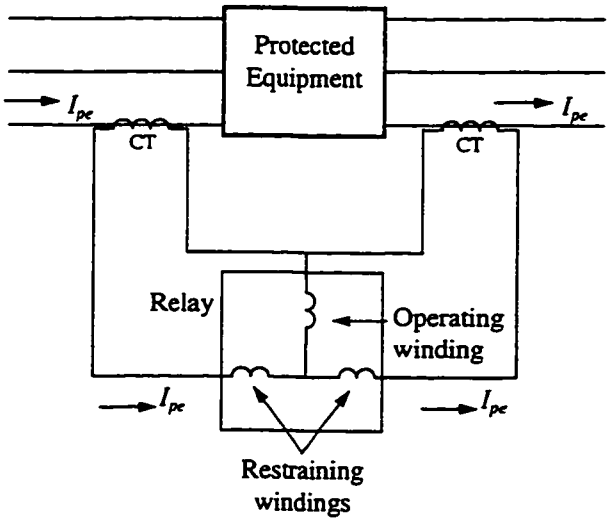

Figure 2.2: Schematic connections of the percentage differential relay.

2.2.2 Digital Differential Protection Using Instantaneous Values

One of the early digital algorithms proposed for generator differential protection is presented in [26]. This algorithm uses the instantaneous differences between the currents entering the generator, i.e. neutral-end currents, and

the currents leaving the generator, i.e. line-side currents, for detecting stator winding faults. The algorithm consists of three parts: a fault monitor, a phase allocation sequence and a fault verification sequence.

The fault monitor checks if the absolute value of the instantaneous difference between the neutral-end and line-side currents has exceeded a prespecified software threshold. Should the absolute value exceed the threshold, the monitor relinquishes control to the phase allocation sequence.

On activation by the monitor, the phase allocation sequence determines the faulted phase. The phase allocation sequence issues a read direct to the analog-to-digital converter to sample the difference current of each phase. The difference current sample of each phase is then stored and its absolute value is calculated. The absolute values of the three samples are compared and the phase with the largest sample is determined. Sequential sampling continues and the procedure described above is repeated until the largest samples from different passes twice indicate the same phase as probably faulted. The phase allocation sequence then branches to the appropriate fault verification routine.

The verification sequence decides whether the generator stator is actually faulted or not. One verification sequence is provided for each phase. On commencement of verification the sampling is restricted to the sum and difference currents of the selected phase. The absolute value of the difference current is multiplied by 128, using an arithmetic left shift of seven bits, and divided by the sum current. The result is compared with a percentage threshold. Should the threshold be exceeded a counter is incremented. In case the result is less than the percentage threshold, the counter is decremented. After the counter has been either incremented or decremented, it is compared with the positive and the negative threshold values. If the value of the counter is between the two threshold values, the issue is undecided and the sequence

returns for another verification pass. If the positive threshold is reached a trip signal is issued, while if the negative threshold value is reached then it is concluded that activation occurred due to a transient condition and the fault monitor is reinstated.

2.2.3 Cross-Correlation Techniques

Cross-correlation techniques have been used in the literature to obtain faithful representation of the signals used in digital protection schemes [27–30]. In cross correlation the signal from the protected system is compared to standard reference signals to extract the real and imaginary parts of the required frequency component of the signal, i.e. the fundamental frequency component and/or the second harmonic component depending on the protection scheme. It should be noted that the cross-correlation techniques are essentially the convolution techniques used in the signal processing literature [31, 32].

Reference [27] uses cross-correlation of an input current signal with sine and cosine waves to extract the real and imaginary parts of the fundamental frequency component of the signal. From the real and imaginary parts of the fundamental frequency of the line-side and neutral-end currents so obtained, the root mean square values of the fundamental frequency components of the differential, I_{diff}, and the sum, I_{sum}, currents are computed. The differential current, I_{diff}, is the difference between the line-side and neutral-end currents, while I_{sum} is the summation of these two currents. Hence, the following trip criterion

$$I_{diff} > Sen \ I_{sum} \tag{2.1}$$

is checked, where Sen is a prespecified sensitivity factor.

At the onset of a fault in the armature winding a second harmonic is pro-

duced in the field current. An algorithm that extracts the second harmonic in the field current, by cross-correlating the field current with sine and cosine references, and then uses it to detect generator faults is presented in [28]. As both internal and external faults produce a second harmonic in the field current, so the direction of negative sequence power flow at the generator terminals is used to differentiate between internal and external faults.

To reduce the computation requirement of the relaying algorithm, cross-correlation with a heptagonal wave for the extraction of fundamental frequency components of the differential and sum currents is implemented in [29,30]. The trip criterion used in this algorithm is the same as that shown in (2.1), but real parts instead of real and imaginary parts are used in that algorithm.

2.2.4 Digital Filter Based Algorithms

Fault current waves contain dc offsets and superimposed harmonics. Digital filters, when used in a protection algorithm, efficiently remove the distortion present in the fault current waves [9,13]. These protection algorithms use finite-duration impulse response (FIR) digital filters to accurately estimate the magnitude of the fundamental component [31,32]. Recently a number of integrated generator protection systems have been reported in the literature [33–35]. These systems use digital filters to compute the phasors of voltages and currents, and apply appropriate digital algorithms for providing a variety of protection functions including stator winding protection.

2.2.5 Symmetrical Components Based Algorithms

An algorithm that uses positive and negative sequence models of the generator, and voltages and currents measured at the generator terminals to discriminate between internal and external faults is given in [36]. Fault dis-

crimination criterion in that algorithm is based on the signs of positive and negative sequence impedances seen by the relay. These impedances are negative for faults internal to the generator and positive for faults external to the generator.

The algorithm first calculates the 60 Hz voltage and current phasors for the three phases of the generator, and subsequently computes the positive and negative sequence phasors. The most recent voltage and current samples are then compared with voltage and current samples from the previous cycle. If the change is greater than a predefined threshold, an impedance calculation procedure is initialized to determine whether an internal fault or an external fault has occurred. Otherwise, the algorithm waits for a new set of samples to arrive and repeats the procedure described above.

2.2.6 Limitations of Existing Digital Techniques

The majority of the previously proposed algorithms are based on fault detection principles that are used in their electro-mechanical counterparts. Moreover, the extensive computations performed to obtain accurate estimates of phasors prevent the relay from taking a quick trip decision. The majority of these digital techniques take at least one cycle after fault inception to issue a trip signal.

2.3 Neural Networks

Neuron is the basic element of a neural network. The manner in which the neurons of a NN are connected and the method by which a NN is trained distinguish one NN from another. As detailed introduction and classification are already available in [15, 16, 22, 37], only a brief summary of the structure of a NN is given in Appendix A. In this section some of the concepts of NNs

that are of importance to this project are reviewed.

2.3.1 Suitability of the Multi-Layer FNN in Power System Protection Applications

The multi-layer feed-forward neural network (MFNN) is currently receiving the most attention as a viable candidate for applications to power systems [11,23]. The MFNN is taught by example, and the hidden layers enable it to extract higher-order statistics, as indicated in Appendix A. The preponderance of data typically available from the power industry, coupled with the ability of the MFNN to learn significantly nonlinear input/output relationships, reveals it as a viable candidate among other solutions [9–11] for solving significant power system protection problems.

Moreover, MFNN can be used to process time series data, which is the main core of digital protection algorithms [11]. As shown in Fig. 2.3 the input sequence is fed into a tapped delay line with each delay element Z^{-1} providing a time delay equal to one sampling interval and then feeding the taps from the delay line into a static MFNN. The index n in Fig. 2.3 is used to indicate the most recent sample of the input and q is the total number of inputs.

In this dissertation, the MFNN is employed to build the proposed neural network based digital differential relay.

2.3.2 Back-Propagation Training Algorithm

Multi-layer feed-forward neural networks are usually trained using the back-propagation algorithm [15,20,21]. As the back-propagation algorithm is used in this dissertation, a brief description of it is given in this section.

The learning procedure here involves the presentation of a set of pairs

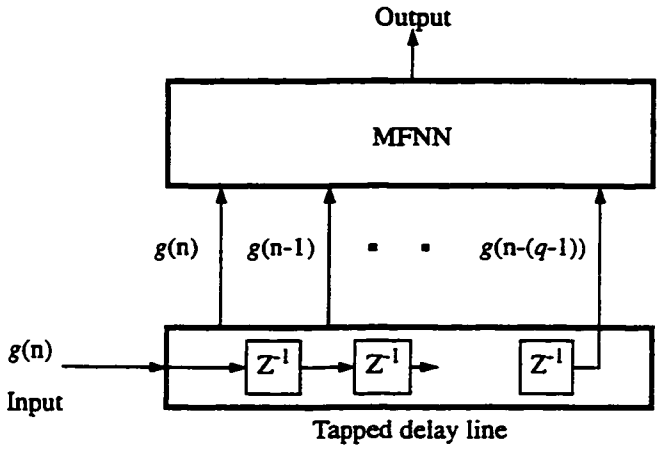

Figure 2.3: A MFNN processing time series data.

of input and output patterns. For each input and output pattern, x, the system first uses the input vector to produce its own output vector and then compares this with the desired output, or target vector. If there is no difference, no learning takes place. If a difference exists, the weights are adjusted to eliminate the total squared error, $E(x)$, which is the sum of the squared differences between the set of desired outputs and the set of actual outputs of the neural network [15]:

$$E(x) = \frac{1}{2}\sum_{k}[d_k(x) - y_k(x)]^2 \tag{2.2}$$

where $d_k(x)$ is the desired output and $y_k(x)$ is the actual output of neuron k for pattern x.

The weights w_{kj} (see Appendix A for a description of weights) can be adjusted to minimize $E(x)$ for the set of training patterns by a gradient descent method, given by:

$$w_{kj}(x+1) = w_{kj}(x) + \Delta w_{kj}(x) \tag{2.3}$$

where

$$\Delta w_{kj}(x) = \eta \delta_k(x) y_j(x) \tag{2.4}$$

where η is the learning rate. If neuron k is in the output layer:

$$\delta_k(x) = \frac{dy_k(x)}{dv_k(x)}[d_k(x) - y_k(x)] \tag{2.5}$$

where $v_k(x)$ is the total weighted sum of neuron k as expressed in (A.3). If neuron k is not in the output layer:

$$\delta_k(x) = \frac{dy_k(x)}{dv_k(x)} \sum_i \delta_i(x) w_{ik}(x) \tag{2.6}$$

where $\delta_i(x)$ is from the neurons in the layer following the layer where neuron k is located.

The objective of the back-propagation algorithm is to update the weights in (2.3) such that the NN can have the lowest error possible, i.e. achieve a global minimum. However, NNs with more than one hidden layer may have several local minima. Adding a momentum factor to (2.4) decreases the sensitivity of the back-propagation algorithm to small details in the error surface [15]. This helps the network to avoid getting stuck in shallow minima, which would prevent the network from finding a lower error solution. The momentum term is added to (2.4) as follows:

$$\Delta w_{kj}(x) = \eta \delta_k(x) y_j(x) + \alpha \Delta w_{kj}(x-1) \tag{2.7}$$

where α is the momentum factor. In the above equations, the learning rate, η, and the momentum factor, α, are between 0 and 1, and are determined by experience.

2.3.3 Use of Neural Networks in Protection Schemes

Investigations into the use of NNs for relaying purposes started about seven years ago. Researchers have applied NNs to solve relaying problems in a number of different areas. This section describes how, in general, a NN can be used in a protection scheme.

The information that can be obtained from a power system is in the form of voltage and current signals. For most NN based protection applications, voltages and currents in one form or another are used to train a NN to distinguish between a fault or a healthy condition in the power system. Once a NN is trained, it is then used by the protection scheme to detect faults. The structure of a NN is application specific. Structural differences might come on account of the number and type of inputs, number and type of outputs and complexity of the application which would then govern the number of layers and the number of neurons in different layers. These parameters of the network are decided by experimentation which involves training and testing a number of network configurations. The process is terminated when the chosen network configuration has satisfactory performance. A NN is considered to have a satisfactory performance when the averaged squared error is at an acceptably minimum value and it is able to respond adequately to patterns which are different from the ones used in training [11, 15, 23]. As discussed in Appendix A, a three layer FNN can emulate any shape of the decision boundary reasonably well and has, therefore, been used for a number of protection functions.

For high impedance fault detection, a three layer FNN has been proposed to distinguish arcing fault currents from non-fault and fault like currents [38]. In transmission line protection, MFNNs have been proposed for fault direction discrimination [39,40], fault classification [41], time zone classification [42] and adaptive reclosing [43]. Since the complex variation of line

impedance is accentuated by the use of the capacitors in series compensated transmission systems, conventional distance protection schemes are limited to certain applications. MFNNs have been proposed to aid in the process of fault detection and fault classification for series compensated transmission systems [44, 45].

MFNNs are also helpful in differentiating between magnetizing inrush current waveforms and fault current waveforms, hence assisting in transformer protection [46–48]. A NN has also been proposed to detect incipient faults, in the form of turn-to-turn stator insulation fault and bearing wear in single phase induction motors [49–51]. The use of NNs in predicting the field current of an alternator and then detecting the field winding interturn fault is described in [52]. Another approach for the localization of field winding shorts, using a NN with a fuzzified output, has been proposed in [53]. In this approach two similar traveling waves are injected simultaneously at both ends of the field winding. Selected features of the received signals are used as inputs to the FNN, which is used to detect and localize shorted turns in the field winding.

As explained previously MFNNs have been extensively used in protection applications, however, few researchers have used self organizing neural networks for fault classification in transmission systems [54, 55].

2.4 Generator Representation in Direct Phase Quantities

Methods of predetermining the transient performance of synchronous machines have, in the past, made use of a number of approximations, in view of the fact that a closed form solution of the performance equations was laborious and in some cases was not feasible [56]. To overcome some of the

difficulties, various transformations, such as $d-q-0$ and $\alpha-\beta-0$, were introduced. The $d-q$ axes model yields differential equations with constant coefficients. They are linear provided that speed is assumed to be constant, which rules out logical and rigorous analysis of power swings. In addition, study of unsymmetrical faults necessitates further transformation of $d-q-0$ equations [57]. In such cases, the $\alpha-\beta-0$ model has been found more convenient to use [58]. The $\alpha-\beta-0$ model results in differential equations with variable coefficients and an approximate solution has been suggested [59]. As stated earlier, the performance equations become nonlinear once the speed variation is taken into account, making it imperative to resort to a computer solution if exact analysis is required.

With the advent of modern computers, numerical methods can be employed efficiently for solving nonlinear differential equations. In such a case, a direct 3-phase model is used for a more exact study of synchronous machine performance [60, 61]. With direct representation, the normal operation can be simulated. Also, various external fault conditions, such as symmetric and unsymmetric conditions, can be simulated, by doing slight modifications in the basic direct 3-phase model.

This section describes a mathematical model of a synchronous machine in direct phase quantities and the procedure for simulating normal operation and external faults using numerical techniques. This model and the required modifications for simulating external faults have already been presented in [60]. However, the modifications that enabled that model to be used to simulate internal faults have been developed in this dissertation and are considered as a part of the dissertation contribution. The internal faults algorithm is described in Chapter 3.

2.4.1 Normal Operation

Figure 2.4 shows a schematic representation of a synchronous generator with two damper windings. In Fig. 2.4, the letters a, b and c refer to the stator phases: phase a, phase b and phase c, respectively, while the letters f, kd and kq refer to the rotor windings: the field winding, the direct axis damper winding and the quadrature axis damper winding, respectively. In direct phase quantities, the performance of a synchronous generator connected to an infinite bus through a short transmission line (TL) having a resistance R_{TL} and an inductance L_{TL}, Fig. 2.5, can be described by equations given below.

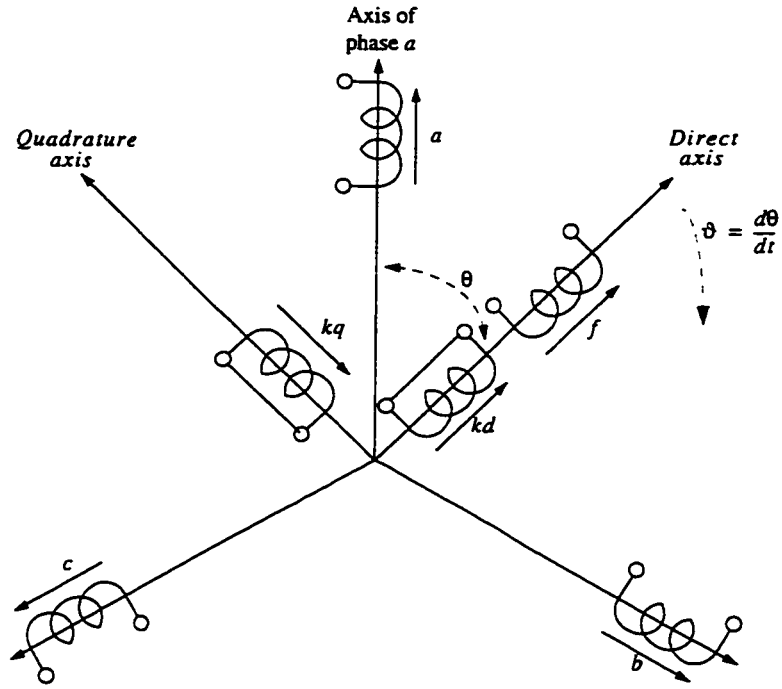

Figure 2.4: Schematic representation of a synchronous machine.

Voltage Relationships

The position of the rotor at any instant is specified with reference to the axis of phase a by the angle θ, Fig. 2.4. In terms of flux linkages, Ψ_1, voltage

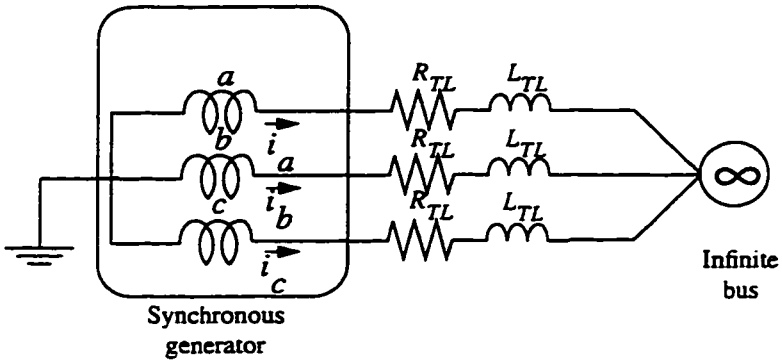

Figure 2.5: System representation.

relationships for the stator and rotor circuits, $\mathbf{e_1}$, are linked with the winding resistances, $\mathbf{R_1}$, and instantaneous currents, $\mathbf{i_1}$, as follows:

$$\mathbf{e_1} = \frac{d\mathbf{\Psi_1}}{dt} - \mathbf{R_1 i_1} \tag{2.8}$$

where

$$\mathbf{e_1} = [e_a e_b e_c e_f e_{kd} e_{kq}]^t \tag{2.9}$$

$$\mathbf{\Psi_1} = [\psi_a \psi_b \psi_c \psi_f \psi_{kd} \psi_{kq}]^t \tag{2.10}$$

$$\mathbf{R_1} = diagonal[R_a R_a R_a - R_f - R_{kd} - R_{kq}] \tag{2.11}$$

$$\mathbf{i_1} = [i_a i_b i_c i_f i_{kd} i_{kq}]^t \tag{2.12}$$

When the machine is supplying a load through a short TL, Fig. 2.5, the machine terminal voltages can be expressed as follows:

$$e_a = -E_{bus}\sin(\omega t) + i_a R_{TL} + \frac{di_a}{dt} L_{TL} \tag{2.13}$$

$$e_b = -E_{bus}\sin(\omega t - \frac{2\pi}{3}) + i_b R_{TL} + \frac{di_b}{dt} L_{TL} \tag{2.14}$$

$$e_c = -E_{bus}\sin(\omega t + \frac{2\pi}{3}) + i_c R_{TL} + \frac{di_c}{dt} L_{TL} \tag{2.15}$$

where $\omega t = \theta + \delta$, ω being the synchronous speed and δ is the load angle with reference to the infinite bus, and E_{bus} is the peak value of the infinite bus phase voltage.

Flux Linkage Relationship

The flux linkage relationship of a synchronous generator can be expressed in symbolic form as:

$$\mathbf{\Psi_1} = \mathbf{L_1 i_1} \tag{2.16}$$

where

$$\mathbf{L_1} = \begin{array}{c} \begin{matrix} a & b & c & f & kd & kq \end{matrix} \\ \begin{bmatrix} L_a & M_{ab} & M_{ac} & M_{af} & M_{akd} & M_{akq} \\ M_{ba} & L_b & M_{bc} & M_{bf} & M_{bkd} & M_{bkq} \\ M_{ca} & M_{cb} & L_c & M_{cf} & M_{ckd} & M_{ckq} \\ M_{fa} & M_{fb} & M_{fc} & L_f & M_{fkd} & 0 \\ M_{kda} & M_{kdb} & M_{kdc} & M_{kdf} & L_{kd} & 0 \\ M_{kqa} & M_{kqb} & M_{kqc} & 0 & 0 & L_{kq} \end{bmatrix} \end{array} \begin{matrix} a \\ b \\ c \\ f \\ kd \\ kq \end{matrix} \tag{2.17}$$

where the term L indicates the self-inductance of either the a, b, c, f, kd or kq winding, and the term M indicates the mutual inductance between any two of these windings. The formulas of the components of the $\mathbf{L_1}$ inductance matrix in (2.17) are given in Appendix B.1.

Torque

Owing to inertia, the instantaneous electric torque, T_{elc1}, differs from the prime-mover mechanical torque, T_{mec}, if the speed varies. At any instant, T_{mec} is equal to T_{elc1} plus the accelerating torque [56,60]. Hence, the equation

of motion of a synchronous generator can be expressed by:

$$\frac{d^2\delta}{dt^2} = \frac{\omega}{2H}(T_{mec} - T_{elc1}) \tag{2.18}$$

where H is the inertia constant. The formula of T_{elc1} is given by:

$$T_{elc1} = \frac{1}{3}(\frac{1}{2}\mathbf{i_{11}}\frac{d\mathbf{L_{11}}}{d\theta}\mathbf{i_{11}}^t + \mathbf{i_{11}}\frac{d\mathbf{L_{12}}}{d\theta}\mathbf{i_{12}}) \tag{2.19}$$

where

$$\mathbf{i_{11}} = [i_a i_b i_c] \tag{2.20}$$

$$\mathbf{i_{12}} = [i_f i_{kd} i_{kq}]^t \tag{2.21}$$

$$\mathbf{L_{11}} = \begin{bmatrix} L_a & M_{ab} & M_{ac} \\ M_{ba} & L_b & M_{bc} \\ M_{ca} & M_{cb} & L_c \end{bmatrix} \tag{2.22}$$

$$\mathbf{L_{12}} = \begin{bmatrix} M_{af} & M_{akd} & M_{akq} \\ M_{bf} & M_{bkd} & M_{bkq} \\ M_{cf} & M_{ckd} & M_{ckq} \end{bmatrix} \tag{2.23}$$

The formula given in (2.19) is based on the fact that an electrical torque is produced in a machine when a change in the energy stored in its coupling field, W_{fld}, occurs, i.e. $T_{elc1} = -dW_{fld}/d\theta$, [61].

General

Equations (2.8,2.13-2.16,2.18) form the complete model for a synchronous machine in direct phase quantities. The elements of the $\mathbf{L_1}$ matrix in (2.17) are dependent on rotor position, which varies with time. Hence the performance equations are differential equations with variable coefficients. As

the speed of the generator varies under transient operating conditions, the performance equations are nonlinear. Generally, solutions in closed form can not be obtained, and a numerical solution has to be resorted to.

Simulation Procedure

The simulation involves the solution, by a numerical method, of the mathematical model presented above. In this dissertation the Runge-Kutta method as modified by Gill is used. This is the same numerical method used in [60]. The basic algorithm for the simulation of the 3-phase model is as follows:

1. The initial voltages, currents, current derivatives, and rotor position, as specified by the problem, are used to start the computation.

2. The flux linkage derivative, $d\mathbf{\Psi_1}/dt$, is computed at the beginning of the n^{th} step with the knowledge of $\mathbf{e_1}$ and $\mathbf{i_1}$ using (2.8).

3. On integration, this gives the flux linkage vector $\mathbf{\Psi_1}$.

4. The electrical angle θ at the n^{th} step, which defines the rotor position at that instant, is obtained by solving (2.18) for δ.

5. The angle θ computed at the end of a step is used in forming the inductance matrix $\mathbf{L_1}$ in (2.17).

6. The currents at the end of the n^{th} step are obtained from:

$$\mathbf{i_1} = \mathbf{L_1}^{-1}\mathbf{\Psi_1} \tag{2.24}$$

7. The current derivative vector, $d\mathbf{i_1}/dt$, is obtained from the following matrix equation, making use of the currents computed above:

$$\frac{d\mathbf{i_1}}{dt} = \mathbf{L_{mod}}^{-1}\mathbf{V} + \mathbf{L_{mod}}^{-1}\mathbf{R_{mod}}\mathbf{i_1} - \mathbf{L_{mod}}^{-1}\frac{d\mathbf{L_1}}{dt}\mathbf{i_1} \tag{2.25}$$

where

$$\mathbf{V}=[-E_{bus}\sin(\omega t)\ -E_{bus}\sin(\omega t-\frac{2\pi}{3})\ -E_{bus}\sin(\omega t+\frac{2\pi}{3})e_f e_{kd} e_{kq}]^t \quad (2.26)$$

$$\mathbf{R_{mod}} = dig[(R_a + R_{TL})(R_a + R_{TL})(R_a + R_{TL}) - R_f\ -R_{kd}\ -R_{kq}] \quad (2.27)$$

The elements of the modified matrix, $\mathbf{L_{mod}}$, are the same as the $\mathbf{L_1}$ matrix except for the following:

$$L_{mod}(1,1) = L_1(1,1) - L_{TL} \quad (2.28)$$

$$L_{mod}(2,2) = L_1(2,2) - L_{TL} \quad (2.29)$$

$$L_{mod}(3,3) = L_1(3,3) - L_{TL} \quad (2.30)$$

The derivation of (2.25) is obtained by equating the derivative of (2.16) with (2.8).

8. The currents and their derivatives calculated above are utilized in calculating the machine terminal voltage given in (2.13-2.15), and the same procedure above is repeated for the (n+1) step.

2.4.2 External Faults

For various faults occurring at the terminals of a loaded machine, the constraints to be imposed, and the corresponding modifications required in the mathematical model described in Section 2.4.1, are described below. This model is also capable of simulating external faults at any location along the TL, but as the constraints of imposing a fault along the line resemble those for a terminal fault, only terminal faults are described in this section. In this dissertation this model has been used for simulating terminal faults as well as faults along the TL.

The necessary changes to simulate faults can be incorporated at any stage

of the simulation by a few simple instructions in the program. It thus allows any kind of fault to be simulated at any required fault inception time. For the sake of clarity, only those expressions or matrices that require to be modified, to simulate a terminal fault, are given.

Three Phase Fault

For a three phase fault, at the instant of the fault,

$$e_a = e_b = e_c = 0 \tag{2.31}$$

This will necessitate the following modifications:

$$V(1) = V(2) = V(3) = 0 \tag{2.32}$$

$$\mathbf{L_{mod}} = \mathbf{L_1} \tag{2.33}$$

$$\mathbf{R_{mod}} = \mathbf{R_1} \tag{2.34}$$

Phase to Phase Fault

For a fault on phases b and c,

$$e_{bc} = e_b - e_c = 0 \tag{2.35}$$

Hence

$$e_b = e_c \tag{2.36}$$

Also

$$e_a + e_b + e_c = 0 \tag{2.37}$$

So

$$e_b = e_c = -\frac{e_a}{2} \tag{2.38}$$

at the instant of the fault. This condition is simulated with the indicated changes in the following elements:

$$V(2) = V(3) = \tfrac{1}{2} E_{bus} \sin(\omega t) \tag{2.39}$$

$$L_{mod}(2,1) = L_1(2,1) + \tfrac{L_{TL}}{2} \qquad L_{mod}(2,2) = L_1(2,2) \tag{2.40}$$

$$L_{mod}(3,1) = L_1(3,1) + \tfrac{L_{TL}}{2} \qquad L_{mod}(3,3) = L_1(3,3) \tag{2.41}$$

$$R_{mod}(2,1) = R_{mod}(3,1) = -\tfrac{R_{TL}}{2} \tag{2.42}$$

$$R_{mod}(2,2) = R_{mod}(3,3) = R_a \tag{2.43}$$

Two Phase to Ground Fault

For a fault on phases a and b, $e_a = e_b = 0$. The modified elements are then:

$$V(1) = V(2) = 0 \tag{2.44}$$

$$L_{mod}(1,1) = L_1(1,1) \qquad L_{mod}(2,2) = L_1(2,2) \tag{2.45}$$

$$R_{mod}(1,1) = R_{mod}(2,2) = R_a \tag{2.46}$$

Single Phase to Ground Fault

For a fault on, say, phase a, $e_a = 0$. This will necessitate the following modifications:

$$V(1) = 0 \tag{2.47}$$

$$L_{mod}(1,1) = L_1(1,1) \tag{2.48}$$

$$R_{mod}(1,1) = R_a \tag{2.49}$$

2.5 Summary

The basic concepts and theories of digital differential protection of generators, neural networks and generator representation in direct phase quantities are presented in this chapter. The fundamental digital techniques used in digital differential protection are explained. It is shown that digital techniques require an extensive amount of computations to obtain accurate estimates of phasors and hence a trip decision is delayed by at least one cycle after fault inception.

The multi-layer feed-forward neural network is a static network. It has an output layer, an input layer and one or two hidden layers. The information can only be fed forward between layers. There is no feedback available during the operation. As the three layer FNN can emulate any shape of the decision boundary reasonably well, it is applied in a number of protection functions and is chosen to build the NN based differential relay.

For simulation of normal operation and external faults of generators, it is shown that a direct 3-phase model is well suited for computer simulation. The use of this model allows a uniform approach to the study of both symmetrical and unsymmetrical faults, while retaining the generator nonlinear model. Moreover, the parameters used in the 3-phase model are physical values and it is not necessary to go through complex transformations as in the case of the d–q–0 and α–β–0 models. It should also be noted that the 3-phase model takes into consideration the variation of speed under transient conditions and a numerical method is used to solve the performance nonlinear differential equations in a step by step manner, i.e. without approximations. This leads to the conclusion that using the direct 3-phase model would produce accurate results.

Chapter 3

Internal Faults in Synchronous Generators

3.1 Introduction

Along with the development of electric power industry, the protection of synchronous generators becomes more and more important. The internal short circuit current for the generator may be several times larger than its terminal short circuit current. The strong current could cause severe heat and mechanical damage. Hence, for adequate generator protection, an accurate method for calculating the internal fault currents should be available.

Several articles analyzing the internal faults of *ac* machines have been published [62–64]. In [62, 63] the symmetrical component method is used and only the fundamental and the third harmonic components, of time and space, are considered. In the case of internal faults in the stator windings of electrical machines, there are stronger space harmonics in the air gap magnetic field and stronger time harmonics in winding currents. Therefore, a substantial amount of error would be caused by using the symmetrical component method. In the multi-loop theory the electrical machine is considered

as formed of several electric circuits, each composed of the actual loops that are formed by the coils [64]. The inaccuracies involved with the calculations of loop inductances and the focus of the multi-loop theory on hydro-generators with distributed neutral arrangement only, prevent the generalization of this method for different types of synchronous generators.

In the previous chapter, a mathematical model of a synchronous machine in direct phase quantities was described and was found to be both accurate and suitable for fault studies. In this chapter a new method for simulating internal faults in a synchronous generator, using the direct phase quantities, is described. The developed method follows the same basic approach as followed in [60], Section 2.4.2, for the simulation of external faults. The method for calculating the self and mutual inductances of the faulted phase of the synchronous machine is based on the analysis presented in [62, 63, 65–67]. In Section 3.2 internal single phase to ground faults and internal two phase to ground faults in multi-path generators are covered, while Section 3.3 describes the simulation of internal single phase to ground faults and internal two phase to ground faults in single-path generators.

The stator windings of the generators are usually grounded in a manner to reduce the fault currents. In other words the generator is grounded through a ground resistance to limit the magnitude of fault current during ground faults [3]. Generator grounding practices and the inclusion of a ground resistance in the direct 3-phase model are described in Section 3.4.

3.2 Internal Faults in Multi-Path Synchronous Generators

3.2.1 Internal Single Phase to Ground Faults

A schematic representation of a synchronous machine with two damper coils during an internal single phase to ground fault in phase a is shown in Fig. 3.1. It is assumed that the armature winding of a synchronous machine consisting of X parallel paths per phase is tapped at a certain point of one of the parallel paths of phase a. The tapped parallel path is divided in two parts, one part is adjacent to the neutral, which is referred to as the m winding, and the second part adjacent to the machine terminal, which is referred to as the n winding. The remaining, $X-1$, parallel paths of phase a are lumped into one equivalent winding which is referred to as the p winding. In direct phase quantities, the performance of a synchronous generator, during an internal single phase to ground fault, connected to an infinite bus through a short transmission line (TL), Fig. 3.2, can be described by equations given below.

Voltage Relationships

The position of the rotor at any instant is specified with reference to the axis of phase a by the angle θ, Fig. 3.1. In terms of flux linkages, $\mathbf{\Psi_2}$, voltage relationships for the stator and rotor circuits, $\mathbf{e_2}$, are linked with the winding resistances, $\mathbf{R_2}$, and instantaneous currents, $\mathbf{i_2}$, as follows:

$$\mathbf{e_2} = \frac{d\mathbf{\Psi_2}}{dt} - \mathbf{R_2 i_2} \tag{3.1}$$

where

$$\mathbf{e_2} = [e_p e_m e_n e_b e_c e_f e_{kd} e_{kq}]^t \tag{3.2}$$

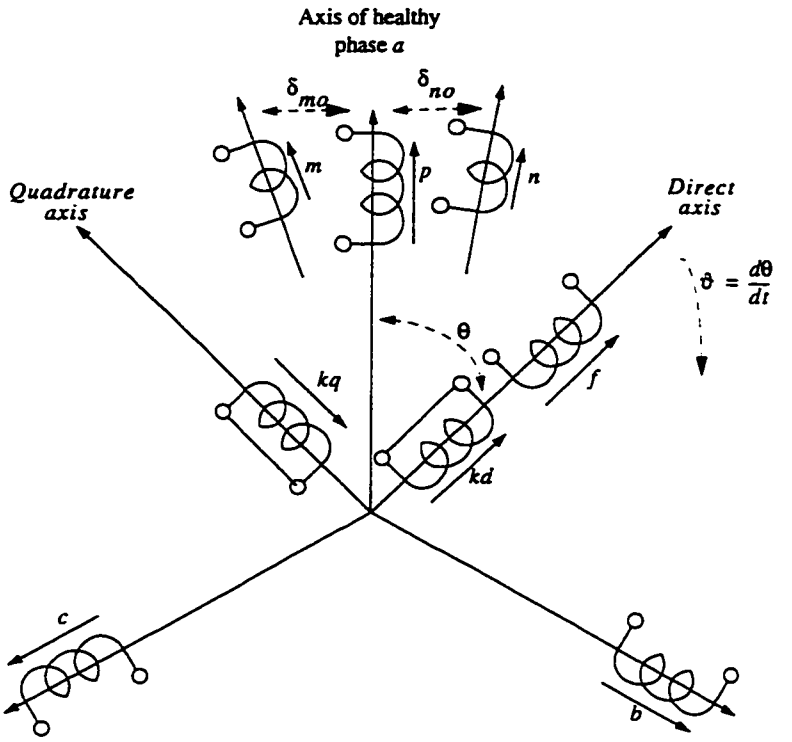

Figure 3.1: Schematic representation of a mutli-path synchronous machine during an internal single phase to ground fault.

$$\mathbf{\Psi_2} = [\psi_p \psi_m \psi_n \psi_b \psi_c \psi_f \psi_{kd} \psi_{kq}]^t \tag{3.3}$$

$$\mathbf{R_2} = diag[R_p R_m R_n R_a R_a \; -R_f \; -R_{kd} \; -R_{kq}] \tag{3.4}$$

$$\mathbf{i_2} = [i_p i_m i_n i_b i_c i_f i_{kd} i_{kq}]^t \tag{3.5}$$

During an internal single phase to ground fault, the machine terminal voltages can be expressed as follows:

$$e_p = -E_{bus}\sin(\omega t) + (i_p + i_n)R_{TL} + (\frac{di_p}{dt} + \frac{di_n}{dt})L_{TL} \tag{3.6}$$

$$e_m = 0 \tag{3.7}$$

$$e_n = e_p \tag{3.8}$$

$$e_b = -E_{bus}\sin(\omega t - \frac{2\pi}{3}) + i_b R_{TL} + \frac{di_b}{dt}L_{TL} \tag{3.9}$$

$$e_c = -E_{bus}\sin(\omega t + \frac{2\pi}{3}) + i_c R_{TL} + \frac{di_c}{dt}L_{TL} \tag{3.10}$$

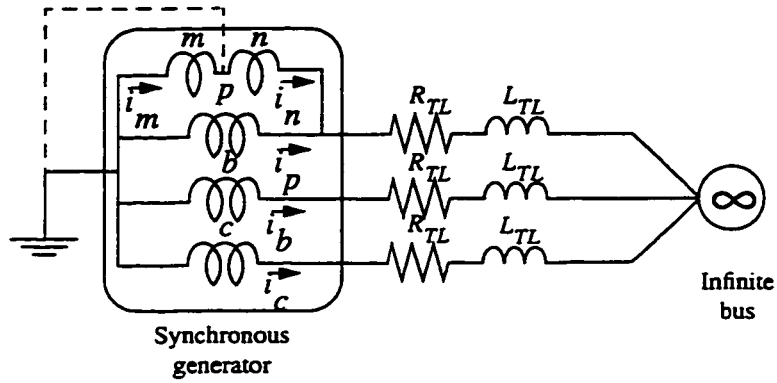

Figure 3.2: System representation for a multi-path machine during an internal single phase to ground fault.

where $\omega t = \theta + \delta$, ω being the synchronous speed and δ is the load angle with reference to the infinite bus, and E_{bus} is the peak value of the infinite bus phase voltage.

Flux Linkage Relationship

The flux linkage relationship during the fault is:

$$\mathbf{\Psi_2} = \mathbf{L_2 i_2} \tag{3.11}$$

where

$$\mathbf{L_2} = \begin{array}{c} \begin{matrix} p & m & n & b & c & f & kd & kq \end{matrix} \\ \begin{bmatrix} L_p & M_{pm} & M_{pn} & M_{pb} & M_{pc} & M_{pf} & M_{pkd} & M_{pkq} \\ M_{mp} & L_m & M_{mn} & M_{mb} & M_{mc} & M_{mf} & M_{mkd} & M_{mkq} \\ M_{np} & M_{nm} & L_n & M_{nb} & M_{nc} & M_{nf} & M_{nkd} & M_{nkq} \\ M_{bp} & M_{bm} & M_{bn} & L_b & M_{bc} & M_{bf} & M_{bkd} & M_{bkq} \\ M_{cp} & M_{cm} & M_{cn} & M_{cb} & L_c & M_{cf} & M_{ckd} & M_{ckq} \\ M_{fp} & M_{fm} & M_{fn} & M_{fb} & M_{fc} & L_f & M_{fkd} & 0 \\ M_{kdp} & M_{kdm} & M_{kdn} & M_{kdb} & M_{kdc} & M_{kdf} & L_{kd} & 0 \\ M_{kqp} & M_{kqm} & M_{kqn} & M_{kqb} & M_{kqc} & 0 & 0 & L_{kq} \end{bmatrix} \end{array} \begin{matrix} p \\ m \\ n \\ b \\ c \\ f \\ kd \\ kq \end{matrix} \tag{3.12}$$

The notations used in (3.12) for the self and mutual inductances are the same as those used for the $\mathbf{L_1}$ matrix in (2.17).

The $\mathbf{L_2}$ inductance matrix can be viewed as having two parts, a healthy part and a faulty part. The healthy part is associated with the self inductances of the healthy windings, i.e. b, c, f, kd and kq, and the mutual inductances between them. In this part the inductances are exactly the same as those of the $\mathbf{L_1}$ matrix in (2.17). The faulty part is associated with the self and mutual inductances of the different parts of the faulty phase a, namely parts p, m and n. The values of the inductances in the faulty part of the $\mathbf{L_2}$ matrix need some modifications from the normal values, and these modifications are described in detail in this section. The formulas of the components of the $\mathbf{L_2}$ matrix in (3.12) are given in Appendix B.2.

The self-inductance of any winding can be viewed as consisting of two parts; a leakage inductance and a main inductance [61]. Based on this assumption, the self-inductance of the m winding is:

$$L_m = -L_{lm} + L_{mam} \tag{3.13}$$

where L_{lm} is the leakage inductance and L_{mam} is the main inductance of the m winding.

The fault current, in a short circuited part of the armature winding, produces a magnetic flux with relatively stronger harmonics than in the case of a whole phase to be short circuited [66]. Consequently, the differential leakage is relatively high for a small part of one parallel path of the armature winding. The differential leakage flux embraces the fundamental flux and all harmonics except the main flux in the air gap, and it can be determined by finding the difference between the total flux in the air gap and the main flux. Detailed analysis of the differential leakage flux and the subsequent

calculation of the leakage inductance of a faulty winding are presented in [66]. In this thesis the analysis presented in [66] is used to calculate L_{lm}.

The differential leakage flux affects the leakage inductance only, thus the ratio between the main inductances is proportional to the ratio between the effective numbers of turns of the corresponding windings, which is [66]:

$$\frac{L_{mam}}{L_{ma}} = \left(\frac{N_m}{N}\right)^2 \tag{3.14}$$

where L_{ma} is the main inductance of healthy phase a, N_m is the effective number of turns of the m winding and N is the effective number of series turns of phase a. Hence, the self-inductance of the m winding is:

$$L_m = -L_{lm} - L_{mam0} - L_{mam1}\cos(2\theta_m) \tag{3.15}$$

where $L_{mam} = -L_{mam0} - L_{mam1}\cos(2\theta_m)$, L_{mam0} being the constant part and L_{mam1} being the variable part of the main inductance of the m winding. The main inductance of the m winding is calculated using (3.14).

The winding of a synchronous machine has coil sides for each phase distributed in several slots per pole [56]. To determine the voltage of an entire phase, the voltages of the component coils must be added as phasors. In the case of the windings p, b and c adding the component coils will result in 3-phase voltages displaced by $\frac{\pi}{3}$ radians from each other. Hence, the axes of these three windings can be displaced by $\frac{\pi}{3}$ radians from each other as shown in Fig. 3.1. However, adding the voltages of the component coils of either the m or n winding will result in a phase shift from the axis of the p winding. As a result the faulted windings, m and n, have rotor displacement angles different from that of the p winding, Fig. 3.1. The displacement angle, θ_m,

corresponding to the m winding is calculated as following:

$$\theta_m = \theta + \delta_{mo} \tag{3.16}$$

where δ_{mo} is the displacement angle of the m winding from the original axis of the a winding due to the fault, Fig. 3.1. In order to calculate the self-inductance of the n winding, the same procedure described above is followed.

Mutual inductance between any two faulty winding parts is proportional to the ratio of their effective number of turns [65, 66], hence:

$$M_{pm} = M_{mp} = \frac{N}{N_m} L_{mam} \tag{3.17}$$

As the internal fault does not affect the main inductance of the faulted phase, the portion of the flux linking a healthy phase, due to a faulted phase, should be the same as before fault occurrence [66].

$$\begin{aligned} i_a M_{ab} &= i_p M_{pb} + i_m M_{mb} + i_n M_{nb} \\ i_a M_{ab} &= \frac{(X-1)i_a}{X} M_{ab} + \frac{i_a}{X}\frac{N_m M_{ab}}{N} + \frac{i_a}{X}\frac{N_n M_{ab}}{N} \end{aligned} \tag{3.18}$$

Based on (3.18) $M_{pb} = M_{bp} = M_{ab} = M_{ba}$, $M_{mb} = M_{bm} = \frac{N_m M_{ab}}{N}$ and $M_{nb} = M_{bn} = \frac{N_n M_{ab}}{N}$.

In keeping with the assumption of (3.18), the flux linking the lumped $X-1$ parallel branches, i.e. p winding, should remain unchanged. This assumption is used to find the self-inductance L_p of the p winding, as follows:

$$\begin{aligned} i_a L_a &= i_p L_p + i_m M_{pm} + i_n M_{pn} \\ i_a L_a &= \frac{(X-1)i_a}{X} L_p + \frac{i_a}{X}\frac{N}{N_m} L_{mam} + \frac{i_a}{X}\frac{N}{N_m} L_{man} \end{aligned} \tag{3.19}$$

where L_a is the self-inductance of healthy phase a and L_{man} is the main

inductance of the n winding. Substituting for L_{mam} and L_{man} in terms of L_{ma} (3.14), and rearranging, yields:

$$L_p = -\frac{X}{X-1}L_{la} + L_{ma}$$
$$L_p = -\frac{L_{la}}{X-1} + L_a \tag{3.20}$$

where $L_a = -L_{la} + L_{ma}$ and L_{la} is the leakage inductance of healthy phase a. The main inductance, $L_{ma} = -L_{ma0} - L_{ma1}\cos(2\theta)$, L_{ma0} being the constant part and L_{ma1} being the variable part of the main inductance of phase a.

It should be noted that, if normal operation is simulated, the above conditions, which are imposed on the inductances of the windings of faulty phase a, (3.14-3.20), would indeed cause the voltage e_p to be equal to e_a. Also, $e_m + e_n$ would be equal to e_a. These are necessary conditions for parallel operation under normal conditions.

Torque

The equation of motion of a synchronous generator can be expressed by [60]:

$$\frac{d^2\delta}{dt^2} = \frac{\omega}{2H}(T_{mec} - T_{elc2}) \tag{3.21}$$

where the formula of the electrical torque in case of a single internal fault, T_{elc2}, is given by:

$$T_{elc2} = \frac{1}{3}(\frac{1}{2}\mathbf{i_{21}}\frac{d\mathbf{L_{21}}}{d\theta}\mathbf{i_{21}}^t + \mathbf{i_{21}}\frac{d\mathbf{L_{22}}}{d\theta}\mathbf{i_{22}}) \tag{3.22}$$

where

$$\mathbf{i_{21}} = [i_p i_m i_n i_b i_c] \tag{3.23}$$
$$\mathbf{i_{22}} = [i_f i_{kd} i_{kq}]^t \tag{3.24}$$

$$\mathbf{L_{21}} = \begin{bmatrix} L_p & M_{pm} & M_{pn} & M_{pb} & M_{pc} \\ M_{mp} & L_m & M_{mn} & M_{mb} & M_{mc} \\ M_{np} & M_{nm} & L_n & M_{nb} & M_{nc} \\ M_{bp} & M_{bm} & M_{bn} & L_b & M_{bc} \\ M_{cp} & M_{cm} & M_{cn} & M_{cb} & L_c \end{bmatrix} \tag{3.25}$$

$$\mathbf{L_{22}} = \begin{bmatrix} M_{pf} & M_{pkd} & M_{pkq} \\ M_{mf} & M_{mkd} & M_{mkq} \\ M_{nf} & M_{nkd} & M_{nkq} \\ M_{bf} & M_{bkd} & M_{bkq} \\ M_{cf} & M_{ckd} & M_{ckq} \end{bmatrix} \tag{3.26}$$

The formula of T_{elc2} given in (3.22) is derived with the same assumptions used to derive T_{elc1} in (2.19), i.e. an electrical torque is produced in a machine when a change in the energy stored in its coupling field occurs [61]. The only difference between T_{elc1} and T_{elc2} is that in calculating T_{elc2} the windings p, m and n have to be accounted for.

General

Equations (3.1,3.6-3.11,3.21) form the complete model for a multi-path synchronous machine during an internal single phase to ground fault in phase a [68]. To simulate an internal single phase to ground fault in phase b or phase c, the same procedure described above is followed, but in that case the faulty phase would be the one composed of three windings and each of the other two phases would be represented by a single winding. In this dissertation internal single phase to ground faults in all three phases are simulated.

The simulation of internal faults involves the solution by a numerical method of the mathematical model developed above, as in the case of normal operation and external faults in Section 2.4. As the simulation procedure

for all three cases is similar, in terms of sequence of steps, the simulation procedure described in Section 2.4.1 is used for simulating all internal faults described in this chapter.

3.2.2 Internal Two Phase to Ground Faults

Figure 3.3 shows a synchronous generator having an internal two phase to ground fault in phases a and b. The faulty path of phase b is divided in two parts, one part is adjacent to the neutral, r winding, and the second part adjacent to the machine terminal, s winding. The remaining, $X-1$. parallel paths of phase b are lumped into one equivalent winding which is the z winding. The relationship expressed in (3.1) will still hold during an internal two phase fault, as shown in (3.27).

$$\mathbf{e_3} = \frac{d\mathbf{\Psi_3}}{dt} - \mathbf{R_3 i_3} \tag{3.27}$$

where

$$\mathbf{e_3} = [e_p e_m e_n e_z e_r e_s e_c e_f e_{kd} e_{kq}]^t \tag{3.28}$$

$$\mathbf{\Psi_3} = [\psi_p \psi_m \psi_n \psi_z \psi_r \psi_s \psi_c \psi_f \psi_{kd} \psi_{kq}]^t \tag{3.29}$$

$$\mathbf{R_3} = diag[R_p R_m R_n R_z R_r R_s R_a - R_f - R_{kd} - R_{kq}] \tag{3.30}$$

$$\mathbf{i_3} = [i_p i_m i_n i_z i_r i_s i_c i_f i_{kd} i_{kq}]^t \tag{3.31}$$

The machine terminal voltages during an internal two phase to ground fault are:

$$e_p = -E_{bus}\sin(\omega t) + (i_p + i_n)R_{TL} + (\frac{di_p}{dt} + \frac{di_n}{dt})L_{TL} \tag{3.32}$$

$$e_m = 0 \tag{3.33}$$

$$e_n = e_p \tag{3.34}$$

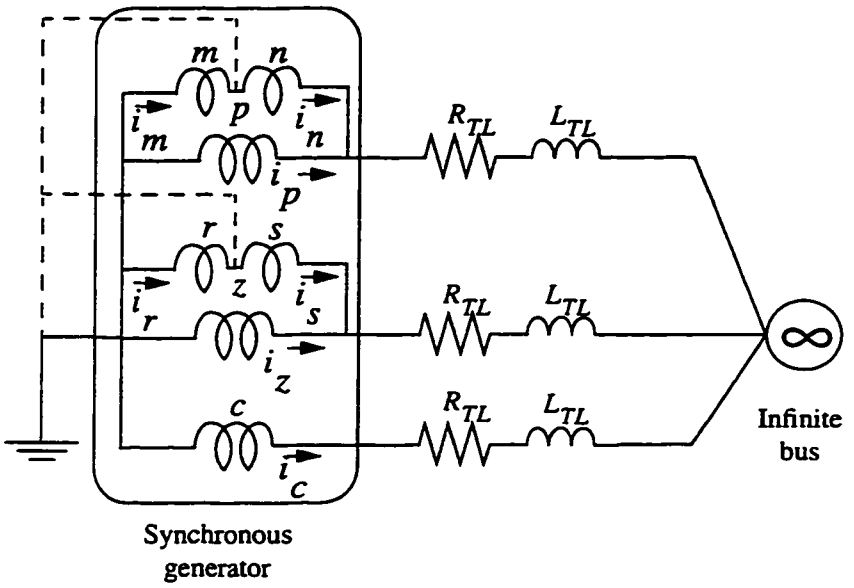

Figure 3.3: System representation for a multi-path machine during an internal two phase to ground fault.

$$e_z = -E_{bus}\sin(\omega t - \frac{2\pi}{3}) + (i_z + i_s)R_{TL} + (\frac{di_z}{dt} + \frac{di_s}{dt})L_{TL} \quad (3.35)$$

$$e_r = 0 \quad (3.36)$$

$$e_s = e_z \quad (3.37)$$

$$e_c = -E_{bus}\sin(\omega t + \frac{2\pi}{3}) + i_c R_{TL} + \frac{di_c}{dt}L_{TL} \quad (3.38)$$

and the flux linkage relationship is:

$$\mathbf{\Psi_3} = \mathbf{L_3 i_3} \quad (3.39)$$

where

$$\mathbf{L_3}=\begin{array}{c} \begin{matrix} p & m & n & z & r & s & c & f & kd & kq \end{matrix} \\ \begin{bmatrix} L_p & M_{pm} & M_{pn} & M_{pz} & M_{pr} & M_{ps} & M_{pc} & M_{pf} & M_{pkd} & M_{pkq} \\ M_{mp} & L_m & M_{mn} & M_{mz} & M_{mr} & M_{ms} & M_{mc} & M_{mf} & M_{mkd} & M_{mkq} \\ M_{np} & M_{nm} & L_n & M_{nz} & M_{nr} & M_{ns} & M_{nc} & M_{nf} & M_{nkd} & M_{nkq} \\ M_{zp} & M_{zm} & M_{zn} & L_z & M_{zr} & M_{zs} & M_{zc} & M_{zf} & M_{zkd} & M_{zkq} \\ M_{rp} & M_{rm} & M_{rn} & M_{rz} & L_r & M_{rs} & M_{rc} & M_{rf} & M_{rkd} & M_{rkq} \\ M_{sp} & M_{sm} & M_{sn} & M_{sz} & M_{sr} & L_s & M_{sc} & M_{sf} & M_{skd} & M_{skq} \\ M_{cp} & M_{cm} & M_{cn} & M_{cz} & M_{cr} & M_{cs} & L_c & M_{cf} & M_{ckd} & M_{ckq} \\ M_{fp} & M_{fm} & M_{fn} & M_{fz} & M_{fr} & M_{fs} & M_{fc} & L_f & M_{fkd} & 0 \\ M_{kdp} & M_{kdm} & M_{kdn} & M_{kdz} & M_{kdr} & M_{kds} & M_{kdc} & M_{kdf} & L_{kd} & 0 \\ M_{kqp} & M_{kqm} & M_{kqn} & M_{kqz} & M_{kqr} & M_{kqs} & M_{kqc} & 0 & 0 & L_{kq} \end{bmatrix} \end{array} \begin{matrix} p \\ m \\ n \\ z \\ r \\ s \\ c \\ f \\ kd \\ kq \end{matrix} \tag{3.40}$$

The formulas of the components of the $\mathbf{L_3}$ inductance matrix in (3.40) are given in Appendix B.3.

Equations (3.21,3.27,3.32-3.39) form the complete model for a synchronous machine during an internal two phase to ground fault [69]. The electrical torque during an internal two phase to ground fault, T_{elc3}, is calculated in a similar manner as T_{elc2} in (3.22), but in this case in addition to windings p, m and n, windings z, r and s have to be accounted for.

3.3 Internal Faults in Single-Path Synchronous Generators

In Section 3.2 an algorithm for simulating internal faults in multi-path synchronous generators is developed. However, a number of synchronous generators have only a single-path per phase. So, in this section the previously described internal faults algorithm is modified to enable the simulation of

internal faults in single-path machines. It should be noted that the single-path machine can be regarded as a special case of the multi-path machine with the lumped $X-1$ parallel paths being omitted, i.e. the p winding in the single phase case and the p and z windings in the two phase case. In order to show the similarity between the multi-path and single-path cases, the steps for simulating internal faults to ground in phase a and in phases a and b are repeated below for the single-path machine.

3.3.1 Internal Single Phase to Ground Faults

A schematic representation of a synchronous machine with two damper coils during an internal single phase to ground fault in phase a is shown in Fig. 3.4. It is assumed that the armature winding of the synchronous machine consisting of a single path per phase is tapped at a certain point of phase a. The tapped phase is divided in two parts, one part is adjacent to the neutral, which is referred to as the an winding, and the second part adjacent to the machine terminal, which is referred to as the aTL winding. The algorithm for simulating internal single phase to ground faults in a single-path per phase synchronous generator connected to an infinite bus, Fig. 3.5, is given below.

Voltage Relationships

The flux linkages, $\mathbf{\Psi_4}$, during an internal fault in a single-path machine are related to the machine voltages, $\mathbf{e_4}$, winding resistances, $\mathbf{R_4}$, and instantaneous currents, $\mathbf{i_4}$, as follows:

$$\mathbf{e_4} = \frac{d\mathbf{\Psi_4}}{dt} - \mathbf{R_4 i_4} \tag{3.41}$$

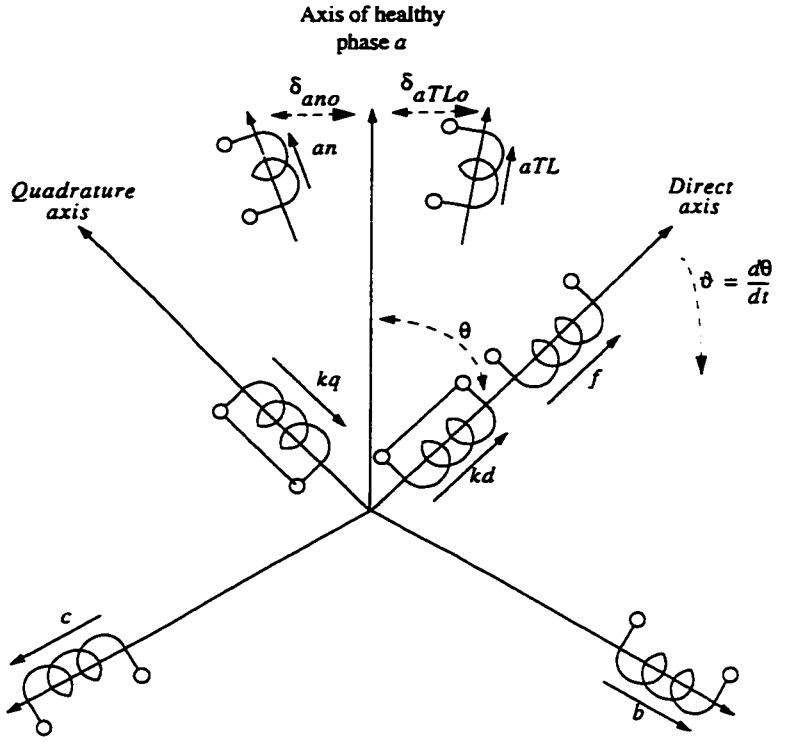

Figure 3.4: Schematic representation of a single-path synchronous machine during an internal single phase to ground fault.

where

$$\mathbf{e}_4 = [e_{an} e_{aTL} e_b e_c e_f e_{kd} e_{kq}]^t \tag{3.42}$$

$$\mathbf{\Psi}_4 = [\psi_{an} \psi_{aTL} \psi_b \psi_c \psi_f \psi_{kd} \psi_{kq}]^t \tag{3.43}$$

$$\mathbf{R}_4 = diag[R_{an} R_{aTL} R_a R_a - R_f - R_{kd} - R_{kq}] \tag{3.44}$$

$$\mathbf{i}_4 = [i_{an} i_{aTL} i_b i_c i_f i_{kd} i_{kq}]^t \tag{3.45}$$

During an internal single phase to ground fault, the machine terminal voltages can be expressed as follows:

$$e_{an} = 0 \tag{3.46}$$

$$e_{aTL} = -E_{bus} \sin(\omega t) + i_{aTL} R_{TL} + \frac{di_{aTL}}{dt} L_{TL} \tag{3.47}$$

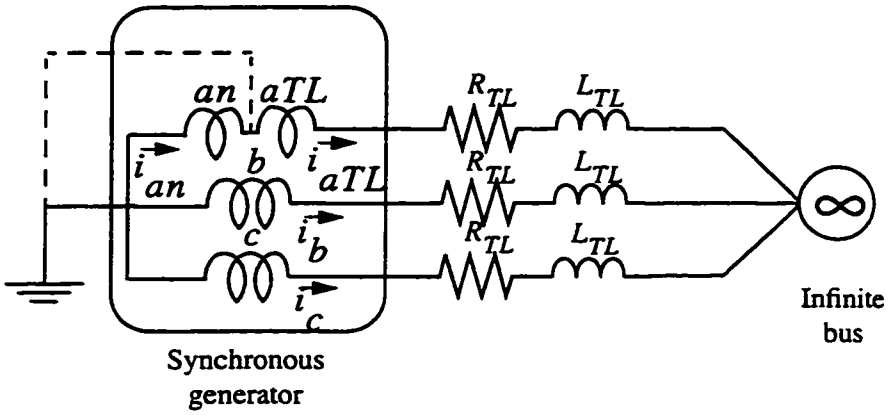

Figure 3.5: System representation for a single-path machine during an internal single phase to ground fault.

$$e_b = -E_{bus}\sin(\omega t - \frac{2\pi}{3}) + i_b R_{TL} + \frac{di_b}{dt}L_{TL} \tag{3.48}$$

$$e_c = -E_{bus}\sin(\omega t + \frac{2\pi}{3}) + i_c R_{TL} + \frac{di_c}{dt}L_{TL} \tag{3.49}$$

Flux Linkage Relationship

The flux linkage relationship during the fault is:

$$\mathbf{\Psi_4} = \mathbf{L_4 i_4} \tag{3.50}$$

where

$$\mathbf{L_4} = \begin{array}{c} \begin{array}{ccccccc} an & aTL & b & c & f & kd & kq \end{array} \\ \left[\begin{array}{ccccccc} L_{an} & M_{anaTL} & M_{anb} & M_{anc} & M_{anf} & M_{ankd} & M_{ankq} \\ M_{aTLan} & L_{aTL} & M_{aTLb} & M_{aTLc} & M_{aTLf} & M_{aTLkd} & M_{aTLkq} \\ M_{ban} & M_{baTL} & L_b & M_{bc} & M_{bf} & M_{bkd} & M_{bkq} \\ M_{can} & M_{caTL} & M_{cb} & L_c & M_{cf} & M_{ckd} & M_{ckq} \\ M_{fan} & M_{faTL} & M_{fb} & M_{fc} & L_f & M_{fkd} & 0 \\ M_{kdan} & M_{kdaTL} & M_{kdb} & M_{kdc} & M_{kdf} & L_{kd} & 0 \\ M_{kqan} & M_{kqaTL} & M_{kqb} & M_{kqc} & 0 & 0 & L_{kq} \end{array}\right] \begin{array}{c} an \\ aTL \\ b \\ c \\ f \\ kd \\ kq \end{array} \end{array} \tag{3.51}$$

The procedure for calculating the self and mutual inductances of the faulty windings, an and aTL, is identical to that for the m and n windings in Section 3.2.1. In fact the $\mathbf{L_4}$ inductance matrix is exactly similar to the $\mathbf{L_2}$ matrix in (3.12) except for omitting the row and column of the p winding.

General

The equation of motion of a synchronous generator can be expressed by [60]:

$$\frac{d^2\delta}{dt^2} = \frac{\omega}{2H}(T_{mec} - T_{elc4}) \tag{3.52}$$

where T_{elc4} in case of a single-path machine is given by:

$$T_{elc4} = \frac{1}{3}(\frac{1}{2}\mathbf{i_{41}}\frac{d\mathbf{L_{41}}}{d\theta}\mathbf{i_{41}}^t + \mathbf{i_{41}}\frac{d\mathbf{L_{42}}}{d\theta}\mathbf{i_{42}}) \tag{3.53}$$

where

$$\mathbf{i_{41}} = [i_{an} i_{aTL} i_b i_c] \tag{3.54}$$

$$\mathbf{i_{42}} = [i_f i_{kd} i_{kq}]^t \tag{3.55}$$

$$\mathbf{L_{41}} = \begin{bmatrix} L_{an} & M_{anaTL} & M_{anb} & M_{anc} \\ M_{aTLan} & L_{aTL} & M_{aTLb} & M_{aTLc} \\ M_{ban} & M_{baTL} & L_b & M_{bc} \\ M_{can} & M_{caTL} & M_{cb} & L_c \end{bmatrix} \tag{3.56}$$

$$\mathbf{L_{42}} = \begin{bmatrix} M_{anf} & M_{ankd} & M_{ankq} \\ M_{aTLf} & M_{aTLkd} & M_{aTLkq} \\ M_{bf} & M_{bkd} & M_{bkq} \\ M_{cf} & M_{ckd} & M_{ckq} \end{bmatrix} \tag{3.57}$$

Equations (3.41,3.46-3.50,3.52) form the complete model for a single-path

synchronous machine during an internal single phase to ground fault [70].

3.3.2 Internal Two Phase to Ground Faults

Figure 3.6 shows a single path per phase synchronous generator having an internal two phase to ground fault in phases a and b. The faulty path of phase b is divided in two parts, one part is adjacent to the neutral, bn winding, and the second part adjacent to the machine terminal, bTL winding. The relationship expressed in (3.41) will still hold during an internal two phase fault, as shown in (3.58).

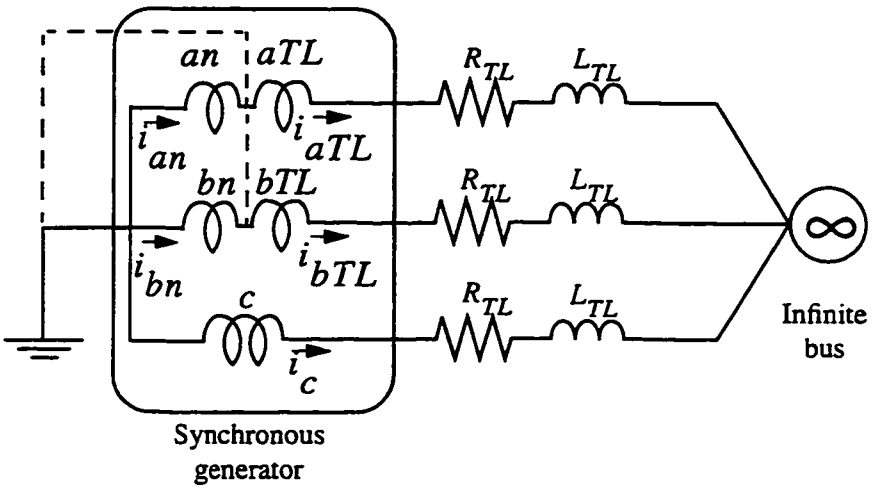

Figure 3.6: System representation for a single-path machine during an internal two phase to ground fault.

$$\mathbf{e_5} = \frac{d\mathbf{\Psi_5}}{dt} - \mathbf{R_5 i_5} \tag{3.58}$$

where

$$\mathbf{e_5} = [e_{an} e_{aTL} e_{bn} e_{bTL} e_c e_f e_{kd} e_{kq}]^t \tag{3.59}$$

$$\mathbf{\Psi_5} = [\psi_{an} \psi_{aTL} \psi_{bn} \psi_{bTL} \psi_c \psi_f \psi_{kd} \psi_{kq}]^t \tag{3.60}$$

$$\mathbf{R_5} = diag[R_{an} R_{aTL} R_{bn} R_{bTL} R_a - R_f - R_{kd} - R_{kq}] \tag{3.61}$$

$$\mathbf{i_5} = [i_{an} i_{aTL} i_{bn} i_{bTL} i_c i_f i_{kd} i_{kq}]^t \tag{3.62}$$

The machine terminal voltages during an internal two phase to ground fault are:

$$e_{an} = 0 \tag{3.63}$$

$$e_{aTL} = E_{bus}\sin(\omega t) + i_{aTL}R_{TL} + \frac{di_{aTL}}{dt}L_{TL} \tag{3.64}$$

$$e_{bn} = 0 \tag{3.65}$$

$$e_{bTL} = E_{bus}\sin(\omega t - \frac{2\pi}{3}) + i_{bTL}R_{TL} + \frac{di_{bTL}}{dt}L_{TL} \tag{3.66}$$

$$e_c = E_{bus}\sin(\omega t + \frac{2\pi}{3}) + i_c R_{TL} + \frac{di_c}{dt}L_{TL} \tag{3.67}$$

and the flux linkage relationship is:

$$\mathbf{\Psi_5} = \mathbf{L_5 i_5} \tag{3.68}$$

where

$$\mathbf{L_5} = \begin{array}{c} \begin{array}{cccccccc} an & aTL & bn & bTL & c & f & kd & kq \end{array} \\ \begin{bmatrix} L_{an} & M_{anaTL} & M_{anbn} & M_{anbTL} & M_{anc} & M_{anf} & M_{ankd} & M_{ankq} \\ M_{aTLan} & L_{aTL} & M_{aTLbn} & M_{aTLbTL} & M_{aTLc} & M_{aTLf} & M_{aTLkd} & M_{aTLkq} \\ M_{bnan} & M_{bnaTL} & L_{bn} & M_{bnbTL} & M_{bnc} & M_{bnf} & M_{bnkd} & M_{bnkq} \\ M_{bTLan} & M_{bTLaTL} & M_{bTLbn} & L_{bTL} & M_{bTLc} & M_{bTLf} & M_{bTLkd} & M_{bTLkq} \\ M_{can} & M_{caTL} & M_{cbn} & M_{cbTL} & L_c & M_{cf} & M_{ckd} & M_{ckq} \\ M_{fan} & M_{faTL} & M_{fbn} & M_{fbTL} & M_{fc} & L_f & M_{fkd} & 0 \\ M_{kdan} & M_{kdaTL} & M_{kdbn} & M_{kdbTL} & M_{kdc} & M_{kdf} & L_{kd} & 0 \\ M_{kqan} & M_{kqaTL} & M_{kqbn} & M_{kqbTL} & M_{kqc} & 0 & 0 & L_{kq} \end{bmatrix} \end{array} \begin{array}{c} an \\ aTL \\ bn \\ bTL \\ c \\ f \\ kd \\ kq \end{array} \tag{3.69}$$

The $\mathbf{L_5}$ matrix is obtained from the $\mathbf{L_3}$ in (3.40) matrix by omitting the rows and columns corresponding to the p and z windings.

Equations (3.52,3.58,3.63-3.68) form the complete model for a single-path synchronous machine during an internal two phase to ground fault [70].

3.4 Generator Grounding

The method of generator grounding used in a generator installation determines the generator's performance during ground fault conditions [1–3]. If the generator is solidly grounded, as is practically never the case, it will deliver a very high magnitude current to a single line to ground fault at its terminals, accompanied by a 58% reduction in the phase to phase voltages involving the faulted phase. If the generator is ungrounded, as is also practically never the case, it will deliver a negligible amount of current to a bolted single line to ground fault at its terminals, accompanied by no reduction in the phase to phase voltages. These represent the extremes in generator grounding with normal practice falling predictably in between.

The high magnitude of fault current which results from solidly grounding a generator is unacceptable because of the damage it can cause during the fault. Isolating the generator by tripping the generator breaker does not cause the fault current to immediately go to zero. The flux trapped in the field will result in the fault current slowly decaying over a number of seconds after the generator is tripped which substantially exacerbates damage. On the other hand, operating a generator ungrounded provides negligible fault current, but the line to ground voltages on the unfaulted phases can rise during arcing type faults to dangerously high levels which could cause insulation failure. As a result, stator windings on major generators are grounded in a manner that will reduce fault current and overvoltages, and yet provide a means of

detecting the ground fault condition quickly enough to prevent iron burning.

3.4.1 Inclusion of a Ground Resistance in the Direct 3-Phase Model

In applying fault conditions for either external faults, Section 2.4.2, or internal faults, Sections 3.2 and 3.3, the generator is assumed to be solidly grounded. The reason, the analysis is done for a solidly grounded generator, is to facilitate the study and development of both algorithms. As these algorithms are used to generate the training data necessary for training the neural networks, as shown in Chapter 5, more realistic data should be obtained. In other words, the generators used in these algorithms have to be grounded through ground resistances that would limit the fault current. Hence, the simulated fault currents would be closer to actual fault currents.

Including a ground resistance in the direct 3-phase model is a very simple task. In the case of normal operation, adding a ground resistance to the neutral of the generator has no effect on the algorithm as the neutral current under balanced operation is zero. In the case of external or internal faults, the effect of the ground resistance would only be on the machine terminal voltage equations, while, the rest of the external or internal faults algorithm is unchanged.

Figure 3.7 shows the multi-path generator of Fig. 3.2 with both the generator and the infinite bus neutrals grounded through resistances R_{g1} and R_{g2}, respectively. In Section 3.2.1 the internal faults algorithm is described for the case shown in Fig. 3.2. To show how to account for the ground resistances in the algorithm, the expressions for the machine terminal voltages are rewritten below:

$$e_p = -E_{bus}\sin(\omega t) + (i_p + i_n)R_{TL} + (\frac{di_p}{dt} + \frac{di_n}{dt})L_{TL}$$

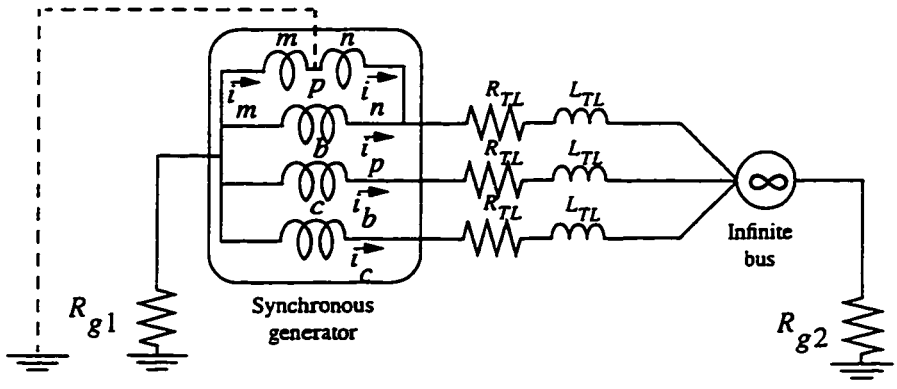

Figure 3.7: System representation during an internal single phase to ground fault in one path of phase a with the ground resistances included.

$$+(i_p + i_m + i_b + i_c)R_{g1} + (i_p + i_n + i_b + i_c)R_{g2} \tag{3.70}$$

$$e_m = (i_p + i_m + i_b + i_c)R_{g1} \tag{3.71}$$

$$e_n = e_p - e_m \tag{3.72}$$

$$\begin{aligned} e_b = & -E_{bus}\sin(\omega t - \frac{2\pi}{3}) + i_b R_{TL} + \frac{di_b}{dt}L_{TL} \\ & +(i_p + i_m + i_b + i_c)R_{g1} + (i_p + i_n + i_b + i_c)R_{g2} \end{aligned} \tag{3.73}$$

$$\begin{aligned} e_c = & -E_{bus}\sin(\omega t + \frac{2\pi}{3}) + i_c R_{TL} + \frac{di_c}{dt}L_{TL} \\ & +(i_p + i_m + i_b + i_c)R_{g1} + (i_p + i_n + i_b + i_c)R_{g2} \end{aligned} \tag{3.74}$$

As indicated above, accounting for R_{g1} and R_{g2} only affects the machine terminal voltages, while, the rest of the algorithm, (3.1-3.5, 3.11-3.26), is unchanged. The previous statment is true for all kinds of external and internal faults presented in this dissertation.

3.5 Summary

In this chapter methods for simulating internal single phase to ground faults and internal two phase to ground faults in multi-path and single-path generators are developed. The internal faults algorithm is based on a direct

3-phase model of the synchronous generator.

In the case of the multi-path machine, the internal faults algorithm regards the faulty phase as composed of three individual windings. The self and mutual inductances of these individual windings are calculated with the aid of special forms. The described model has the advantage of simulating internal faults, while retaining the generator nonlinear model. The ability of the developed algorithm to retain the generator nonlinear model and to take into account the variation of speed under transient conditions enhances its accuracy. The single-path machine can be regarded as a special case of the multi-path machine.

Grounding the generator through a resistance has the beneficial effect of reducing the fault current and the subsequent fault damage. It is shown that including the ground resistance in the direct 3-phase model only affects the machine terminal voltage equations during a fault.

Chapter 4

Generator Simulation Results

4.1 Introduction

The main objective of this thesis is to train different neural network modules to detect and classify faults in the stator windings of generators. Choosing the appropriate inputs to a neural network not only reduces the training time but also increases the classification accuracy of the output. In order to choose the appropriate inputs, generator simulation studies should be done first.

It is the aim of this chapter to present simulation results showing the generator currents during normal operation state, external fault state and internal fault state. Illustrative simulation results showing the normal operation state and external fault state are presented in Sections 4.2 and 4.3, respectively. Simulation results showing internal fault currents are then presented and discussed in Section 4.4. The effect of ground resistance is shown by comparing internal fault currents with and without a ground resistance. The effect of internal fault location is shown by presenting internal faults at different winding percentages.

4.2 Simulation of Normal Operation State

The direct 3-phase model [60], Section 2.4.1, is used to simulate the generator performance during normal operation state. In this thesis all simulation studies are done for a generator connected to an infinite bus through a short TL, as shown in Fig. 2.5, using the per-unit (pu) values of the respective components. The simulation model was written using the *Matlab* software as this facilitated the programming and debugging procedures. Six synchronous generators, G_1, G_2, G_3, G_4, G_5 and G_6, are used throughout the simulation studies presented in this thesis. The parameters of these six generators, short TL, infinite bus and ground resistances, R_{g1} and R_{g2}, are given in Appendix C.

Figure 4.1 shows the stator currents, i_a, i_b and i_c, and the field current, i_f, when the generator G_4 is delivering a power (P) of 0.9 pu at a power factor (pf) of 0.9 lag. During normal operation, the damper winding currents, i_{kd} and i_{kq}, are zero, hence they are not shown. It should also be noted that the field current, i_f, is a constant *dc* value when the generator is operating under balanced three phase conditions.

4.3 Simulation of External Fault State

The modified direct 3-phase model [60], Section 2.4.2, is used to simulate external faults at the machine terminals and along the TL connected to the machine. As mentioned in Section 3.4, ground resistances, R_{g1} and R_{g2} Fig. 3.7, are used throughout the simulations to limit the fault current during ground faults, in particular during single phase to ground faults.

Figures 4.2 and 4.3 show a two phase to ground fault at the middle of the TL. The generator used in this simulation is G_3 and the fault is in phases *a* and *b*. The power before fault inception was 0.75 pu at a power factor of 0.8 lag. It is noticed that during the fault the field current, i_f, contains first

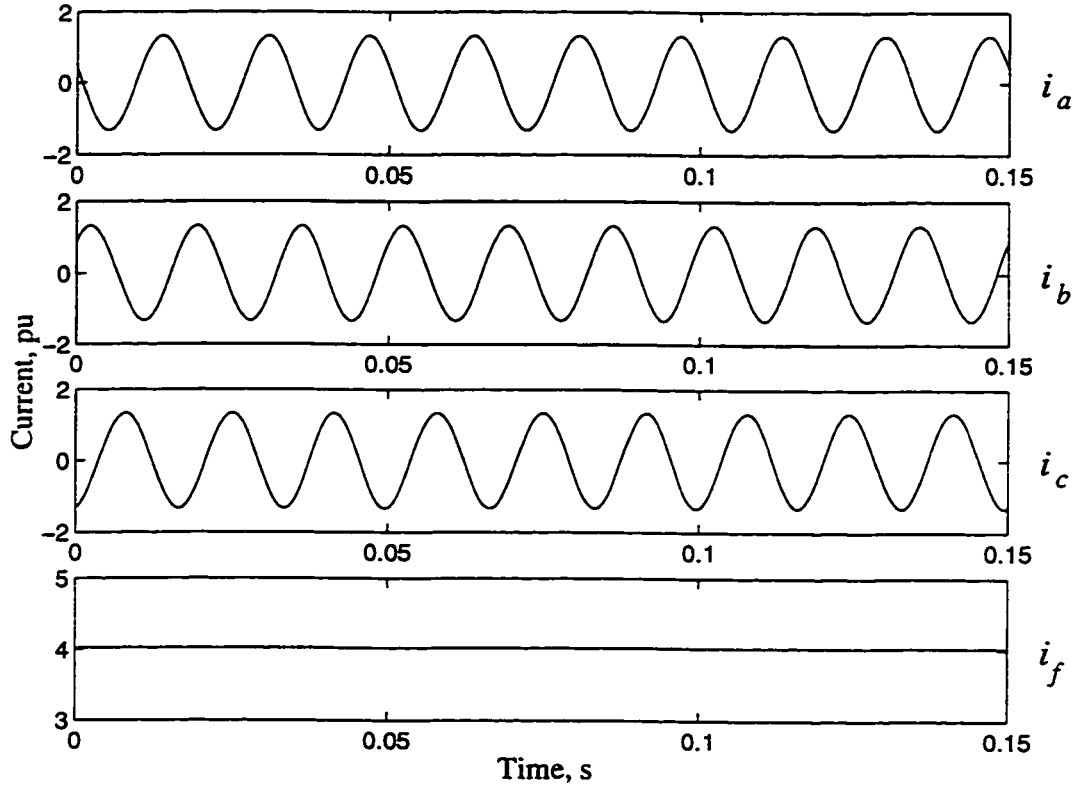

Figure 4.1: Computed currents for generator G_4 during normal operation state, P=0.9 pu and pf=0.9 lag.

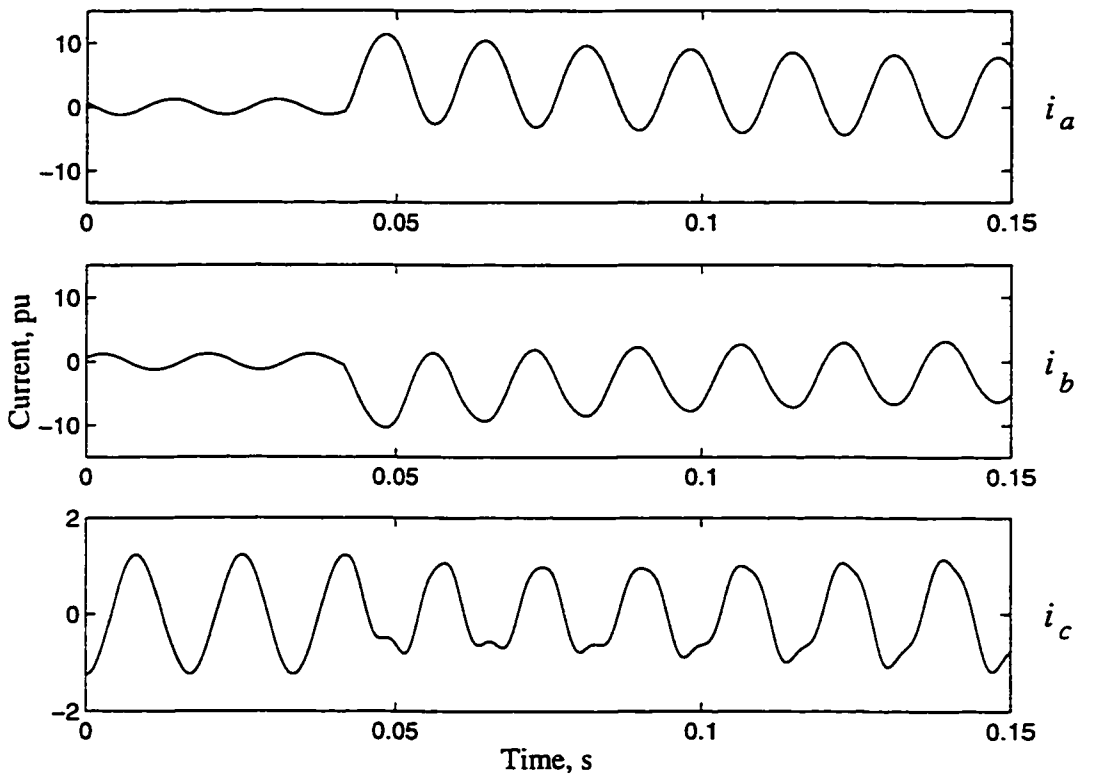

Figure 4.2: Computed stator currents for a two phase to ground fault, phases a and b of G_3, at the middle of the TL, P=0.75 pu, pf=0.8 lag, R_{g1}=1.5 pu and R_{g2}=0.8 pu.

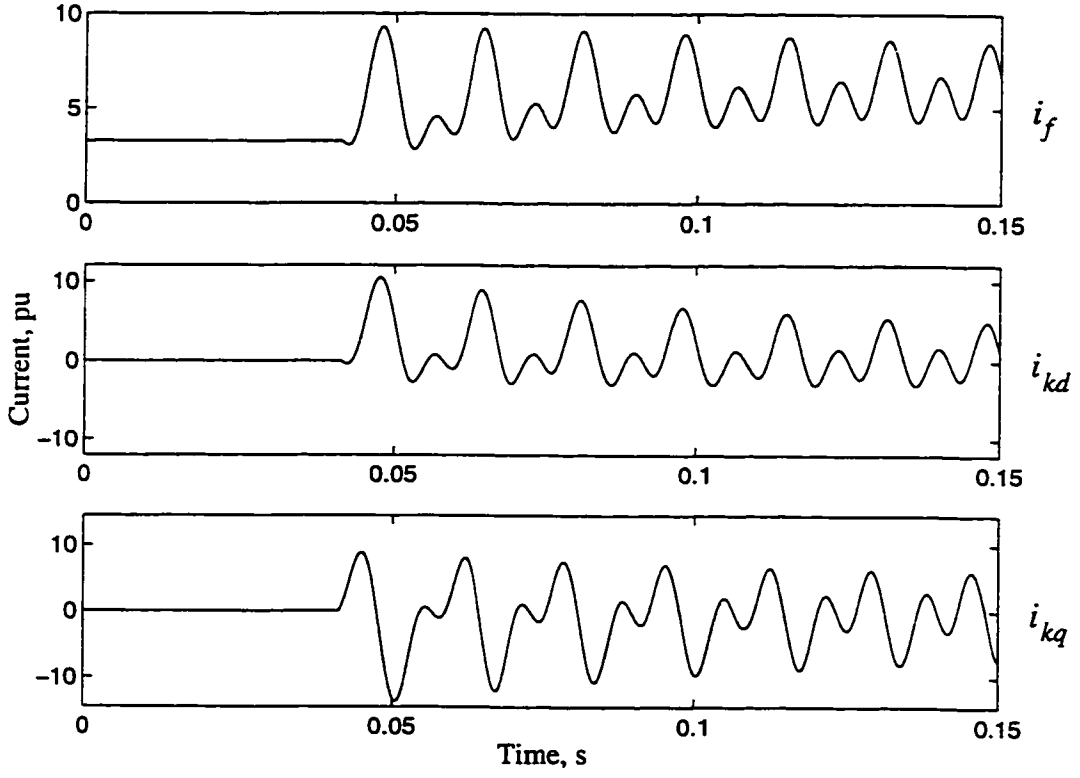

Figure 4.3: Computed rotor currents for a two phase to ground fault, phases a and b of G_3, at the middle of the TL, P=0.75 pu, pf=0.8 lag, R_{g1}=1.5 pu and R_{g2}=0.8 pu.

and second harmonic components, Fig. 4.3.

4.4 Simulation of Internal Fault State

The internal faults algorithm [68–70], Chapter 3, is used to simulate internal single phase to ground faults and internal two phase to ground faults in multi-path and single-path generators. In this section the effects of ground resistance and internal fault location are shown through comparison studies.

4.4.1 Effect of Ground Resistance

The effect of ground resistance on an internal single phase to ground fault is illustrated in Figs. 4.4 through 4.7. The notations of the currents are the same as in Chapter 3, and all winding percentages are measured from the neutral-end of the generator. The effectiveness of R_{g1} and R_{g2}, Fig. 3.7, in limiting the stator currents during the fault can be noticed by comparing Fig. 4.4, which represents a solidly grounded fault, and Fig. 4.5, which represents a fault with ground resistances included. The ground resistances managed to limit the fault currents to around 150% of the rated current, which is the common practice in generator installations [1–3]. This grounding setup not only reduces fault currents, but also provides a means of detecting the ground fault condition quickly enough to prevent iron burning. Henceforth, the values of R_{g1} and R_{g2} are fixed at 1.5 pu and 0.8 pu, respectively.

Figures 4.8,4.9 and 4.10 show an internal two phase to ground fault at 50% of one path of phases b and c of generator G_4. The currents i_{c1}, i_{c2} and i_{c3} represent the currents in the lumped $X-1$ parallel paths, the faulty winding adjacent to the neutral and the faulty winding adjacent to the machine terminal, respectively. It is clear that R_{g1} and R_{g2} are not very effective in limiting the fault currents during internal two phase to ground faults. The simulation studies done in this thesis indicate that R_{g1} and R_{g2} are effective only during single phase to ground faults.

It is shown in Figs. 4.7 and 4.10 that the field current, i_f, contains first and second harmonic components as in the external fault state, Fig. 4.3. However, by comparing Figs. 4.3 and 4.10, it can be seen that the amplitudes of the first and second harmonic components are different for external and internal faults.

4.4.2 Effect of Internal Fault Location

The effect of internal fault location is illustrated by simulating two internal single phase to ground faults at different winding percentages of the same phase as shown in Figs. 4.11 through 4.14. A single-path generator, G_1, is used in this study and the internal faults are at 77% and 10% of phase b. It can be seen from Figs. 4.11 and 4.12 that while the changes in i_{bn} and i_{bTL} are evident for a fault at 77% of the winding, the corresponding changes for a fault at 10% of the winding are hardly noticeable. The same remark can be made about the rotor currents, Figs. 4.13 and 4.14. These remarks lead to the conclusion that faults which involve a higher percentage of the winding provide sufficient changes in the currents, that allow their quick detection by differential protection.

4.5 Summary

In this chapter simulation results showing generator currents during three different states, i.e. normal operation state, external fault state and internal fault state, are presented. Simulation studies indicate that the field current is distinctive for each state. This implies that using the field current as an input to the neural network, in addition to the stator currents, may help in distinguishing between these three states. The simulation results also show that the ground resistance is very effective in limiting the fault currents during single phase faults. Finally, it is shown that the location of the internal fault has an effect on the fault current patterns.

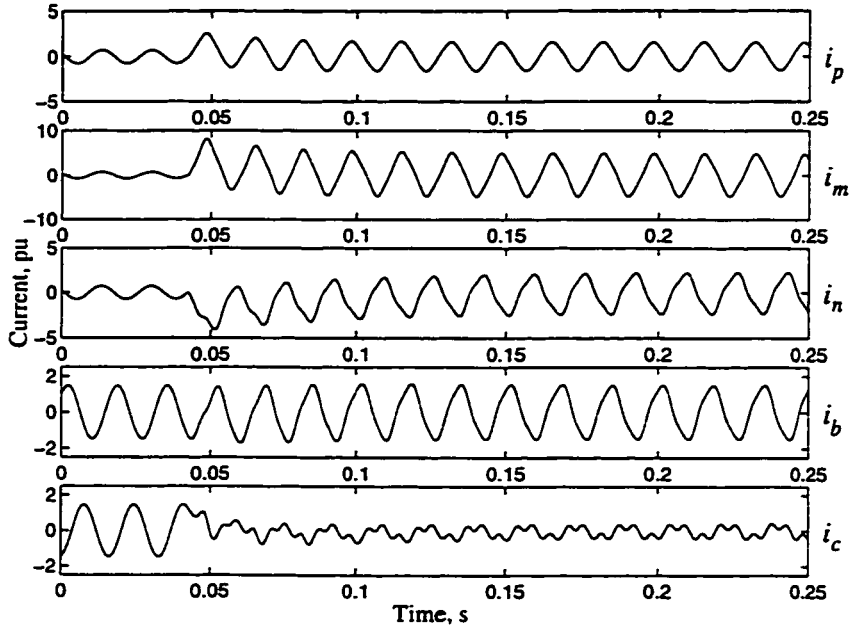

Figure 4.4: Computed stator currents for an internal single phase to ground fault at 62% of one path of phase a of generator G_2, P=1 pu, pf=0.9 lag, R_{g1}=0 and R_{g2}=0.

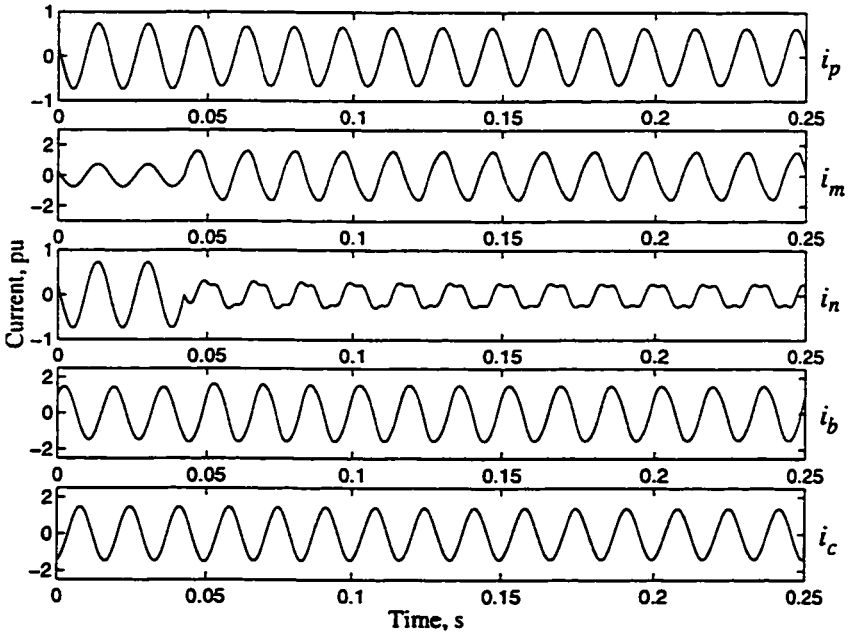

Figure 4.5: Computed stator currents for an internal single phase to ground fault at 62% of one path of phase a of generator G_2, P=1 pu, pf=0.9 lag, R_{g1}=1.5 pu and R_{g2}=0.8 pu.

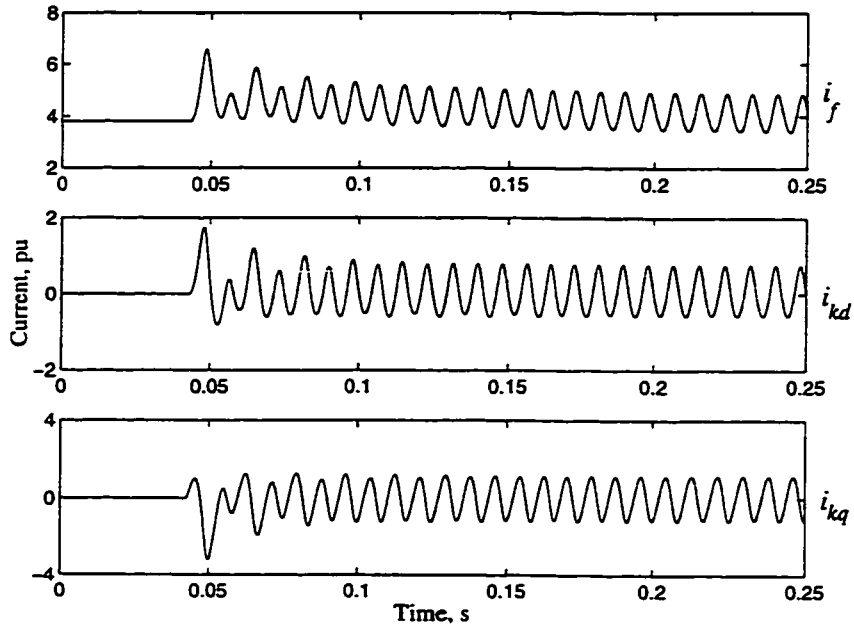

Figure 4.6: Computed rotor currents for an internal single phase to ground fault at 62% of one path of phase a of generator G_2, P=1 pu, pf=0.9 lag, R_{g1}=0 and R_{g2}=0.

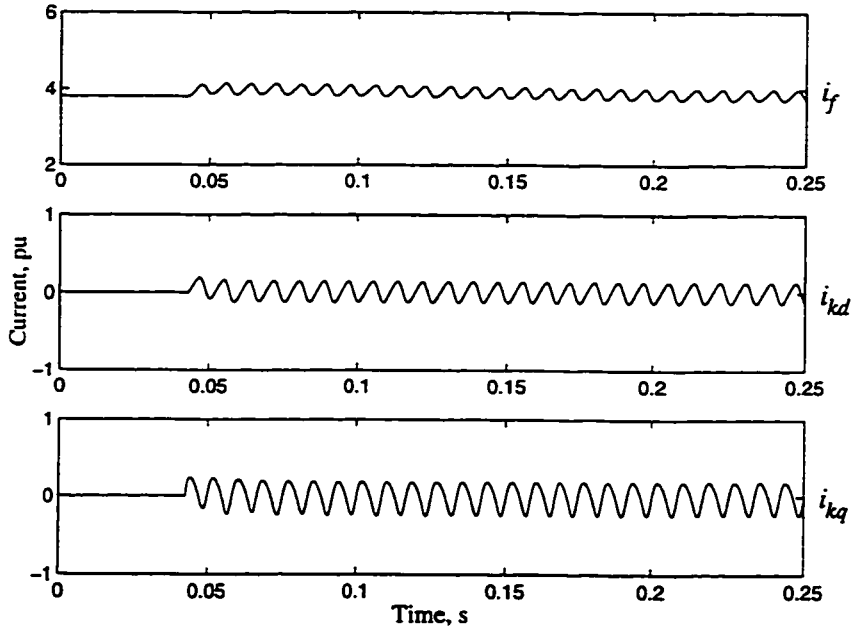

Figure 4.7: Computed rotor currents for an internal single phase to ground fault at 62% of one path of phase a of generator G_2, P=1 pu, pf=0.9 lag, R_{g1}=1.5 pu and R_{g2}=0.8 pu.

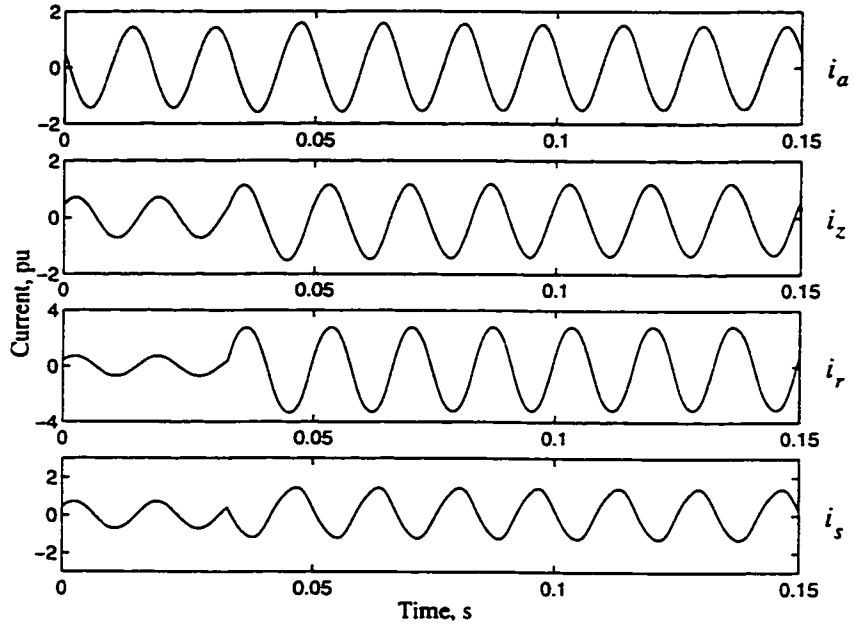

Figure 4.8: Fault currents for windings a, z, r, s for an internal two phase to ground fault at 50% of one path of phases b and c of generator G_4, P=0.95 pu, pf=0.87 lag, R_{g1}=1.5 pu and R_{g2}=0.8 pu.

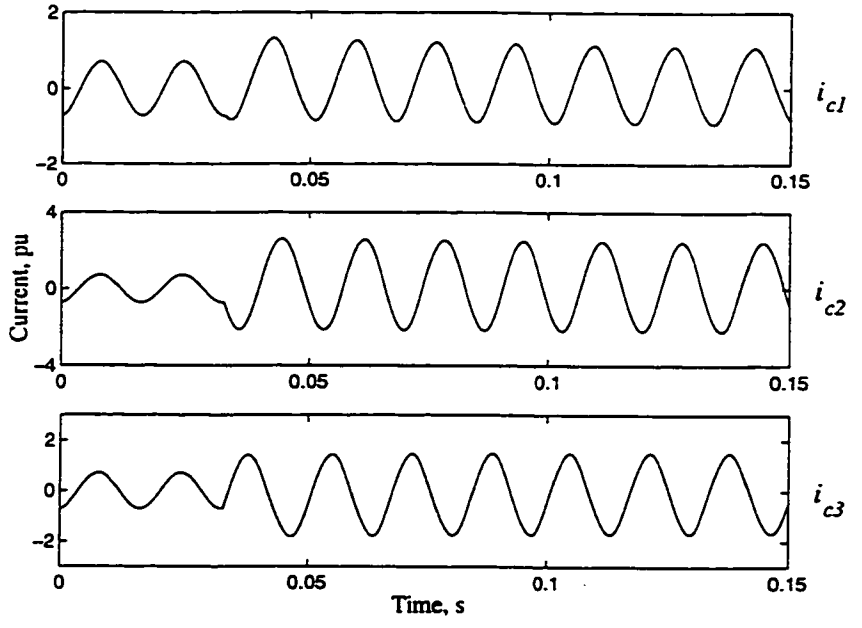

Figure 4.9: Fault currents for windings $c1, c2, c3$ for an internal two phase to ground fault at 50% of one path of phases b and c of generator G_4, P=0.95 pu, pf=0.87 lag, R_{g1}=1.5 pu and R_{g2}=0.8 pu.

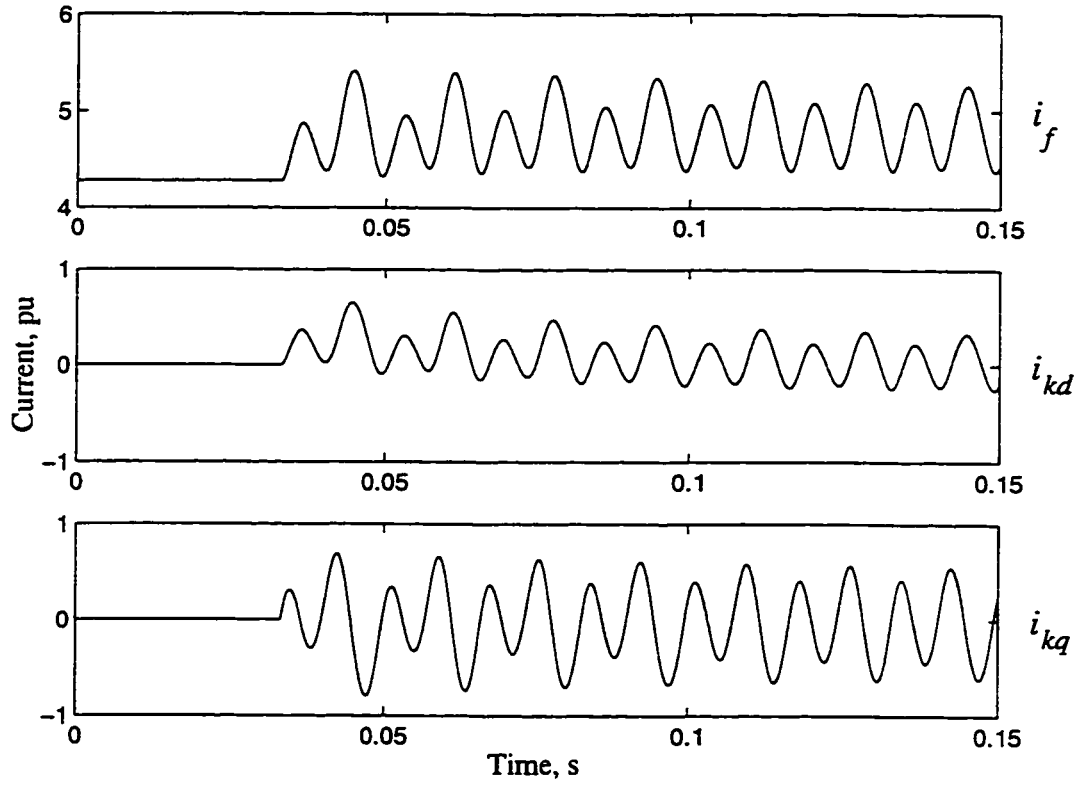

Figure 4.10: Computed rotor currents for an internal two phase to ground fault at 50% of one path of phases b and c of generator G_4, P=0.95 pu, pf=0.87 lag, R_{g1}=1.5 pu and R_{g2}=0.8 pu.

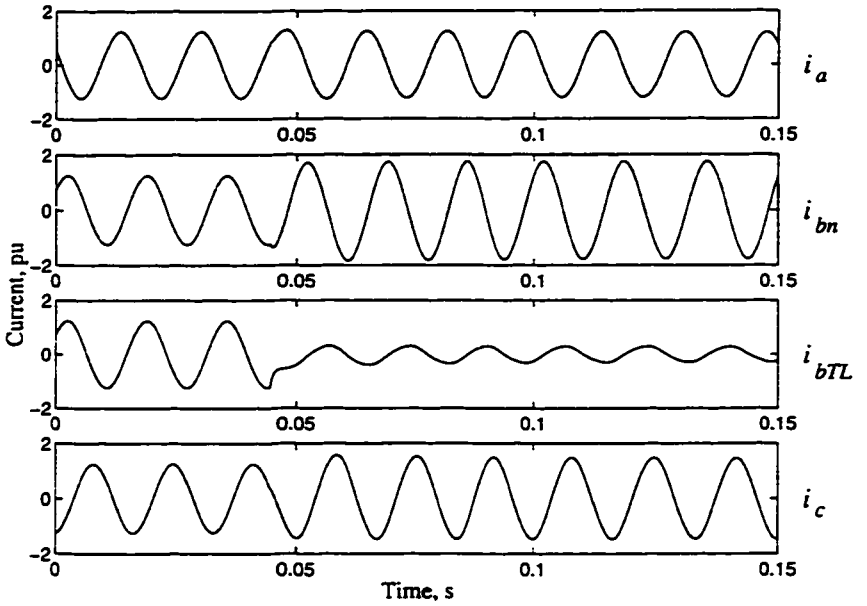

Figure 4.11: Computed stator currents for an internal single phase to ground fault at 77% of phase b of generator G_1, P=0.8 pu, pf=0.85 lag, R_{g1}=1.5 pu and R_{g2}=0.8 pu.

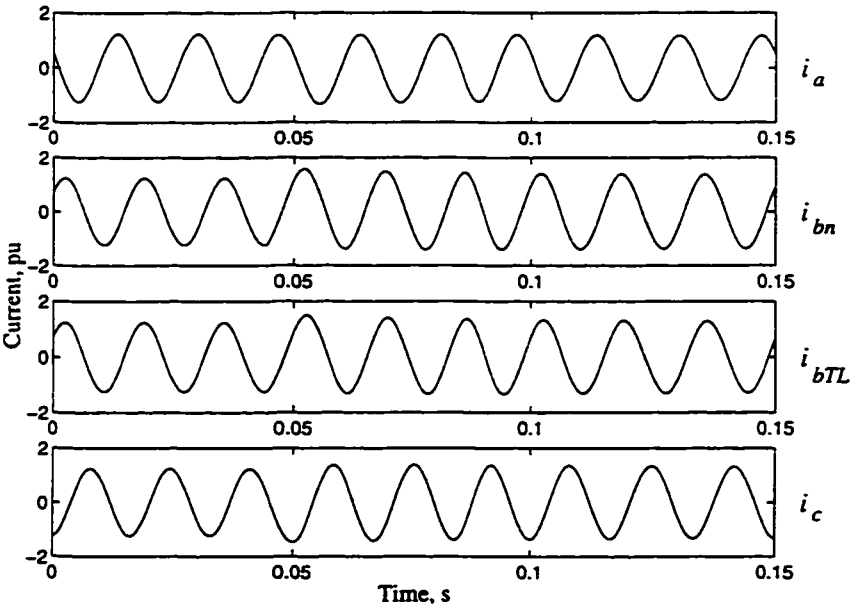

Figure 4.12: Computed stator currents for an internal single phase to ground fault at 10% of phase b of generator G_1, P=0.8 pu, pf=0.85 lag, R_{g1}=1.5 pu and R_{g2}=0.8 pu.

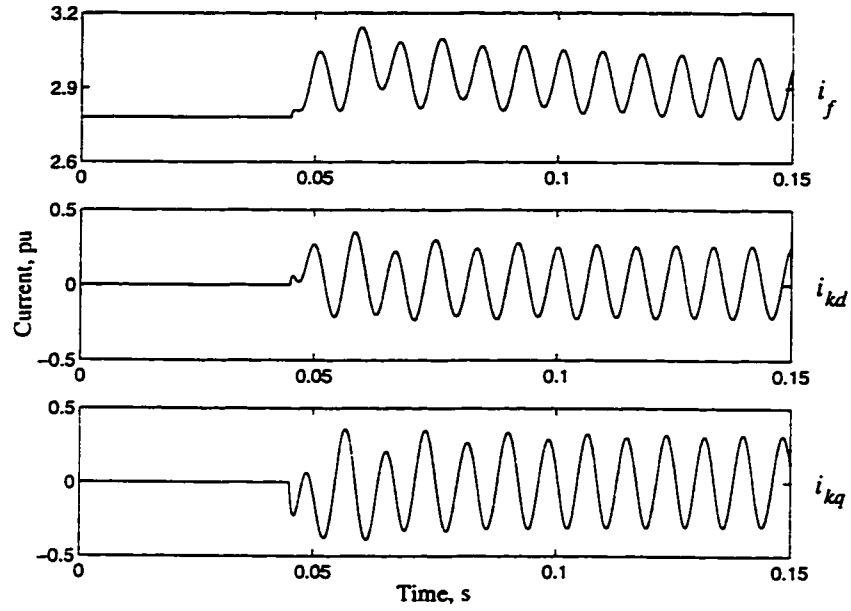

Figure 4.13: Computed rotor currents for an internal single phase to ground fault at 77% of phase b of generator G_1, P=0.8 pu, pf=0.85 lag, R_{g1}=1.5 pu and R_{g2}=0.8 pu.

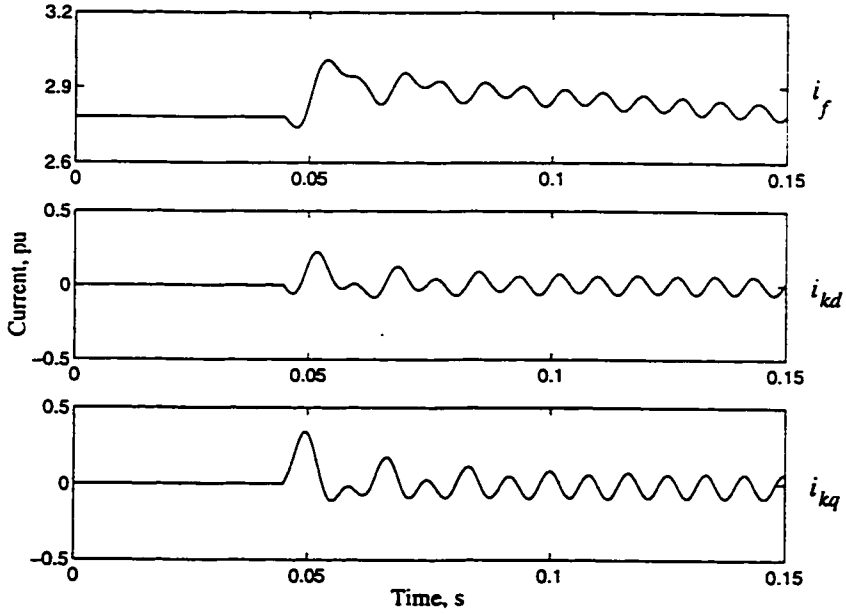

Figure 4.14: Computed rotor currents for an internal single phase to ground fault at 10% of phase b of generator G_1, P=0.8 pu, pf=0.85 lag, R_{g1}=1.5 pu and R_{g2}=0.8 pu.

Chapter 5

Design of the Neural Network Based Digital Differential Relay

5.1 Introduction

The majority of power system protection techniques are involved in defining the system state through identifying the pattern of the associated voltage and current waveforms. This means that the development of protection techniques can be essentially treated as a problem of pattern classification/recognition. However, due to the various distortions and noises that faults generate, conventional digital pattern recognition techniques may not be satisfactory in complex protection applications. Moreover, these techniques use digital signal processing methods which take time (usually one cycle of the system frequency) to determine if a fault has occurred, and hence issue a trip signal.

Successful application of neural networks (NNs) in other areas of power engineering has demonstrated that it can be employed as an alternative method for solving certain long standing problems where conventional digital techniques have had difficulty or have not achieved the desired speed,

accuracy or efficiency [11]. This is so by virtue of the adaptive, learning and parallel processing ability of the NN. Also, the ability of neural networks, in particular multi-layer feed-forward neural networks (MFNNs), to learn by training any complex input/output mapping makes their use as pattern classifiers successful.

Design of a new NN based digital differential relay for generator stator winding protection is presented in this chapter. The relay has two feed-forward neural networks (FNNs): One FNN is used by the fault detector module and the other by the fault classifier module. The FNN based fault detector module is used to discriminate between three generator states, namely the normal operation state, external fault state and internal fault state. In the event of an internal fault the trip logic module issues a trip signal and activates the FNN based fault classifier module, which identifies the faulted phase(s). Current patterns used to train the FNNs were obtained by simulating normal operation state for the generator at different loading conditions and different types of internal and external faults. Simulations were performed using the direct 3-phase model, described in Chapters 2 and 3, which is capable of simulating the three states of the generator.

5.2 Inputs

The structure of the proposed NN based digital differential relay, used for detecting faults and classifying internal faults, is shown in Fig. 5.1. The modules shown in Fig. 5.1 are not the complete modules of a digital relay, but rather the important modules needed for the proposed protection scheme. In each of the following sections the function of each module, shown in Fig. 5.1, is described.

In differential protection it is essential to use both the line-side and

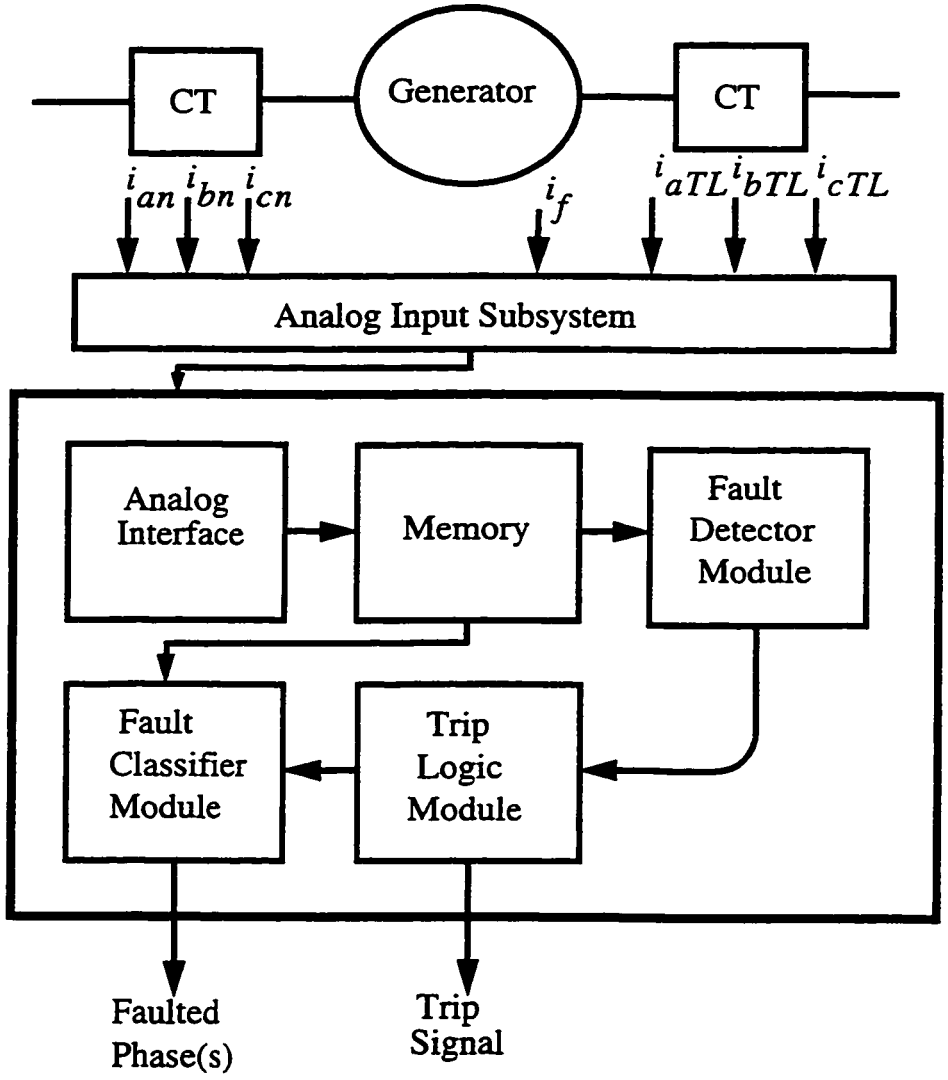

Figure 5.1: Important modules of the NN based digital differential relay.

neutral-end currents of each phase, as the differential relay operates on the difference between these two currents, as explained in Section 2.2.1. Hence, the inputs to the relay are the generator three phase currents from both the line-side ($i_{aTL}, i_{bTL}, i_{cTL}$) and the neutral-end ($i_{an}, i_{bn}, i_{cn}$) in addition to the field current (i_f). In the case of an internal fault in one path of phase a of a multi-path machine, Fig. 3.2, $i_{aTL} = i_p + i_n$ and $i_{an} = i_p + i_m$. The same analogy follows for internal faults in phases b and c of a multi-path machine.

The second harmonic present in the field current, during a fault, has been used previously in a generator digital protection algorithm to indicate the existence of an abnormality [28]. It has also been shown in Chapter 4 that the field current is a constant dc value during normal operation state. Simulation studies in the same chapter also indicated that although the field current, i_f, contains fundamental and/or second harmonic (depending on the type of fault) during both external and internal faults, their amplitudes in external and internal faults are different. Hence, samples of the field current are used to help the NN based fault detector module to differentiate between the three states.

5.3 Analog Input Subsystem

In an actual hardware implementation the inputs to these modules would be the low level signals provided by the current transformers (CTs) [10]. However, in the simulation part of this project the inputs to the analog input subsystem are the instantaneous pu current values provided by the direct 3-phase model, described in Chapters 2 and 3. A sampling frequency of 1200 Hz (20 samples/cycle) is used in this relaying scheme. Hence, to avoid aliasing problems, an antialiasing low pass filter, with a cut-off frequency of 570 Hz, is used at the analog input subsystem. This filter is a second order

Butterworth filter, and its transfer function is:

$$H(s) = \frac{{\omega_o}^2}{s^2 + 2\zeta\omega_o s + {\omega_o}^2} \tag{5.1}$$

where $\omega_o = 2\pi 570$ rad/s and $\zeta = 0.71$. The trapezoidal rule is used in simulating the filter.

5.4 Analog Interface

This module performs two functions. It samples the currents at a sampling rate of 1200 Hz and scales the current values such that they have a maximum value of +1 and a minimum value of -1.

5.5 Memory

The memory is used to store the most recent samples of the 7 inputs, in addition to four previous samples of each input. The stored samples are later used by the fault detector module and the fault classifier module.

5.6 Fault Detector Module

The NN based fault detector module is the main part of the differential relay. Its function is to differentiate between three generator states, namely the normal operation state (NOS), external fault state (EFS) and internal fault state (IFS). The following sections describe the structure of the NN used for fault detection and its training process.

5.6.1 Neural Network Structure

In Section 2.3.1 the reasons that the MFNN is employed in the proposed NN based relay are stated. Among these reasons is the ability of MFNNs to learn by training any required input/output mapping, and subsequently respond to new inputs in the most appropriate manner [15,23]. Two layer FNNs can be used to classify inside, convex and open or closed fields, but three layer FNNs can generate arbitrary complex decision regions. In this project three layer FNNs are used.

The structure of the FNN based fault detector module is shown in Fig. 5.2. The FNN of Fig. 5.2 is fully connected in the sense that every node in each layer, including the input layer, is connected to every other node in the adjacent forward layer. The inputs to the FNN are 7 currents, each current being represented by five consecutive samples, making a total of 35 inputs. The index n in Fig. 5.2 is used to indicate the most recent sample of each current. Five consecutive samples of each current form a 1/4 cycle of fundamental frequency (60 Hz), and the information contained in a 1/4 cycle is sufficient for the FNN to detect a change of state. It is due to this reason that five samples per current are used.

The degree of freedom of the neural network (i.e. number of neurons in the hidden layers) must be matched to the complexity of the classification boundary [15,23]. Currently, in the absence of parametric guidance, the only proposed method of determining the best number of hidden neurons is by comparative cross validation among two or more NNs. Moving from a small number of hidden neurons to a large number should decrease the overall probability of error while maintaining an equivalent error performance for the test and training data. There is always a range where the error of the NN is relatively unchanged. This should be the best range for NN structure. This method was used to test several networks, and finally it was decided to

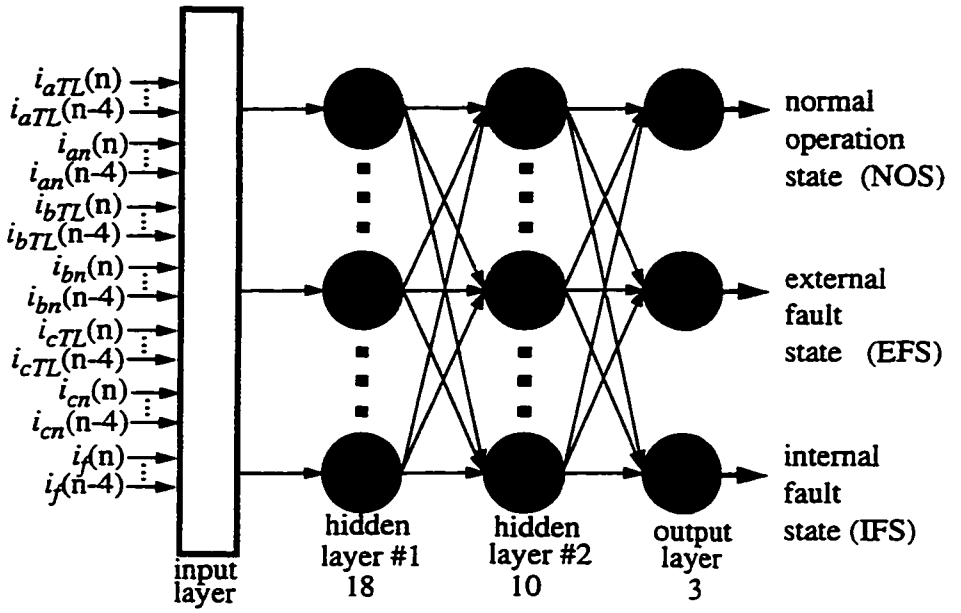

Figure 5.2: Structure of the FNN based fault detector module.

have 18 tan-sigmoid neurons in the first hidden layer, 10 tan-sigmoid neurons in the second hidden layer and 3 log-sigmoid neurons in the output layer.

The sigmoidal functions (A.6,A.7) are used because they help in producing an arbitrary decision boundary with smooth curves and edges [15]. Also, they are differentiable functions, which is an essential feature when the back-propagation algorithm is used in training as indicated in Section 2.3.2. The tan-sigmoid function is used in the hidden layers as the MFNN trained with the back-propagation algorithm may, in general, learn faster when the sigmoidal activation function built into the neuron model of the network is asymmetric than when it is nonsymmetric.

Each neuron in the output layer, Fig. 5.2, is responsible for one fault type, except the first one that signals the 'normal state'. Therefore depending on the state of the generator one output is mapped to a value greater than 0.9 while the two others are less than 0.1.

5.6.2 Training Process

The training algorithm used is the back-propagation algorithm with momentum and adaptive learning rate [15,20,21], Section 2.3.2. The software used for implementing the algorithm is the *Matlab Neural Network Toolbox* [71], and batch mode training was used.

The training data was obtained using the direct 3-phase model, described in Chapters 2 and 3. The power system model consisted of a generator connected to an infinite bus through a short TL, as shown in the figures of Chapters 2 and 3. Ground resistances, R_{g1} and R_{g2} Fig. 3.7, were included in the power system model, and their values were fixed at 1.5 pu and 0.8 pu, respectively, as indicated in Section 4.4.1.

The training set consisted of about 30000 patterns representing different cases of the three generator states. About 10000 patterns were used for each state. Number of training patterns for the three states was kept equal to avoid skewed training. The normal operation state was represented by three phase balanced operation at different loads and power factors. Patterns from different types of external faults at various locations along the TL were used in training. The internal faults training data consisted of various types of faults at different percentages of the stator winding.

Initially training started with a smaller training set, around 15000, but during validation tests it was found that the FNN response to boundary patterns was poor. Those boundary patterns represent normal operation at low power, external single phase to ground faults at the end of the TL and internal single phase to ground faults involving small winding percentages. Hence, more boundary patterns were generated and included in the training set, which finally reached about 30000 patterns.

Three different machine parameters were used to generate the training set to ensure that the FNN is able to identify the three states for any generator.

These three machines were G_2 (22 kVA), G_3 (30 MVA) and G_6 (975 MVA). The parameters of these generators are given in Appendix C.

Training was stopped after the normalized average squared error dropped to 0.019 and the FNN was able to adequately generalize [11,15,23]. The generalization ability of the FNN based fault detector module is shown through simulation studies presented in the next chapter.

5.7 Trip Logic Module

The trip logic module issues a trip signal only when it confirms that the output of the fault detector module is either an internal fault or a prolonged external fault that may affect the generator. In order to confirm the presence of a certain state (normal, external or internal), the fault logic module averages six consecutive outputs of each of the three output neurons. The generator is considered to be operating in its normal state if (5.2) is valid. A trip decision is taken in the case of an internal fault if the conditions specified in (5.3) exist for 3 samples.

$$AVNS > 0.7 \& AVEF < 0.23 \& AVIF < 0.2 \tag{5.2}$$

$$AVNS < 0.42 \& AVEF < 0.4 \& AVIF > 0.8 \tag{5.3}$$

where $AVNS$, $AVEF$ and $AVIF$ are the averaged outputs of NOS, EFS and IFS neurons, respectively. When the trip logic module issues a trip signal based on the detection of an internal fault it also activates the fault classifier module.

In the event of an external fault, this relay is used as a backup relay, in case the responsible relay failed to trip. A delayed trip decision is taken in the case of an external fault if the conditions specified in (5.4) are sustained

for a prespecified number of cycles, Y, and no other relay has tripped. The setting Y is chosen based on the expected operating time of the responsible relay. In this project Y was chosen to be 1.5 cycles (30 samples).

$$AVNS < 0.42 \& AVEF > 0.8 \& AVIF < 0.4 \tag{5.4}$$

At each sampling interval the relay checks whether NOS (5.2) is valid or not. In case NOS is valid, the relay resets its internal and external fault counters, and waits for a new set of samples. In case IFS (5.3) or EFS (5.4) is valid, the relay increments the internal or external fault counter. Should the internal counter reach 3 or the external counter reach 30, the relay issues a trip signal. It can happen during the light internal or external faults that none of the conditions specified in (5.2-5.4) are valid at one sampling interval. Should this occur, the counters are kept at their previous values and the relay waits for a new set of samples for verification.

It should be noted that the conditions specified in (5.2-5.4) were obtained empirically by extensive simulation studies and it is believed that these conditions accurately distinguish all three states. The reason behind averaging six consecutive FNN outputs and then checking the conditions specified in (5.2-5.4) is to make the relay stable during passing transients. At the same time, this will not affect the speed of the relay, in terms of tripping time, as the logic described above can still initiate a trip decision within 7 to 9 samples after the inception of an internal fault.

5.8 Fault Classifier Module

Analysis of the internal faults in the armature winding of a generator is essential to the proper performance of the power system. It is required in monitoring the performance of relays, circuit breakers, and other protective

and control elements. Moreover, identifying the faulted phase or phases speeds up machine repair time.

The internal fault classifier module is activated by the trip logic module only in the event of an internal fault. It is composed of two parts. The first part is a FNN that classifies each of the three phases as faulty or healthy. The second part is a simple fault classifier confirmation logic that first averages the FNN outputs and then uses the averaged outputs to confirm the status of each phase. In the following sections the structure of each part is described.

5.8.1 Feed-Forward Neural Network Fault Classifier

The structure of the FNN, which is also fully connected, is shown in Fig. 5.3. The inputs to the FNN are 6 currents, each current being represented by four consecutive samples, making a total of 24 inputs. Samples of the field current are not used in this module as they do not help in classifying the phases. Also, after several attempts, it was decided that four samples per current are sufficient for fault classification purposes. The information contained in 3 samples per current was not enough for fault classification. Using five samples per current increased the network complexity, while the classification accuracy remained the same as for four samples per current.

The FNN has three layers, with 14 tan-sigmoid neurons in the first hidden layer, 7 tan-sigmoid neurons in the second hidden layer and 3 log-sigmoid neurons in the output layer. It is noticed by comparing Figs. 5.2 and 5.3 that the neurons in the hidden layers of the FNN fault detector are more than those of the FNN fault classifier. This is so because the task required by the FNN fault classifier is less complex, hence it can be accomplished by a smaller network.

Each neuron in the output layer, Fig. 5.3, is responsible for a fault in one of the phases. As an example, suppose there is an internal fault in phase a,

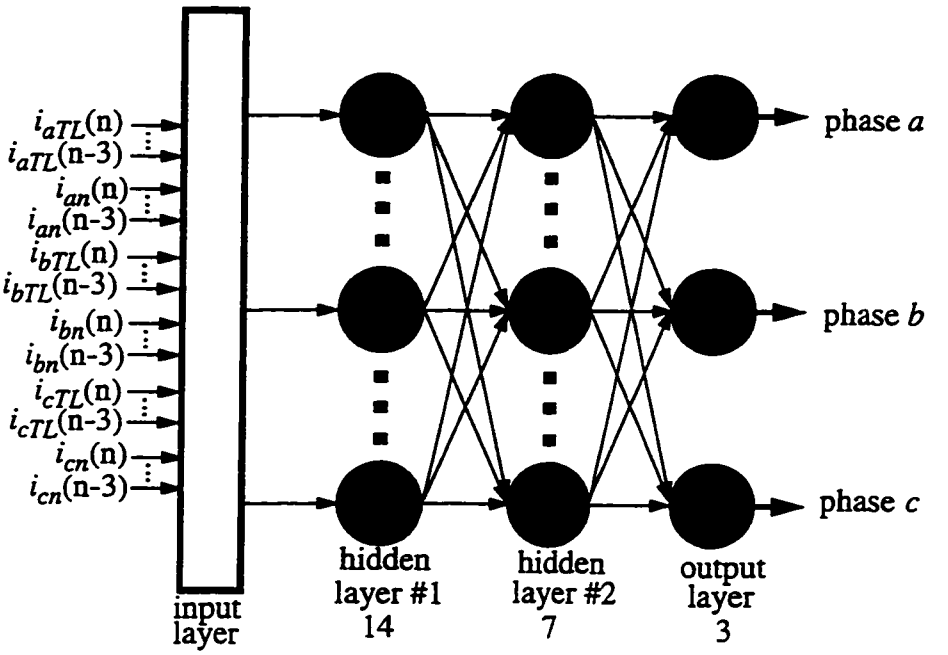

Figure 5.3: Structure of the FNN fault classifier.

then the output of phase *a* neuron will be mapped to a value greater than 0.95, indicating that this phase is faulty, while the outputs of the two other neurons will be less than 0.1, indicating that these two phases are healthy.

The training algorithm used is the back-propagation algorithm with momentum and adaptive learning rate. The training set consisted of about 10000 patterns representing different types of internal faults. These patterns were the internal fault patterns used previously for training the fault detector module. As this module is activated during internal faults only, there was no need to expose it to patterns from other states. Training was stopped after the normalized average squared error dropped to 0.007 and the FNN was able to adequately generalize [11, 15, 23].

5.8.2 Fault Classifier Confirmation Logic

The function of the fault classifier confirmation logic is to confirm the status of each phase. The fault confirmation logic first averages five consecutive outputs of each of the three output neurons, and then uses the averaged outputs to confirm the status of each phase. So, for the fault classifier confirmation logic to confirm that there is an internal single phase fault in phase a, or b, or c, the conditions specified in either (5.5), or (5.6), or (5.7), respectively, should exist for 3 samples. For a two phase fault, the fault classifier confirmation logic would not indicate that phases a and b, or b and c, or c and a, are faulty unless the boundary conditions of either (5.8), or (5.9), or (5.10), respectively, exist for 3 samples.

$$AVFA > 0.8 \& AVFB < 0.3 \& AVFC < 0.3 \tag{5.5}$$

$$AVFA < 0.3 \& AVFB > 0.8 \& AVFC < 0.3 \tag{5.6}$$

$$AVFA < 0.3 \& AVFB < 0.3 \& AVFC > 0.8 \tag{5.7}$$

$$AVFA > 0.8 \& AVFB > 0.8 \& AVFC < 0.15 \tag{5.8}$$

$$AVFA < 0.15 \& AVFB > 0.8 \& AVFC > 0.8 \tag{5.9}$$

$$AVFA > 0.8 \& AVFB < 0.15 \& AVFC > 0.8 \tag{5.10}$$

where $AVFA$, $AVFB$ and $AVFC$ are the averaged outputs of phase a, phase b and phase c neurons, respectively. In the event of a three phase internal fault, the boundary conditions are:

$$AVFA > 0.8 \& AVFB > 0.8 \& AVFC > 0.8 \tag{5.11}$$

5.9 Summary

A new multi-neural network based digital differential relay for stator winding protection is presented. The relay has two main tasks. The first task is to differentiate between normal operation state, external fault state and internal fault state. The output of the FNN based fault detector module is used by the trip logic module to issue a trip signal in the event of an internal fault or a prolonged external fault. The second task is classifying the stator phases as faulty or healthy in the event of an internal fault.

Chapter 6

Evaluation of the Relay Performance

6.1 Introduction

Neural networks are difficult to account for and explain their results. The analytical methods for explaining the weights and biases of a trained network are not yet available. The only means of verifying the performance of a trained network is to perform extensive testing. For that reason the proposed NN based relay [72–74], Chapter 5, was tested using a large set of independent test patterns. In addition to using the three machine parameters previously used for training (G_2, G_3, G_6) to simulate new faults for testing, three more machine parameters (G_1, G_4, G_5) were also used. The parameters were for 15 kVA (G_1) and 100 MVA (G_5) cylindrical type machine and a 40 MVA (G_4) salient pole type machine. The parameters of these six generators are given in Appendix C.

The results of the relay modules, when exposed to severe faults, light faults and transients, are illustrated through simulation studies presented in this chapter. In Section 6.2 the results of the fault detector module, Fig. 5.2,

are presented. The results of the trip logic module, Fig. 5.1, are presented in Section 6.3, and the results of the fault classifier module, Fig. 5.3, are presented in Section 6.4.

6.2 Fault Detector Module Results

The function of the FNN based fault detector module is to differentiate between three generator states, namely the normal operation state (NOS), external fault state (EFS) and internal fault state (IFS), Section 5.6. There are three neurons in the output layer, as shown in Fig. 5.2, and each neuron is responsible for one state. Therefore, when the generator is at a certain state, the output of the corresponding neuron is mapped to a value greater than 0.9 while the two other neurons are less than 0.1.

Figures 6.1,6.2 and 6.3 show the results of the FNN based fault detector module. The internal fault percentages mentioned throughout this dissertation are measured from the neutral-end of the generator. In the figures presented in this chapter the term pg indicates a single phase to ground fault, ppg indicates a two phase to ground fault, pp means a phase to phase fault and FI is the fault inception time in samples. In all the results presented in this thesis, the generator is in NOS before a fault is applied. The results shown in Figs. 6.1,6.2 and 6.3 indicate that the fault detector module is not affected by different loading conditions, fault types, fault locations and fault inception times. It takes the FNN 1 to 5 samples (0.83 to 4.2 ms) to change its output, as a change from one state to another occurs.

In protection it is more important to ensure proper relay operation during transients and light faults. Transients can be in the form of a slight unbalance in the phase currents, which could happen due to an unbalanced fault occurring far away from the generator or due to an unbalanced load.

Another form of transients is a step change in power, which may occur due to switching loads or even increasing the generator power. A differential relay, protecting the generator winding, should remain inoperative and stable under these transients. Figure 6.4-a shows the success of the FNN in detecting a normal operation state, even though there was a 2% unbalance in the phase currents. The response of the FNN to a step change of 0.15 pu in power is shown in Fig. 6.4-b. Each neuron in the output layer had a constant value during the transient period.

Percentage differential protection is mainly used to compensate for current transformers (CTs) mismatches [3, 25]. CTs errors are obvious in the event of high currents associated with severe external fault conditions, and could cause the relay to falsely identify the fault as an internal fault and maloperate. The outputs of the FNN during a 3 phase fault at the machine terminals, where there was a 15% difference between line-side and neutral-end currents, are shown in Fig. 6.5-a. The FNN based fault detector module accurately classified the fault as an external fault.

In general, relays have difficulty detecting light faults, mainly because their current patterns are similar to those of normal operation. Figure 6.5-b shows the success of the proposed NN based relay in detecting an external fault at the end of the TL, i.e. on the infinite bus side.

The performance of the FNN based fault detector module was checked for light internal faults. The response of the FNN to internal single phase to ground faults at 20% and 10% of phase a is shown in Fig. 6.6. A similar study for internal two phase to ground faults involving 25% of phases b and c and 4% of phases a and b is presented in Fig. 6.7. The results of Figs. 6.5-b, 6.6 and 6.7 show that the FNN is able to indicate the correct state of the generator, even for light faults. It can also be noticed that the NOS neuron, Fig. 5.2, has the tendency to be active during light faults, while for

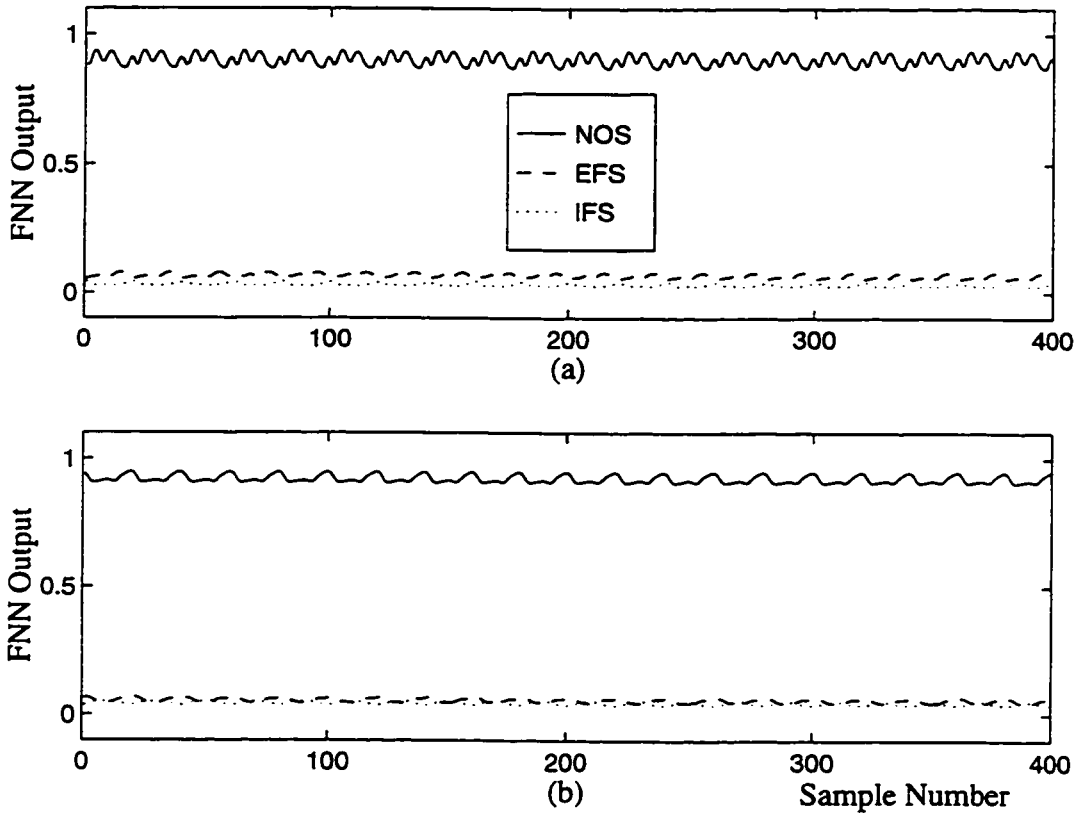

Figure 6.1: Results of the FNN based fault detector module for NOS. (a) G_4, P=0.8 pu and pf=0.9 lag. (b) G_1, P=0.4 pu and pf=0.8 lag.

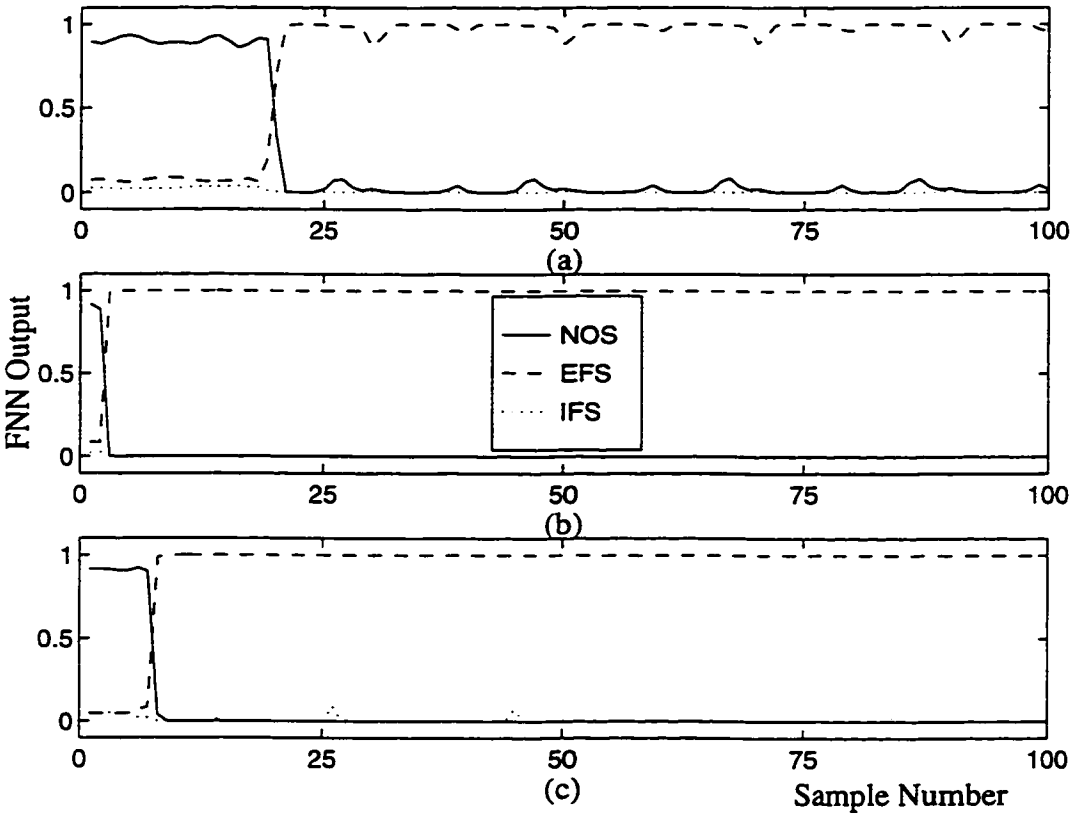

Figure 6.2: Results of the FNN based fault detector module for EFS. (a) G_3, pg b, at middle of TL, P=0.9 pu, pf=0.9 lag and FI=19. (b) G_1, ppg a, b, at 80% of TL, P=0.7 pu, pf=0.8 lag and FI=2. (c) G_5, pp b, c, at machine terminals, P=0.93 pu, pf=0.9 lag and FI=7.

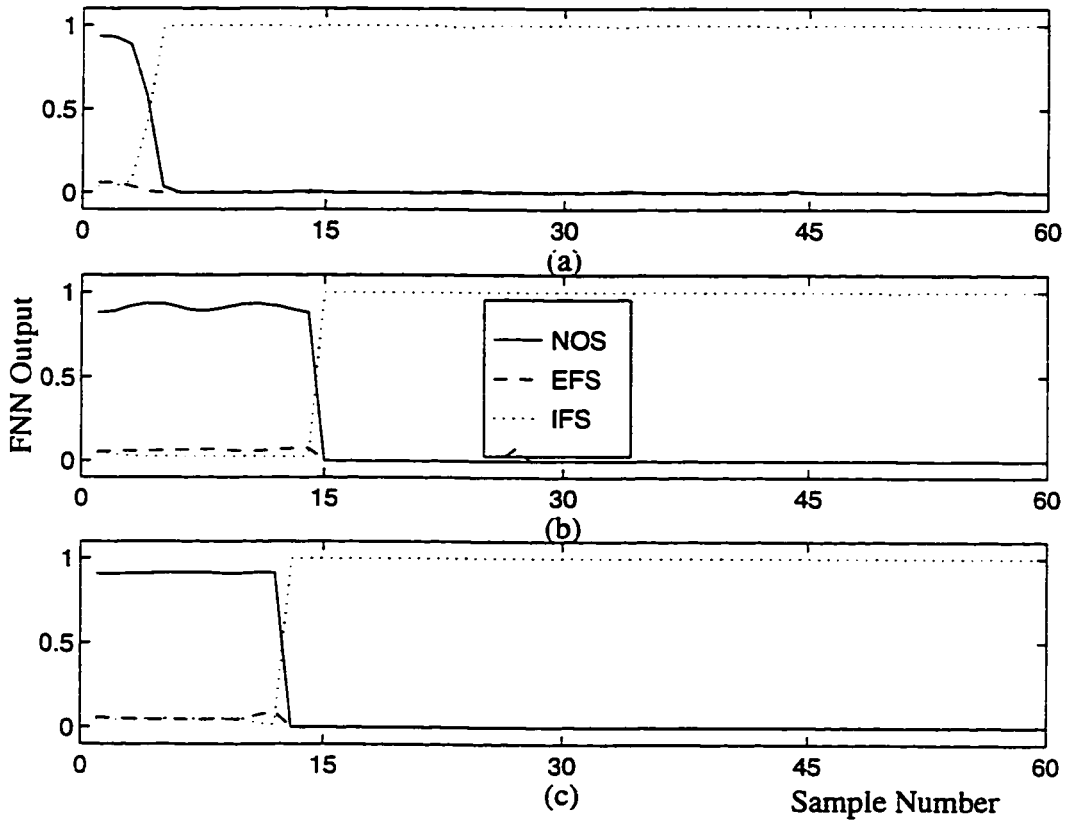

Figure 6.3: Results of the FNN based fault detector module for IFS. (a) G_2, pg at 37% of c, P=0.55 pu, pf=0.86 lag and FI=2. (b) G_1, ppg at 62% of b & 88% of c, P=0.77 pu, pf=0.82 lag and FI=14. (c) G_4, ppg at 50% of a & 50% of c, P=0.92 pu, pf=0.9 lag and FI=12.

easily detectable faults its value is less than 0.1. This is due to the fact that light faults resemble normal operation, so the weaker the fault is, the more active the NOS neuron is, as can be observed by comparing Figs. 6.6-a and 6.6-b. However, the averaging scheme used by the trip logic module makes the overall protection scheme insensitive to the fluctuations, occurring during light faults, in the output neurons.

6.3 Trip Logic Module Results

The trip logic module uses an averaging scheme, as explained in Section 5.7. to make a trip decision. This module issues a trip signal when an internal fault or a prolonged external fault is confirmed. In the case of an internal fault the conditions specified in (5.3) should exist for 3 samples, while for an external fault the conditions specified in (5.4) should exist for 30 samples.

Figure 6.8 shows the outputs of the trip logic module for the two internal faults shown in Figs. 6.3-c and 6.6-a. The outputs are shown up to the sample the trip logic module issued its first trip signal. The simulation studies done indicate that for internal faults involving more than one phase, the relay trips after 7 to 9 samples (5.8 to 7.5 ms) from fault inception. The results of the sensitivity analysis show that the smallest fault detectable is 4% of the winding to winding faults.

The relay tripping characteristic for internal single phase to ground faults is shown in Fig. 6.9. It can be seen from Fig. 6.9 that the relay tripping time for faults involving 30% or more of the winding is 7 to 10 samples (one half cycle or less), and for faults involving 20% to 10% is 13 to 20 samples (one cycle or less). Internal single phase to ground faults which involve 9% or less of the winding are not detected by the proposed NN based relay. Ground fault protection should be provided for this small percentage of the winding

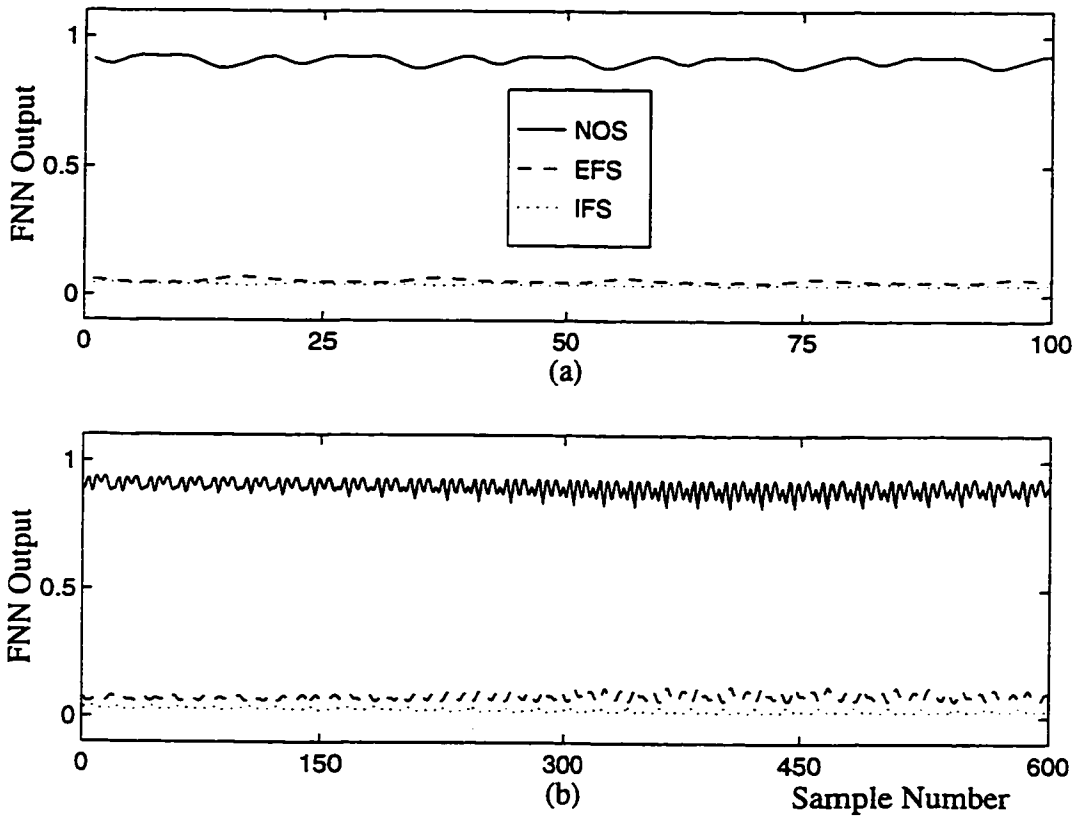

Figure 6.4: Outputs of the FNN based fault detector module during transients. (a) NOS with 2% unbalance, G_5, P=0.5 pu and pf=0.8 lag. (b) Step change of 0.15 pu in power at sample number 22, G_3, P=0.8 pu and pf=0.9 lag.

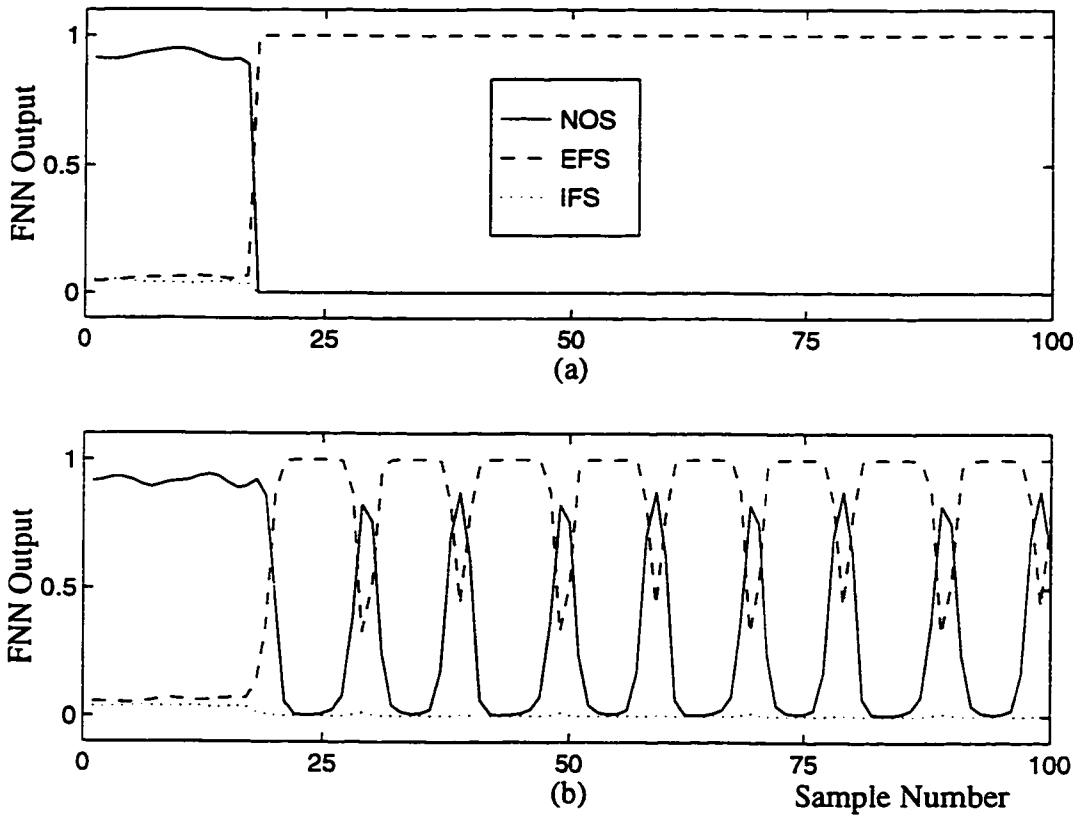

Figure 6.5: Outputs of the FNN based fault detector module during CT mismatch and light external faults. (a) EFS, G_6, 3 phase, at machine terminals with a CT mismatch of 15%, P=0.8 pu, pf=0.9 lag and FI=16. (b) EFS, G_4, pg *b*, at end of TL, P=0.6 pu, pf=0.8 lag and FI=18.

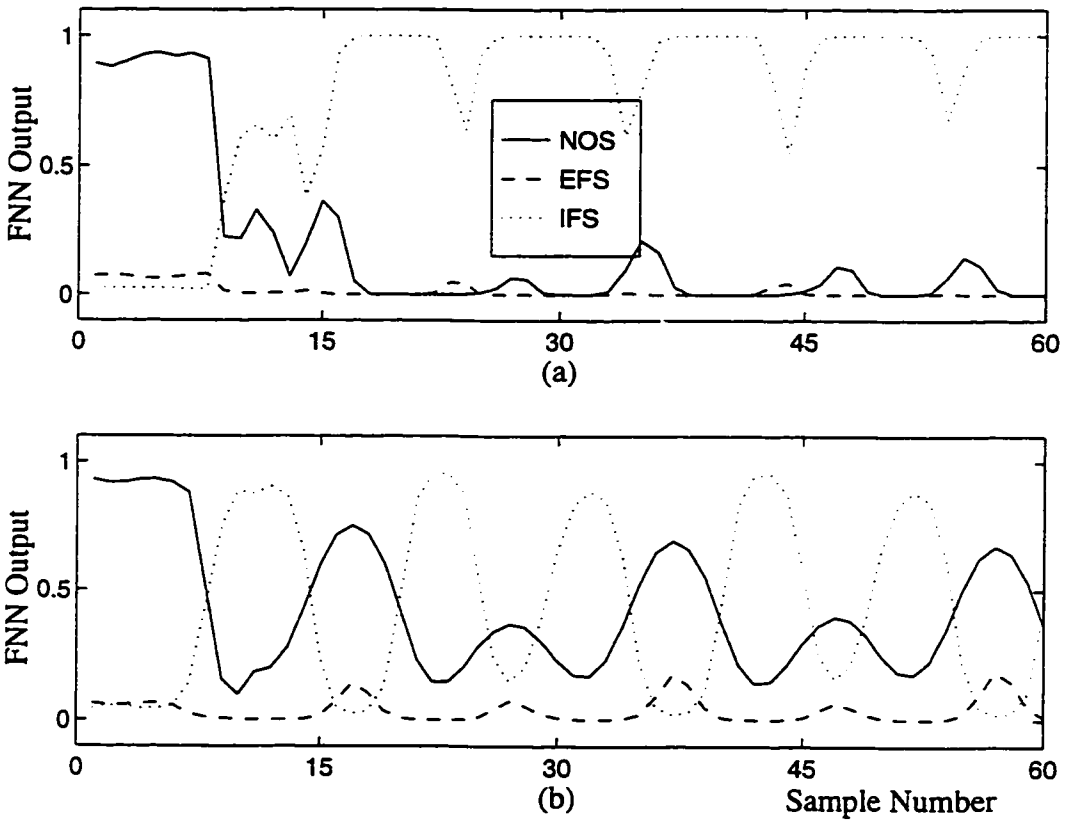

Figure 6.6: Outputs of the FNN based fault detector module during light internal faults. (a) IFS, G_4, pg at 20% of a, P=0.75 pu, pf=0.8 lag and FI=8. (b) IFS, G_4, pg at 10% of a, P=0.6 pu, pf=0.9 lag and FI=6.

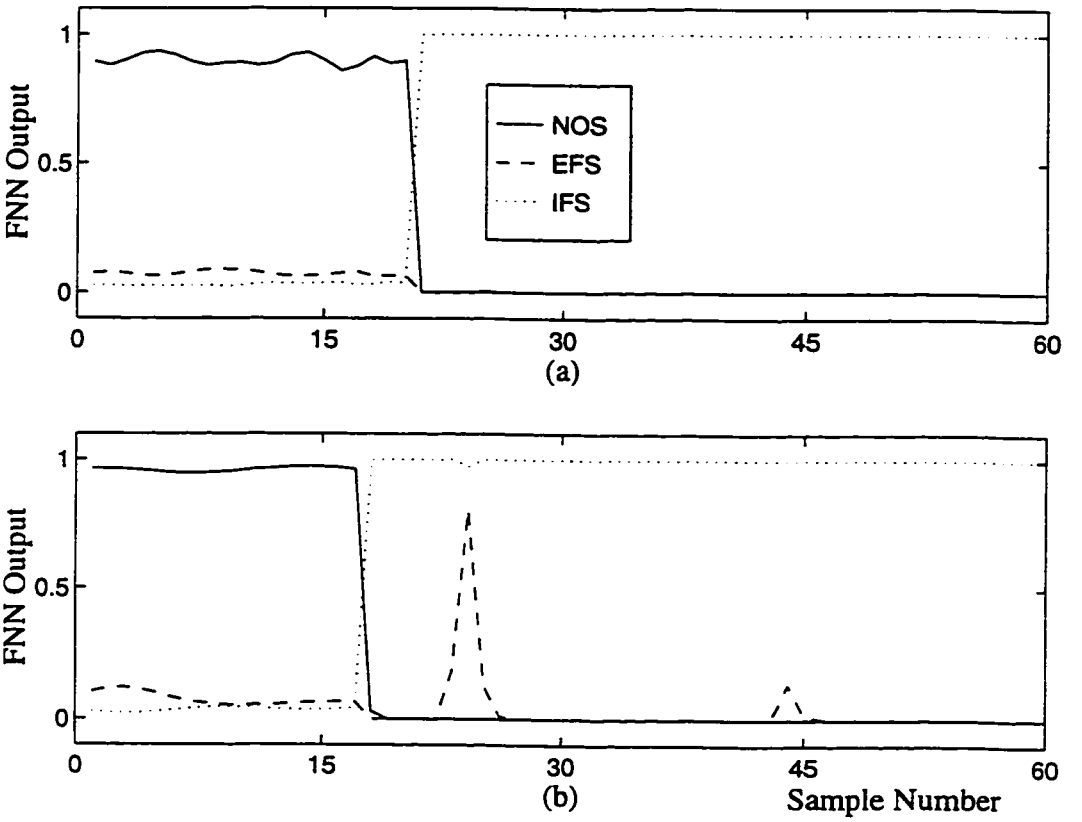

Figure 6.7: Outputs of the FNN based fault detector module during light internal faults. (a) IFS, G_6, ppg at 25% of b & 25% of c, P=0.63 pu, pf=0.9 lag and FI=19. (b) IFS, G_5, ppg at 4% of a & 4% of b, P=0.4 pu, pf=0.8 lag and FI=17.

as described in Section 1.2.

The response of the trip logic module to external faults is shown in Fig. 6.10. The results, shown in Fig. 6.10, are up to the sample the relay issued its first trip signal, based on the detection of a prolonged external fault. In this project it is assumed that prolonged external faults have occurred and that the primary protection failed to operate. The purpose of this assumption is to check the ability of the NN based relay to operate during external faults. However, in a utility the primary protection will isolate the external fault, causing the NN based relay to reset its counters, as described in Section 5.7. The response of the FNN based fault detector module to the two external faults presented in Fig. 6.10 is shown in Figs. 6.2-b and 6.5-b. It is noticed that tripping times are shorter for severe external faults and longer for light external faults. Longer tripping times occur due to the fluctuations of the NOS and EFS neurons, Fig. 6.5-b, which make the external fault conditions in (5.4) invalid at some sampling intervals. This causes the trip logic module to take a longer time to verify the existence of a fault.

Current transformer saturation can present a problem to differential relaying during severe external fault conditions [26, 27]. However, as fault detection is fast, the fault detector module will detect the presence of an external fault prior to CT saturation. So, the external fault counter in the trip logic module will build up, hence preventing maloperation. In the simulation part of this project, the reaction of the relay to CT saturation is not shown. However, in the implementation part, Chapter 8, the relay is exposed to external faults that caused CT saturation. The results showing the success of the relay in detecting internal phase to phase faults and the ability to handle noisy patterns are also presented in Chapter 8.

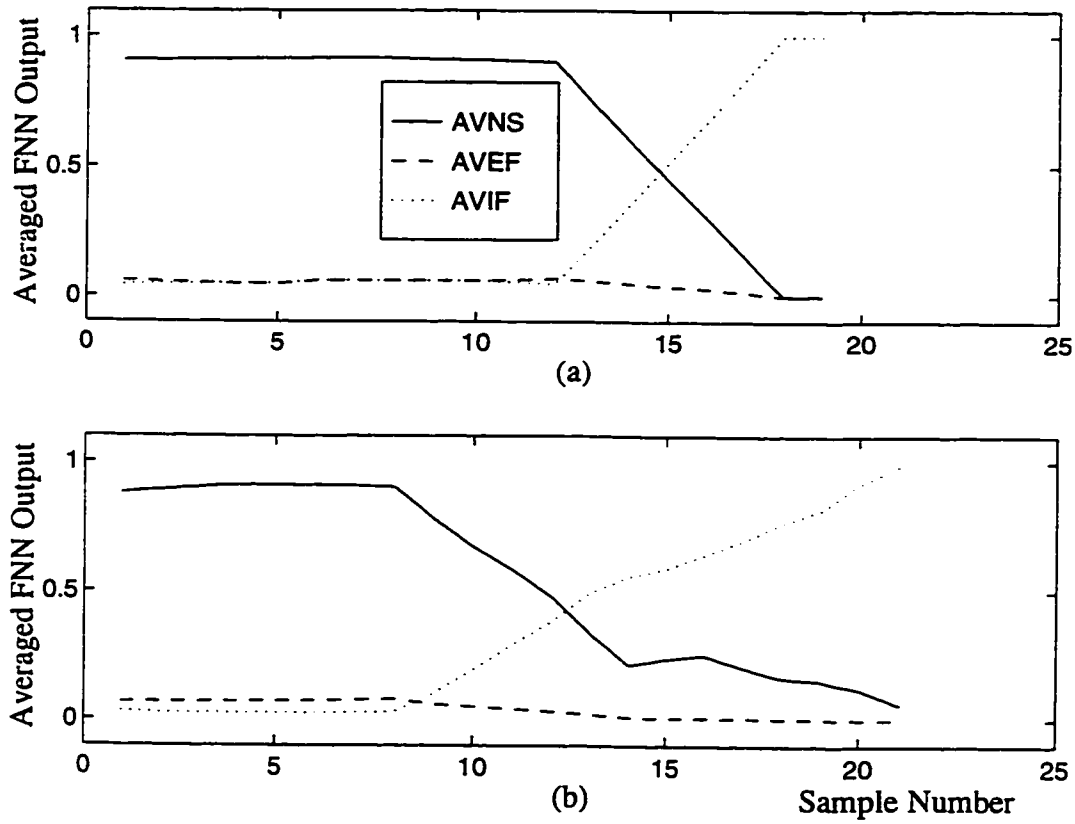

Figure 6.8: Outputs of the trip logic module for IFS. (a) G_4, ppg at 50% of a & 50% of c, P=0.92 pu, pf=0.9 lag and FI=12. (b) G_4, pg at 20% of a, P=0.75 pu, pf=0.8 lag and FI=8.

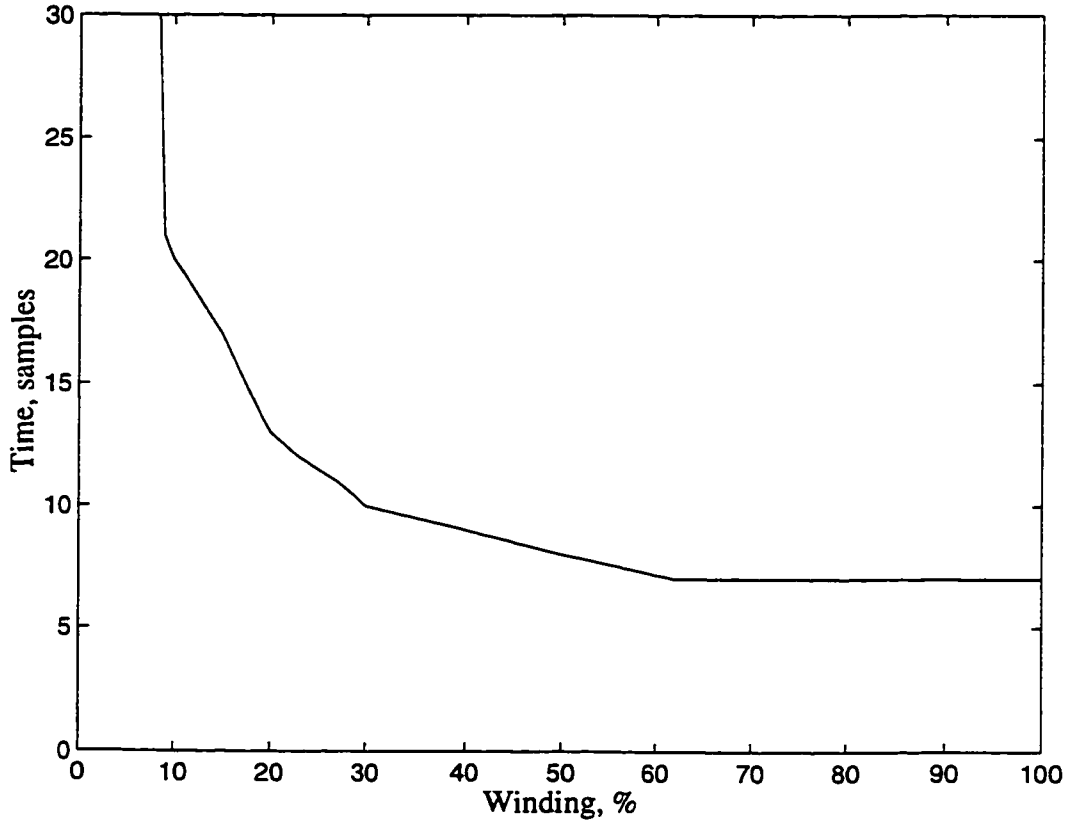

Figure 6.9: Relay tripping characteristic for internal single phase to ground faults.

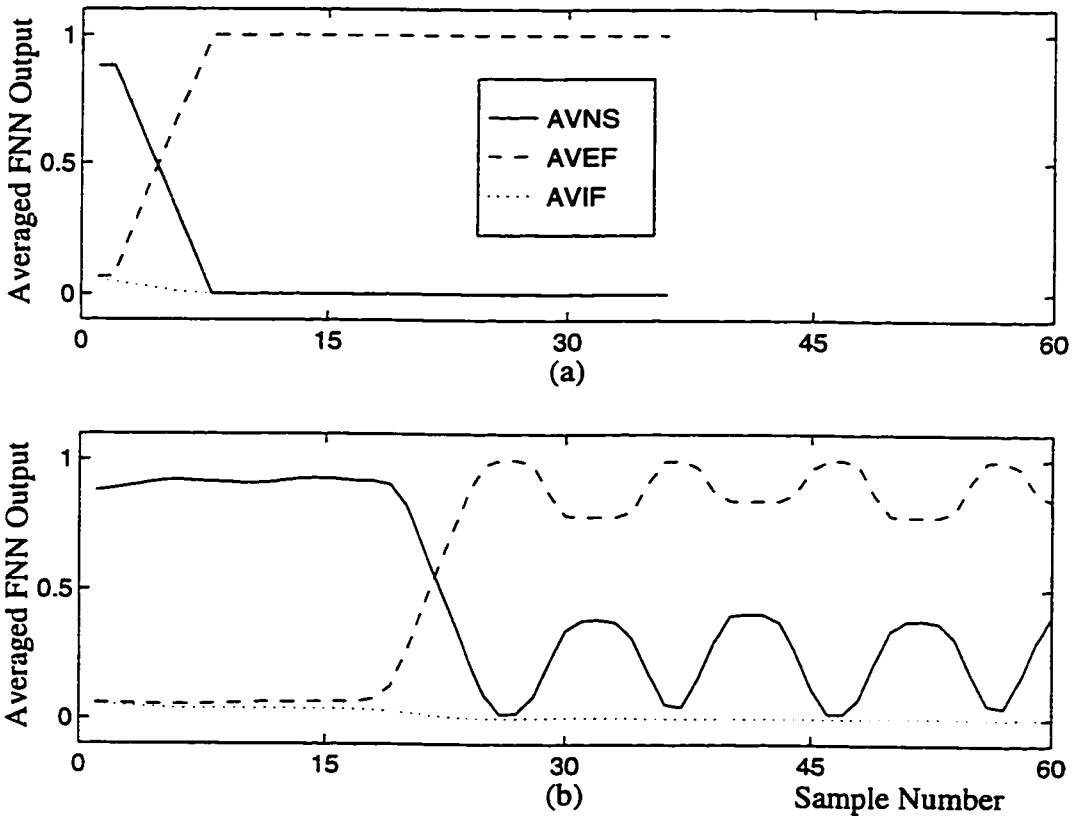

Figure 6.10: Outputs of the trip logic module for EFS. (a) G_1, ppg a, b, at 80% of TL, P=0.7 pu, pf=0.8 lag and FI=2. (b) G_4, pg b, at end of TL, P=0.6 pu, pf=0.8 lag and FI=18.

6.4 Fault Classifier Module Results

The internal fault classifier module is activated by the trip logic module only in the event of an internal fault, Section 5.8. It is composed of two parts. The first part is a FNN that classifies the phases as faulty or healthy. The second part is a simple fault classifier confirmation logic that first averages the FNN outputs and then uses the averaged outputs to confirm the status of each phase, in accordance with (5.5-5.11).

The FNN fault classifier was subjected to different types of internal faults at different percentages of the windings, to check its performance. Figures 6.11,6.12 and 6.13 show the results of the FNN fault classifier. The results shown in Figs. 6.11,6.12 and 6.13 indicate that the FNN is accurate, robust and is not affected by different prefault loading conditions, fault types and fault locations. The results of the sensitivity analysis, performed on the FNN fault classifier, indicate that the smallest fault detectable by that module is 10% of the winding for phase to ground faults and 4% of each winding for two phase to ground faults.

Figure 6.14 shows the outputs of the fault classifier confirmation logic for the internal faults shown in Figs. 6.11-b, 6.12-a and 6.13-a. The outputs are shown from the sample the fault classifier module was activated up to sample the logic confirmed the status of each phase. It takes the fault classifier module (FNN+logic) 6 to 13 samples (5 to 10.8 ms) after its activation to identify the faulty phase(s), as shown in Fig. 6.14. It should be noted that longer confirmation times are only associated with internal single phase to ground faults involving smaller percentages of the winding.

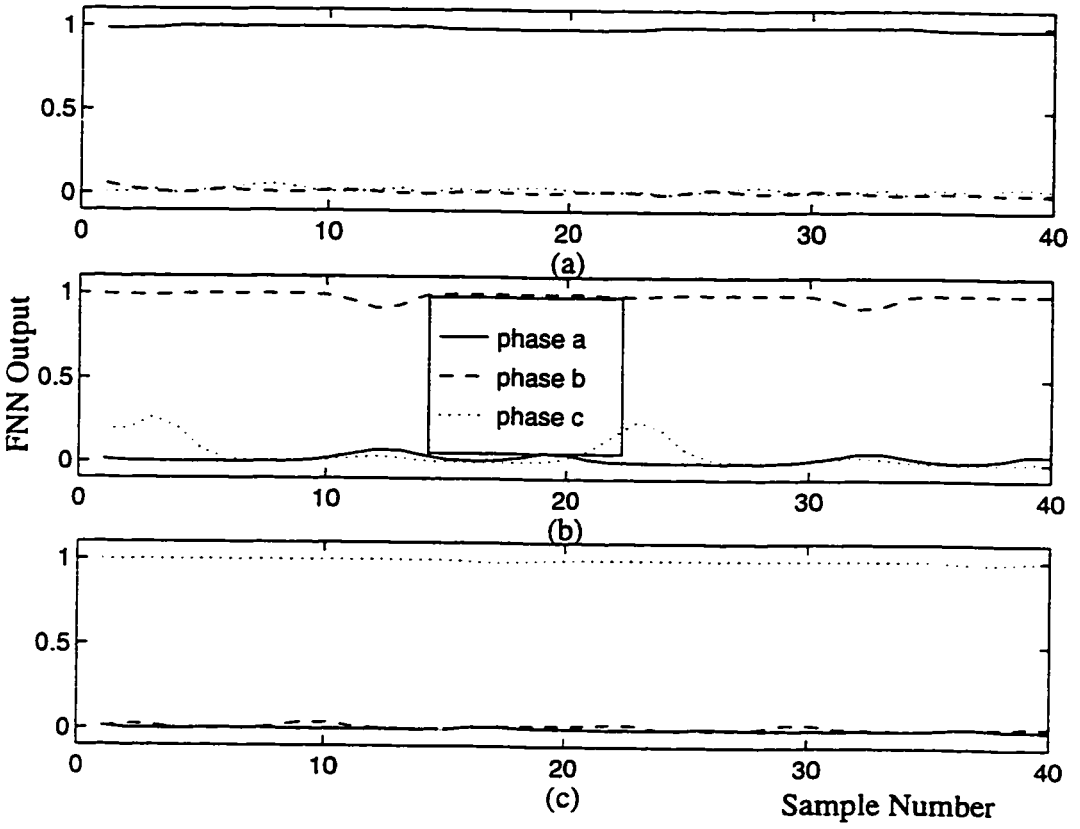

Figure 6.11: Results of the FNN fault classifier for internal single phase to ground faults. (a) G_3, fault at 77% of a, P=1.0 pu and pf=0.8 lag. (b) G_4, fault at 20% of b, P=0.8 pu and pf=0.8 lag. (c) G_6, fault at 88% of c, P=0.4 pu and pf=0.9 lag.

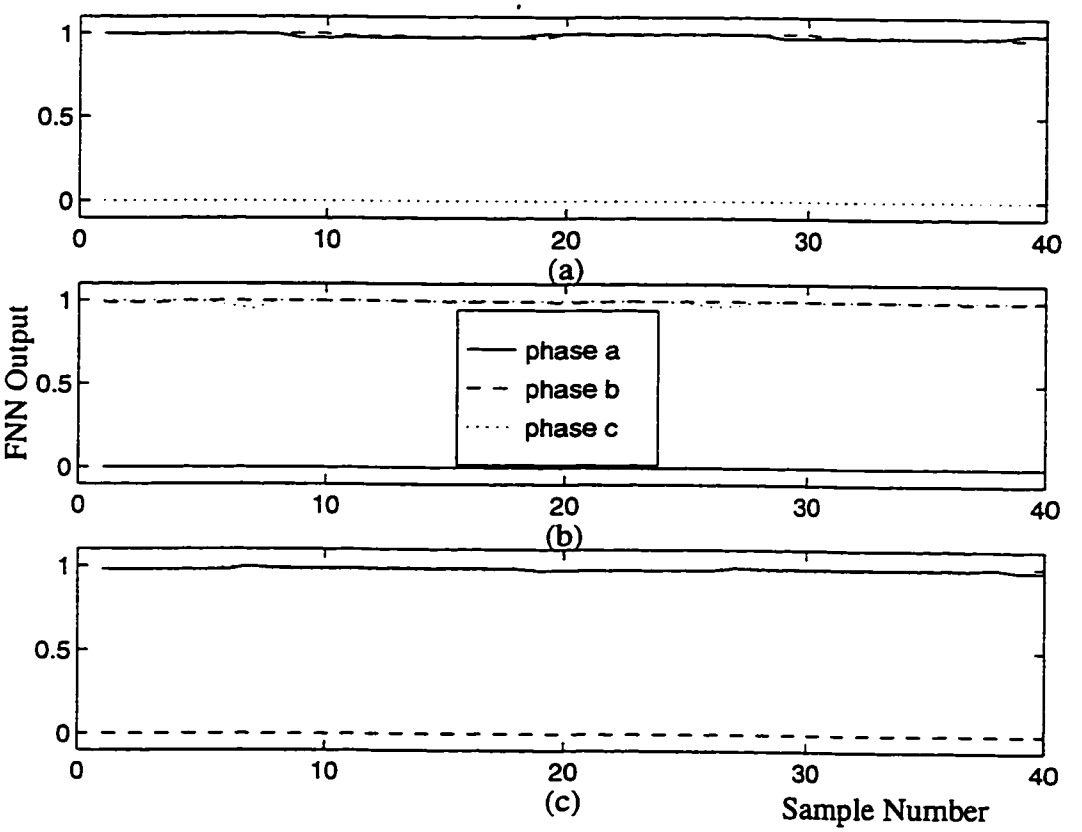

Figure 6.12: Results of the FNN fault classifier for internal two phase to ground faults. (a) G_5, fault at 62% of a & 50% of b, P=0.8 pu and pf=0.9 lag. (b) G_2, fault at 62% of b & 88% of c, P=0.5 pu and pf=0.9 lag. (c) G_5, fault at 25% of a & 37% of c, P=0.85 pu and pf=0.85 lag

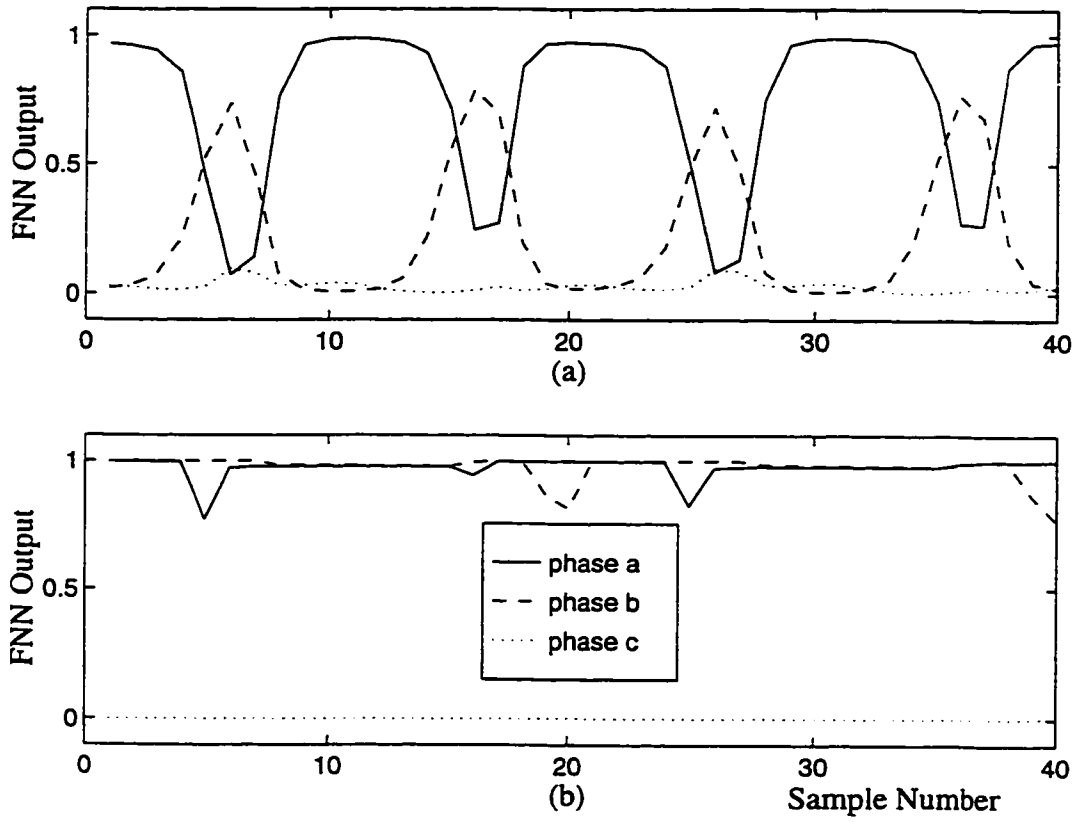

Figure 6.13: Results of the FNN fault classifier for light internal faults. (a) G_4, pg at 10% of a, P=0.6 pu and pf=0.9 lag. (b) G_5, ppg at 4% of a & 4% of b, P=0.4 pu and pf=0.8 lag.

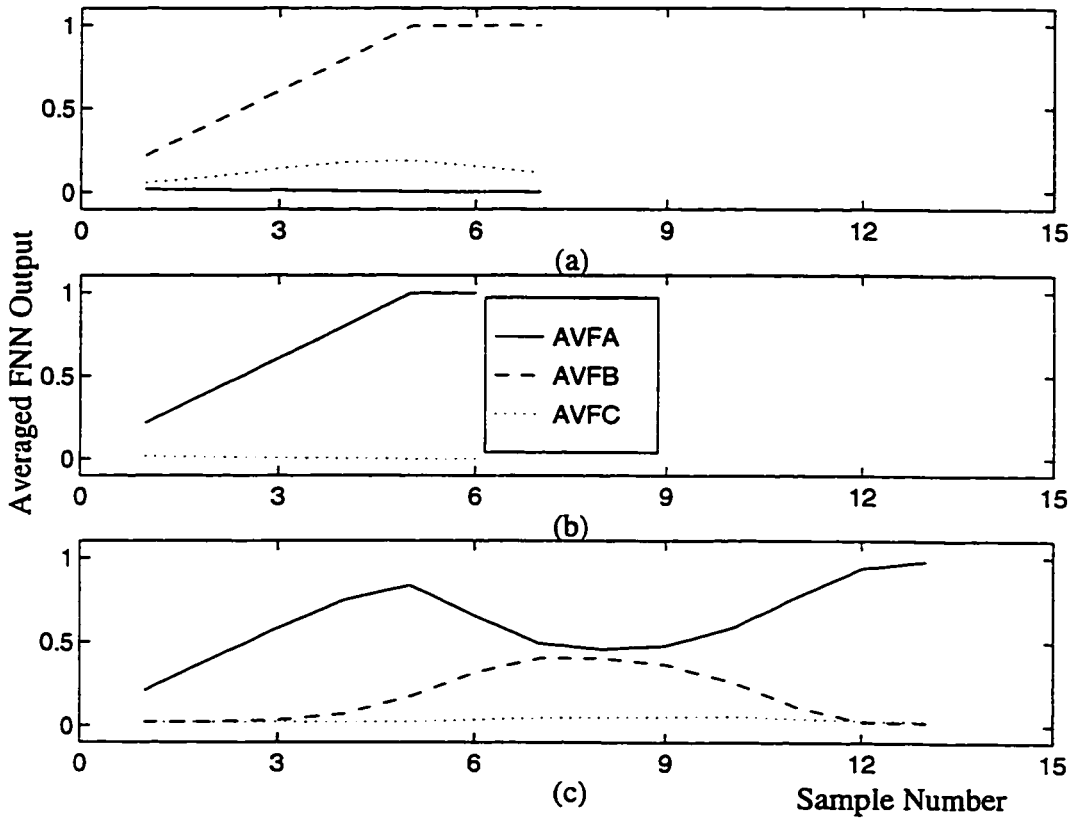

Figure 6.14: Outputs of the fault classifier confirmation logic. (a) G_4, pg at 20% of b, P=0.8 pu and pf=0.8 lag. (b) G_5, ppg at 62% of a & 50% of b, P=0.8 pu and pf=0.9 lag. (c) G_4, pg at 10% of a, P=0.6 pu and pf=0.9 lag.

6.5 Summary

The performance of the proposed protection scheme was tested using a set of independent test patterns in this chapter. Fault detection is fast, accurate and reliable even in the presence of current transformer mismatches or system transients. The relay tripping time, for the majority of internal faults, is well within half a cycle. This is faster than the conventional digital relays. The proposed relay also manages to detect light faults, which are normally not detected by the conventional digital relays. The results of the fault classifier module indicate that it is fast, robust and accurate, even for internal faults involving smaller percentages of the winding.

Chapter 7

Experimental Verification of Internal Faults

7.1 Introduction

Simulated current patterns representing different generator states have been used in Chapters 5 and 6 to train and test the NN based relay. In these simulations a direct 3-phase model of the generator, Section 2.4, was used to simulate normal operation and external faults. In Chapter 3 an internal faults algorithm, capable of simulating single and two phase to ground faults, was developed. While the methods of simulating normal operation and external faults are well documented in the literature [56–58, 60, 61], the internal faults algorithm [68–70] needs further experimental verification.

In this chapter simulation results showing the internal fault currents, during single phase to ground faults and two phase to ground faults, are compared with actual fault currents to verify the developed algorithm. The laboratory physical model, which consists of the power system model and the associated hardware, is described in Section 7.2. Results confirming the accuracy of the internal faults algorithm are then presented in Section 7.3.

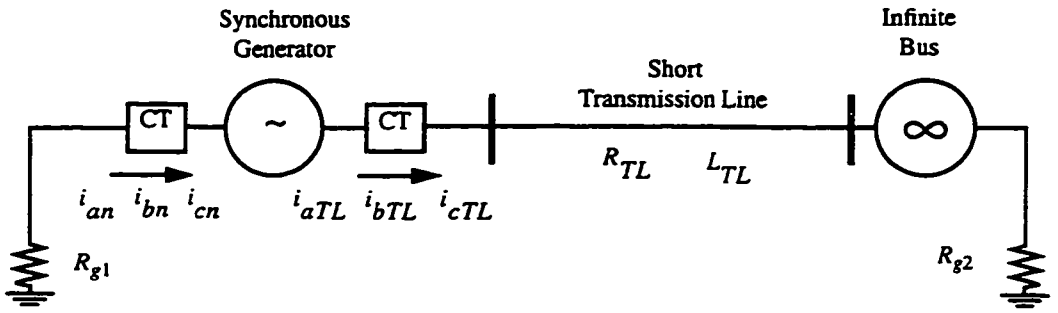

Figure 7.1: Single line diagram of the power system model implemented in the laboratory.

The effect of magnetic saturation on the performance of the algorithm is discussed in Section 7.4.

7.2 Physical Model

7.2.1 Power System Model

Figure 7.1 shows the single line diagram of the power system model implemented in the laboratory. It consists of a synchronous generator connected to an infinite bus (city power system) through a short TL, represented by a resistance R_{TL} and an inductance L_{TL}. Both the generator and the infinite bus neutrals are grounded through resistances R_{g1} and R_{g2}, respectively, in order to limit the short circuit currents. The synchronous generator is rated at 5 kVA, 210 V, 13.75 A, 1800 RPM. The synchronous machine is driven by a 4.5 kW, 250 V *dc* machine and does not have damper windings. The operating condition of the generator, i.e. active power and power factor, can be changed by changing the field currents of the *dc* motor and generator, respectively. Details of the model parameters are given in Appendix D.

The armature winding of the generator consists of two paths per phase. For the purpose of implementing internal faults, the two paths of each phase are connected in series, and the mid point of one or more of the phases (50%

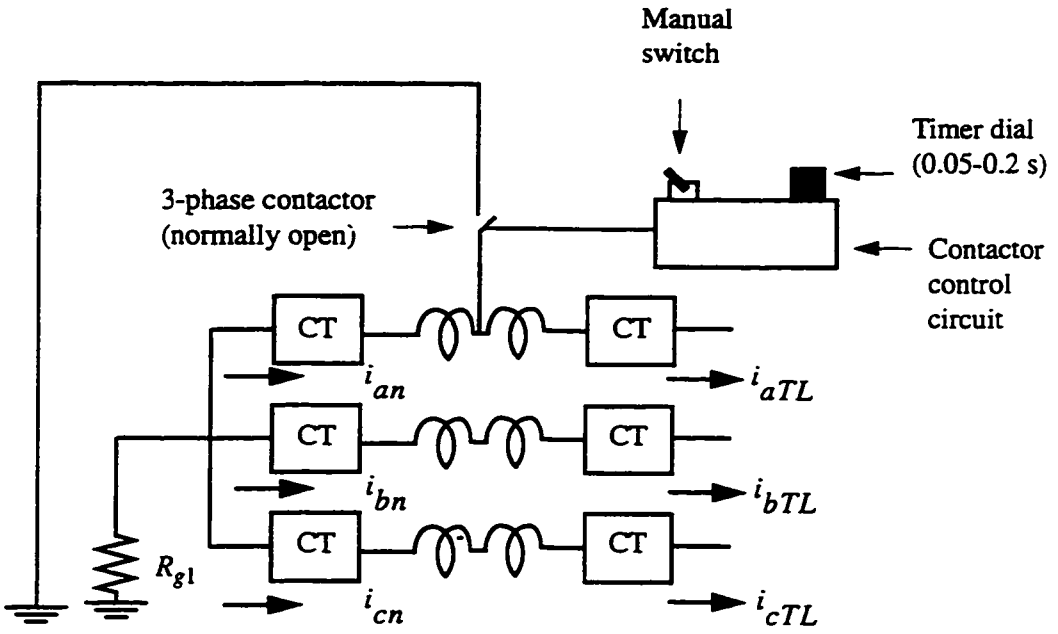

Figure 7.2: Detailed drawing of a single phase internal fault connection.

of the winding) is connected to the ground through a 3-phase contactor, Fig. 7.2. A timer is inserted in the control circuit of the contactor that allows for an internal fault to occur for a period ranging from 0.05 to 0.2 s. In order to initiate and record an internal fault, the procedure is:

1. Connect the mid point of the desired phase(s) to the 3-phase contactor.
2. Operate the generator at the desired power and power factor.
3. Adjust the timer dial to a specified time.
4. Operate the manual switch of the contactor control circuit. This will cause an internal fault to occur for a specified time, then the machine will return to normal operation. Prefault, fault and post-fault currents are recorded by means of the implemented hardware, which is described in the next section.

7.2.2 Hardware Structure

Current transformers, having turns ratio of 50/5 A, are used in this laboratory setup with current shunts (5A/100mV) connected to their secondaries. Fig. 7.3. An additional current shunt (2A/100mV) is connected in the field circuit, to enable recording the field current. As the produced voltage signals are in the millivolt range, it is essential to amplify the signals before converting them to digital form. A 6-channel amplifier, available at the power system laboratory of the University of Calgary, is used for amplification purposes. As there are only 6-channels available, so in addition to the field current, five more currents (3 line-side and 2 neutral-end currents) can be recorded. These channels are sufficient for all types of tests that are required to be done in this dissertation. The amplifier is adjusted to have a gain of 25, so the input voltage signals under normal conditions would be in the range of 0.7 V, and under fault conditions they would range from 2 to 12 V (depending on the type of fault).

A data acquisition system (DAS) is connected to the amplifier output to record the internal fault currents, as shown in Fig. 7.3. The DAS is connected to a digital signal processing (DSP) board, supplied by Spectrum Signal Processing Inc., via two links. One link is for the multiplexing command and the other for the analog voltage signals to pass on to the analog to digital converter (A/D) of the DSP board. The DSP board contains a Texas Instruments TMS320C30 DSP chip. The chip is a 32-bit floating point device with a speed of 16.7 million instructions per second. Its performance is further enhanced through its large on-chip memories, direct memory access (DMA) controller, two external interface ports and an instruction cache. The board is mounted inside an 80486 PC which is equipped with corresponding development and debugging tools. The recorded currents of different internal faults are finally saved in files in the PC. These files are later used to compare

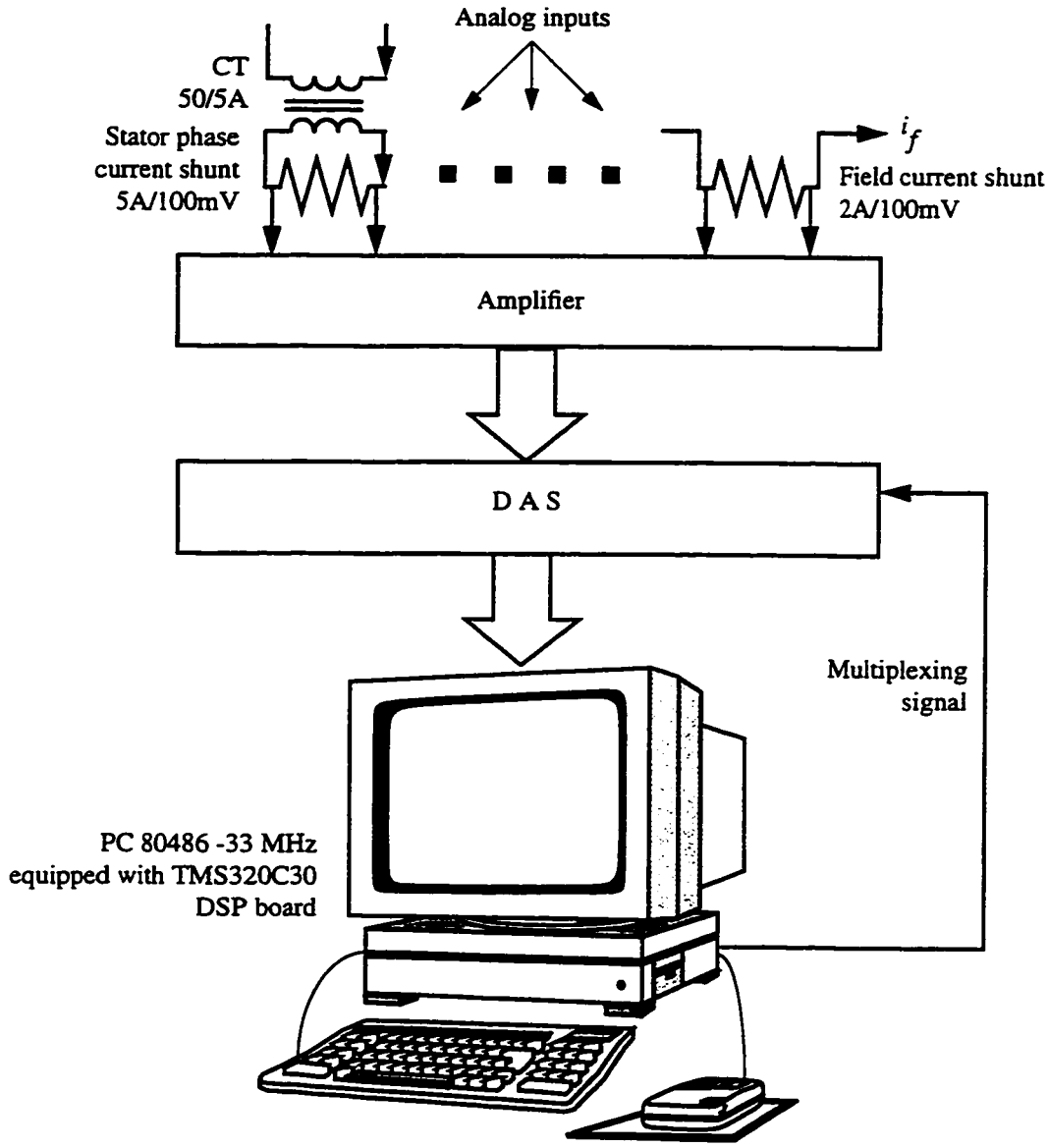

Figure 7.3: Hardware structure.

actual and simulated fault currents.

7.3 Comparison Between Laboratory and Simulation Results

Several internal single phase to ground and two phase to ground faults, at different prefault loading conditions, power factors and fault inception times, were performed using the previously described laboratory setup. The parameters of the power system model, Appendix D, and the prefault data have been used by the internal single phase to ground and two phase to ground faults algorithm, Section 3.3, to simulate fault currents similar to the obtained test fault currents, for comparison purposes.

Comparisons between laboratory and simulation results for internal single phase to ground faults are shown in Figs. 7.4,7.5 and 7.6. The fault currents shown in Fig. 7.4 are for an internal single phase to ground fault at 50% (tap-to-neutral) of phase a. As the fault occurred in phase a, the currents on the line-side of phases b and c would be equal to their counterparts on the neutral-end, i.e. i_b=i_{bTL}=i_{bn} and i_c=i_{cTL}=i_{cn}, hence it is sufficient to show only one current for each healthy phase. The fault currents shown in Figs. 7.5 and 7.6 are for similar faults in phases b and c,respectively. It can be concluded from Figs. 7.4,7.5 and 7.6 that the computed fault currents closely match the recorded fault currents. The maximum difference between fault currents obtained by the proposed method and their recorded counterparts is 1% to 12%. An additional 10 internal single phase to ground faults were performed and compared to the simulation results. All results are similar to those in Figs. 7.4,7.5 and 7.6.

The proposed internal two phase to ground faults algorithm, Section 3.3.2, has been used to simulate an internal fault at 50% of phases a and b, Fig. 7.7.

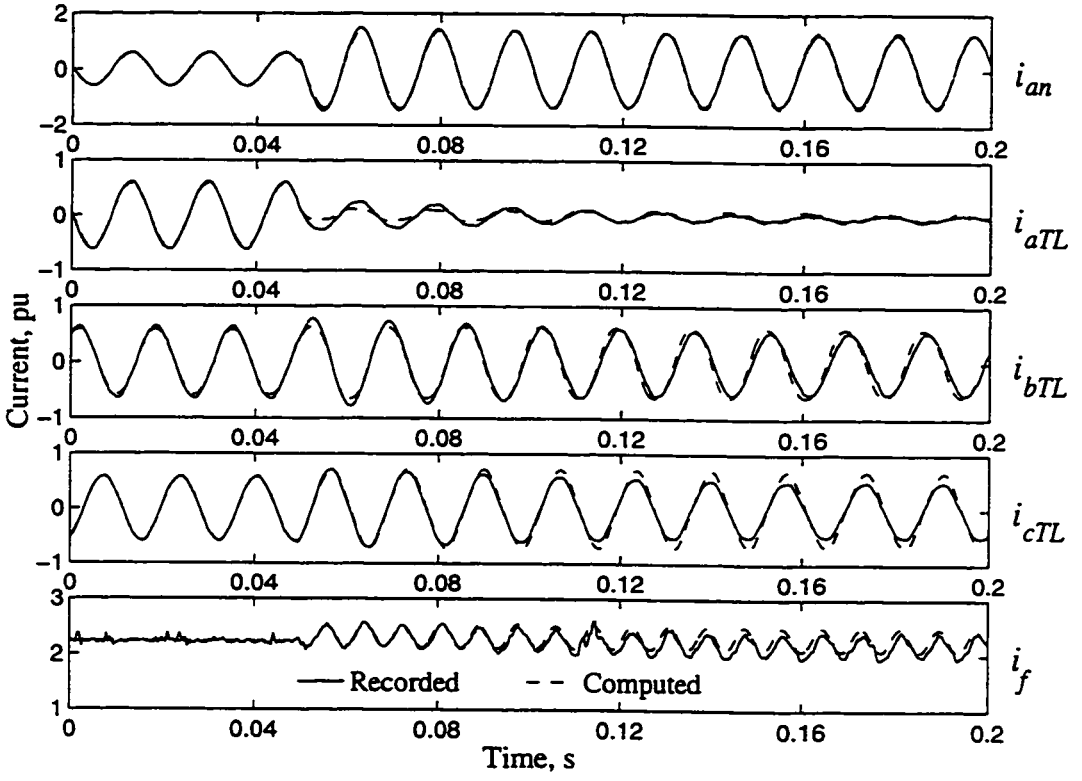

Figure 7.4: Computed and recorded currents for an internal single phase fault at 50% of phase a, P=0.42 pu and pf=0.86 lag.

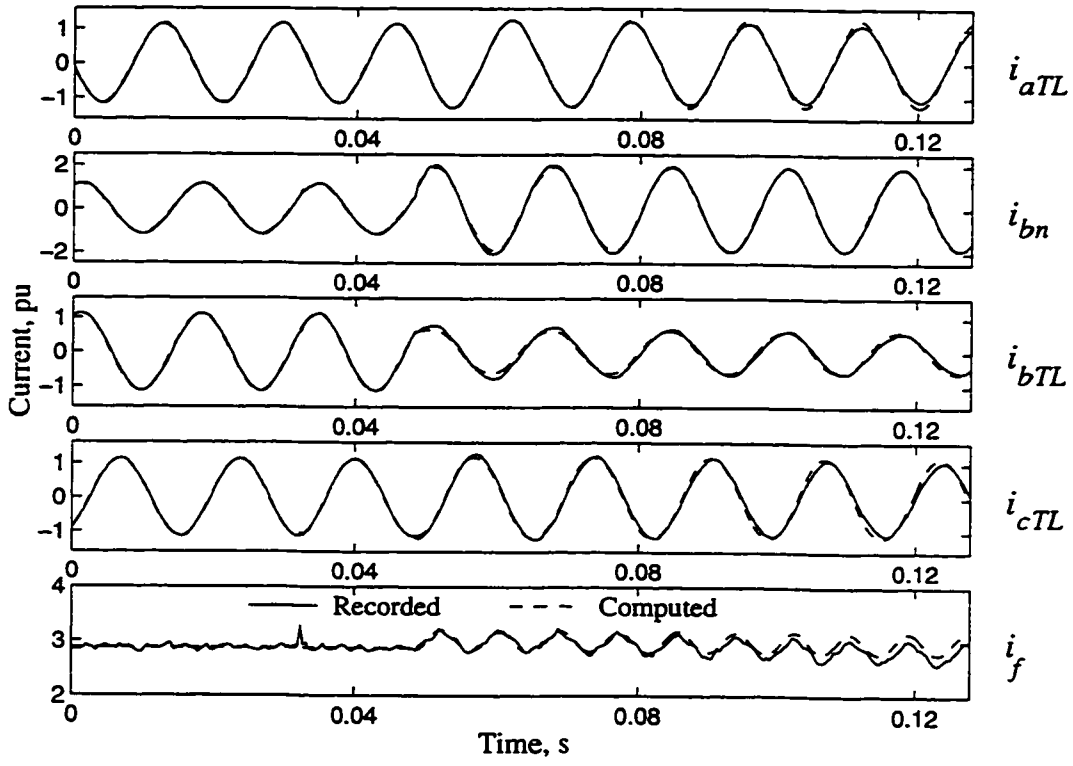

Figure 7.5: Computed and recorded currents for an internal single phase fault at 50% of phase *b*, P=0.81 pu and pf=0.95 lag.

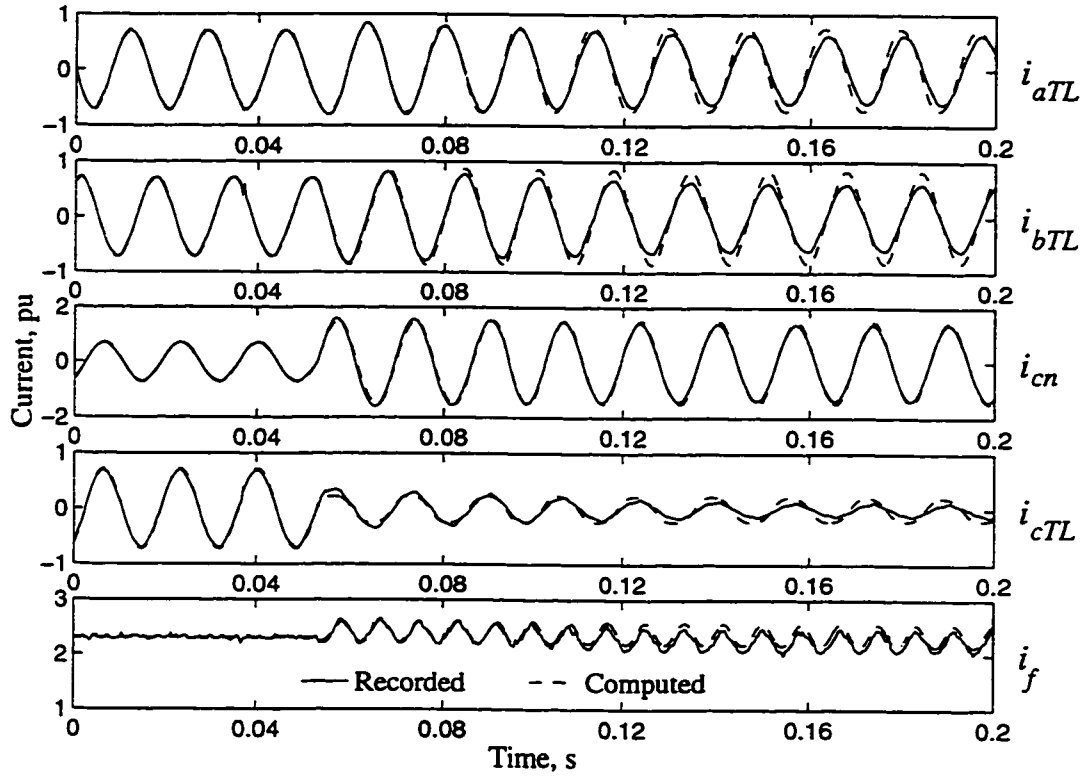

Figure 7.6: Computed and recorded currents for an internal single phase fault at 50% of phase *c*, P=0.52 pu and pf=0.97 lag.

Although there exists a resemblance between the computed and the recorded currents for $i_{an}, i_{aTL}, i_{bn}, i_{bTL}$ and i_f, there is a significant difference in phase between computed and recorded currents for the healthy phase, i.e. phase c. The same results were obtained when comparisons were done for internal two phase to ground faults at 50% of phases a and c and phases b and c. It should be noted that the unsaturated parameters of the machine are used in the simulations. So, in order to improve the performance of the internal two phase to ground faults algorithm some form of magnetic saturation has to be considered. Inclusion of magnetic saturation is described in the next section. At the same time, the results of the internal two phase to ground faults algorithm should not affect the NN based relay for two reasons. The first is that fault detection and classification occur in the first cycle following the fault, and as shown in Fig. 7.7 the computed and recorded currents do match in the first cycle. The other reason is that the phase difference occurs in the healthy phase and not in the faulty phases, which have more influence in the relay fault detection and classification decisions. Real-time results. validating these claims, are presented in the next chapter.

7.4 Magnetic Saturation

Different saturation formulas are available for the $d-q-0$ model of the synchronous machine [75–77]. However, formulas for saturation in direct phase quantities, in-particular with the machine suffering from an internal fault, are unavailable. But, it is often recognized that machines operate in the saturated region under both steady-state and transient conditions [78]. Hence, in an attempt to improve the simulation results of the internal two phase to ground faults, the saturated steady-state parameters of the machine are used, i.e. those parameters that correspond to the prefault operating point

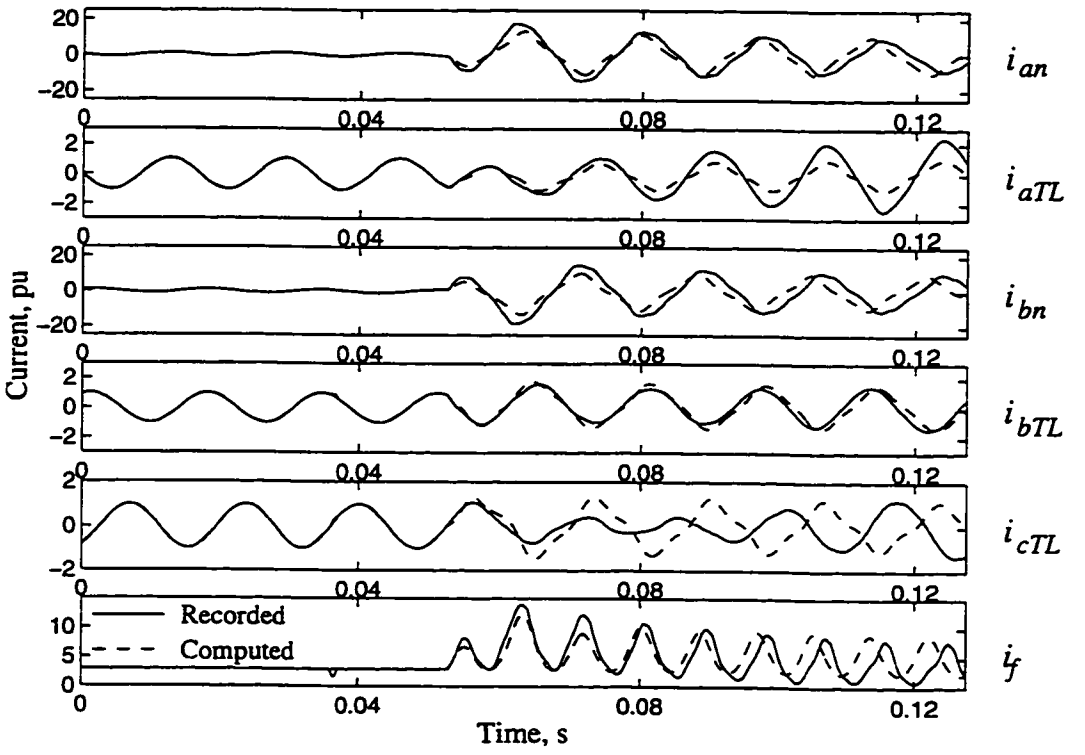

Figure 7.7: Fault currents, computed and recorded, for an internal two phase to ground fault at 50% of phases a and b, obtained using the unsaturated parameters, P=0.73 pu and pf=0.95 lag.

of the machine.

To obtain the saturated parameters of the machine, the information used is the open circuit characteristics (OCC) that represent the saturated relationship between the magnetizing current and the mutual flux linkage in the direct axis, and the results of the asynchronous test that gives the relationship between the direct axis and the quadrature axis. The accuracy of the obtained saturated steady-state parameters is confirmed by using them to solve the steady-state equations of the machine [56], and then comparing the value of the obtained field current with the measured one.

The internal two phase to ground fault, shown in Fig. 7.7, was simulated again using the saturated steady-state parameters that correspond to the prefault operating point. Figure ..5 shows a comparison between the computed and the recorded fault currents. It is clear that there is a significant improvement in the simulation results. There is a closer match between simulation and real fault currents, in-particular in the first few cycles following the fault. At a few cycles after the fault, the difference between both currents increases. This may be attributed to a change in the machine parameters, that is not accounted for in the simulations.

Comparisons are also done for internal faults to ground at 50% of other phases, i.e. a, c and b, c, as shown in Figs. 7.9 and 7.10. The results of Figs. 7.9 and 7.10 are identical to those in Fig. 7.8 in terms of resemblance with real fault currents. Using the saturated steady-state parameters for simulating internal single phase to ground faults produces almost the same results as those shown in Figs. 7.4,7.5 and 7.6.

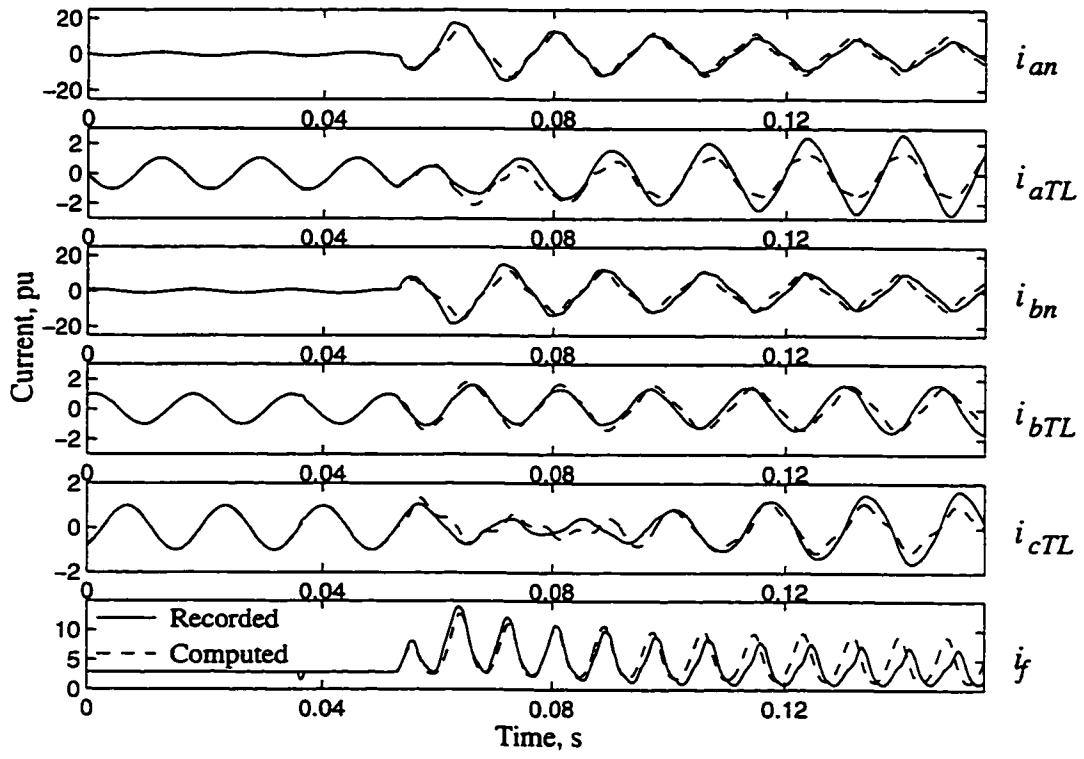

Figure 7.8: Fault currents, computed and recorded, for an internal two phase to ground fault at 50% of phases a and b, obtained using the saturated parameters, P=0.73 pu and pf=0.95 lag.

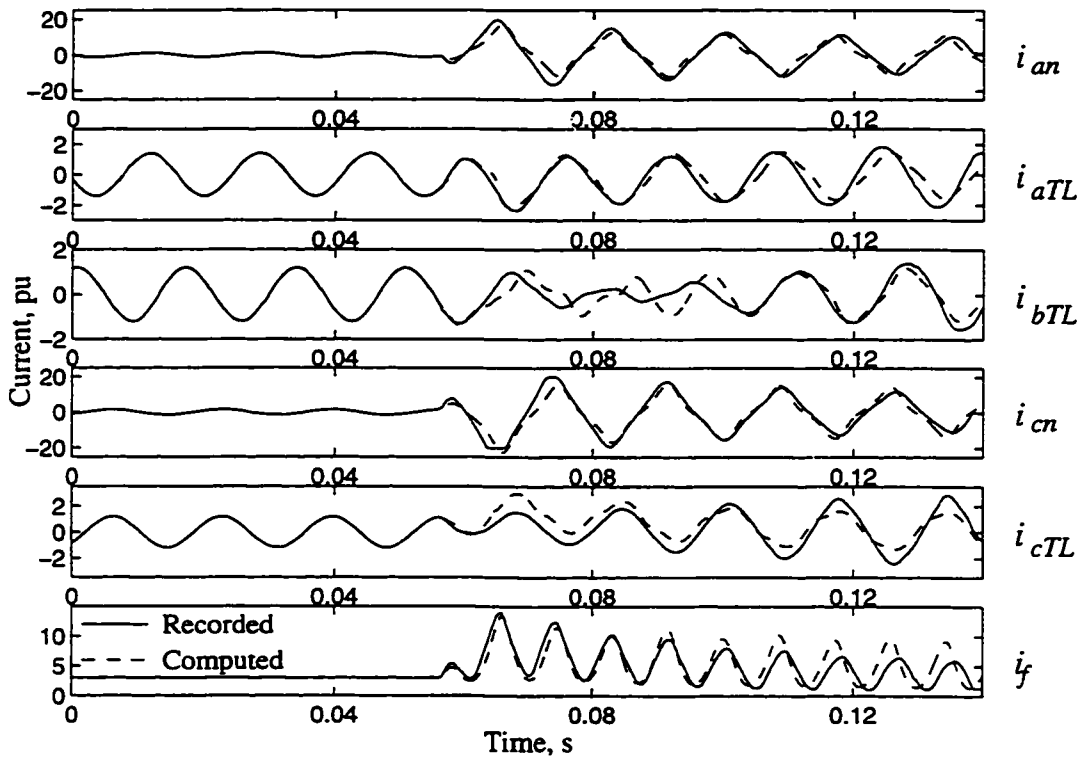

Figure 7.9: Fault currents, computed and recorded, for an internal two phase to ground fault at 50% of phases a and c, obtained using the saturated parameters, P=0.86 pu and pf=0.95 lag.

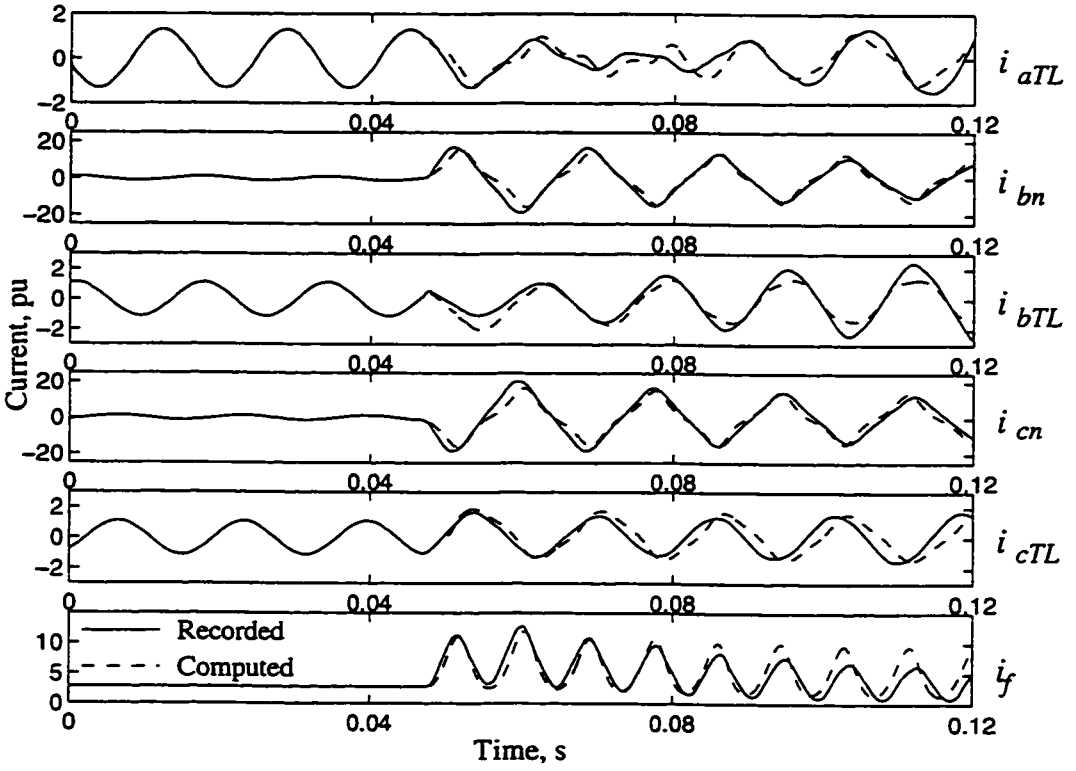

Figure 7.10: Fault currents, computed and recorded, for an internal two phase to ground fault at 50% of phases b and c, obtained using the saturated parameters, P=0.8 pu and pf=0.95 lag.

7.5 Summary

In this chapter simulation results, obtained by the developed internal faults algorithm, are compared with actual fault currents. The model has high accuracy in the case of internal single phase to ground faults. In the case of internal two phase to ground faults, the unsaturated parameters cause a phase shift to occur between the computed and recorded currents for the healthy phase. Saturated steady-state parameters, when used in the internal two phase to ground faults algorithm, produce more accurate results. Saturated steady-state parameters do not affect the internal single phase to ground faults algorithm.

Chapter 8

Relay Laboratory Implementation and Real-Time Test Results

8.1 Introduction

Results in Chapter 6 have shown that the NN based relay exhibits very good performance [72–74]. Like most other neural network based research, the results in Chapter 6 are based on computer simulations. In these simulations, the generator states were simulated using a set of simultaneous differential equations, and NNs were simulated by using a sequential algorithm to simulate the parallel distributed nature of NNs. The simulation results presented may be said to be close to the expected in a physical system for the following reasons:

- The direct 3-phase model represents fairly closely the physical system, as it retains the generator nonlinear model and takes into consideration the variation of speed during transient conditions [60, 61]

- The developed internal faults algorithm produces fault currents which are very similar to actual fault currents, as shown in Chapter 7.

- The sequential algorithm can obtain the same output of a dedicated NN hardware, except for a longer computation time [71].

Computer simulation is still different from the real physical system since the operating environment of the physical system is not ideal, due to the existence of noise, CT mismatches and CT saturation. Therefore, after theoretical development and computer simulation, the next desirable step is to evaluate the relay performance on a physical model.

As it is necessary to implement a NN based relay in hardware and make sure that the calculation time is less than the inter-sampling period, very few laboratory implementations of NN based relays are reported in the literature. A FNN based technique, that distinguishes between magnetizing inrush and internal fault currents of a power transformer, has been implemented in a laboratory environment [79]. The FNN based technique is a part of a transformer protection algorithm.

The implementation of a NN based relay in a laboratory environment is reported in this chapter. The physical model, used to implement the NN based relay and test it, is the same one described in Section 7.2 and shown in Figs. 7.1,7.2 and 7.3. Since a dedicated NN hardware was not available at the time of implementation, a sequential simulation method was employed to implement the NN based relay in software on the DSP board described in Chapter 7. Details of the relay implementation are described in Section 8.2. Effectiveness of the NN based relay, in response to different operating conditions and various types of faults, is demonstrated in Section 8.3.

8.2 Relay Implementation

8.2.1 Neural Network Weights

The FNNs used in the relay operate in a static manner. In other words, they were trained off-line, and once the desired performance was achieved the weights and biases of the FNNs were frozen. So, the main objective of the experimental work is to verify that the previously trained FNNs can perform well when exposed to actual current patterns. For that reason the weights and biases of the FNNs used in the relay implementation are the same ones obtained from the off-line training process described in Chapter 5.

8.2.2 Sequential Implementation of Parallel Mechanism

Parallel processing is one of the most important properties of the neural networks. The neurons in a layer operate in parallel. This results in high speed operation. Research on designing NNs by using modern technology is advancing very fast. However, because NN hardware was not available in the laboratory at the time of implementation, a sequential implementation method was designed to simulate the parallel mechanism.

The sequential implementation method is very similar to the NN simulation used in the simulation studies in the previous chapters. Instead of allowing all neurons in the same layer to compute simultaneously, this method only allows neurons to compute one after another. The computation starts from the first neuron of the first layer and ends with the last neuron of the output layer. The output of each neuron is held constant until the next computation cycle starts. This method results in an output similar to that of a real NN except that the computation time is longer here.

8.2.3 Physical Model

As mentioned in the introduction, the physical model, which was used to verify the internal faults algorithm in Chapter 7, is used to implement and test the relay. So, the power system model, Fig. 7.1, is not changed, but the location and type of fault are changed by changing the connection of the 3-phase contactor, Fig. 7.2. In this way internal faults at 50% and 100% of the winding can be carried out, as well as external faults at the machine terminals and at the end of the TL. The type of the fault can be either a ground fault, a phase to phase fault or a 3-phase fault.

In this dissertation a sampling rate of 1200 Hz (20 samples/cycle) is used as mentioned in Section 5.3. Hence, to avoid aliasing problems, an antialiasing low pass filter, with a cut-off frequency of 600 Hz, is inserted between the amplifier and the DAS. The amplifier and the DAS are shown in Fig. 7.3.

8.2.4 Software Structure

The relay software, running on DSP, is developed in C language. In addition, a communication routine, running on PC, is also developed to further facilitate the implementation process. Flow chart of the PC communication routine is shown in Fig. 8.1. This routine functions as a man machine interface. It first initializes vectors and flags for DSP-PC communication. Then, it loads the DSP code into the chip. It then reads the FNNs weights and biases and sends them to the DSP chip through dual access RAM (DARAM). After the inception of the main relay loop by the DSP, the PC communication routine reads the outputs of the fault detector module and trip logic module. It should be noted that once the relay detects an internal fault, it activates the fault classifier module, and subsequently the communica-

tion routine reads the outputs of the fault classifier module. Once the DSP program is stopped, as explained below, the output data is saved in a file.

Flow chart of the program running on the DSP board is shown in Fig. 8.2. This program first initializes the vectors and flags for DSP-PC communication, reads the FNNs parameters from DARAM, reset all counters and set all the scales. The setting of the scales is very important as all inputs should have a value between ± 1, so they can be processed by the FNNs. After initializing the DAS and the sampling time counter, the DSP program enters the main relay loop. The relay then waits for the DAS program to be executed. The DAS program is a very small program, which is also performed by the DSP board. In this program multiplexing, A/D conversion and scaling of each input signal is done at the beginning of each inter-sampling period. The DAS program is executed in about 0.12 ms. Following that, the main relay loop proceeds in the same manner as described in Chapter 5 for the relay operation. The DSP program is stopped if an internal fault is detected and classified or if an external fault is detected, as indicated in Fig. 8.2.

In order to improve the computation speed of the DSP program, Fig. 8.2, the tan-sigmoid neurons in the hidden layers of the FNNs are calculated by means of a look-up table. The tan-sigmoid function in (A.7) is broken-into 14000 points in the look-up table. In this manner, the total weighted sum, v, of each neuron is calculated and the output of the neuron is obtained by means of the look-up table. This will speed-up the computation time of the program. Hence, the main relay loop, including the DAS program, is executed in 0.76 ms. This time is well within the available inter-sampling time of 0.833 ms.

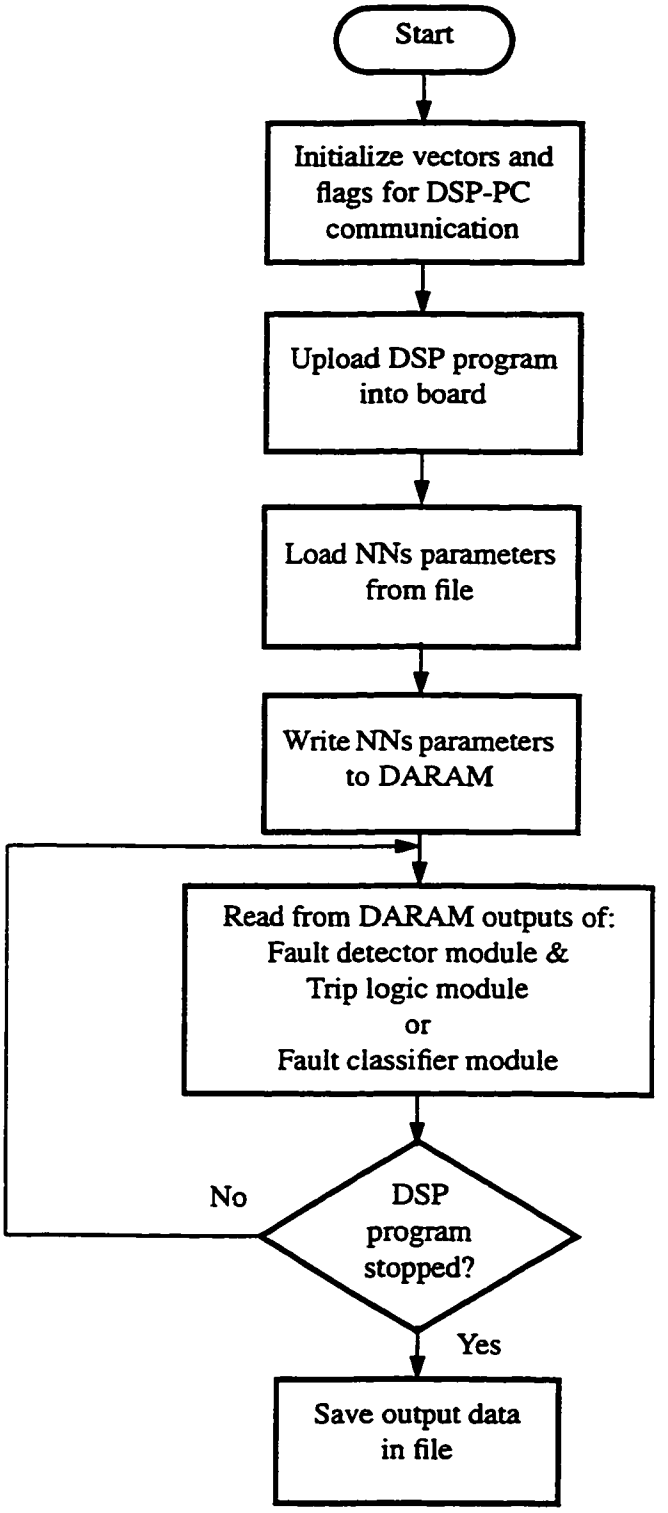

Figure 8.1: Flow chart of the PC communication routine.

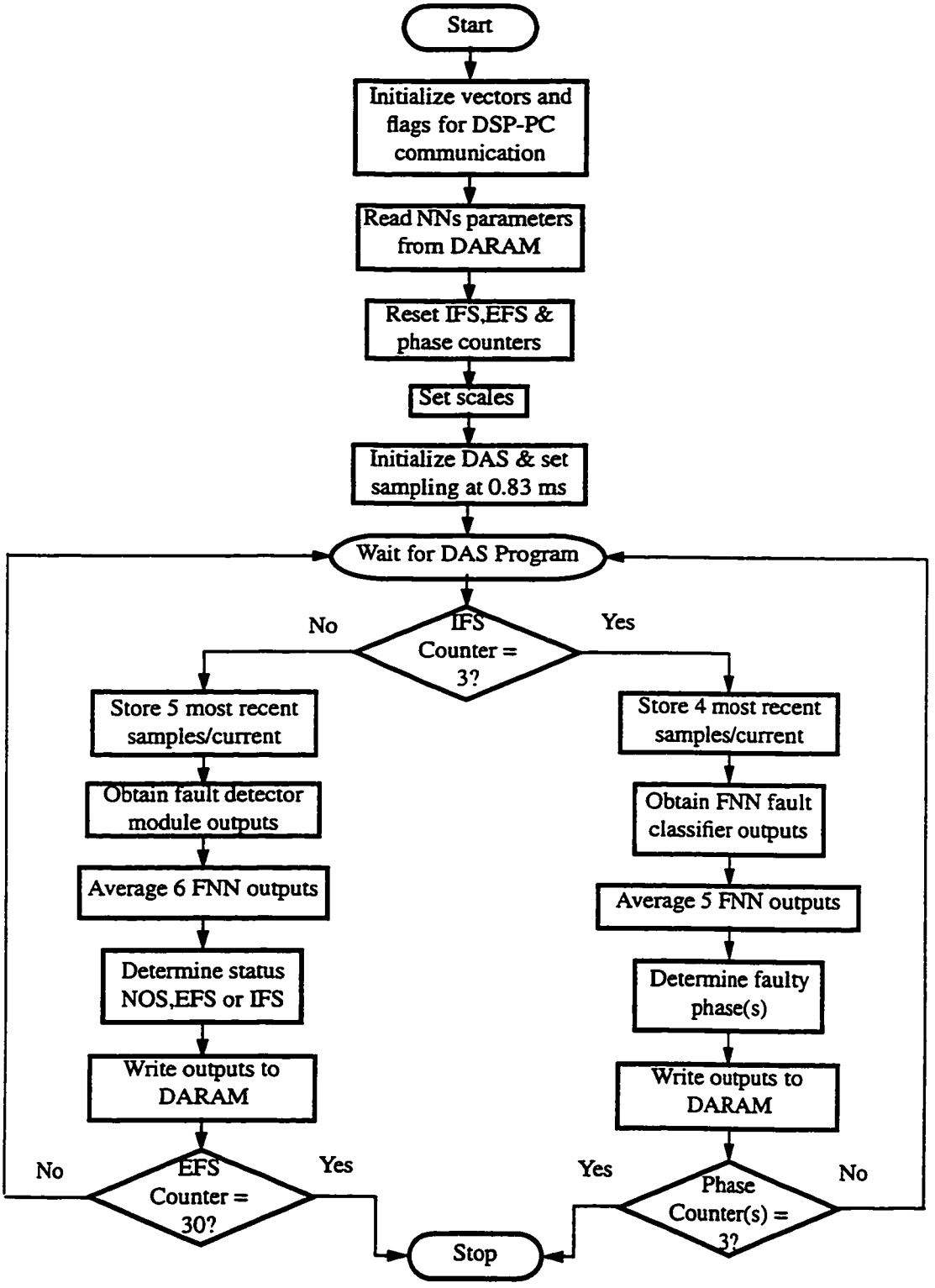

Figure 8.2: Flow chart of the DSP program.

8.3 Real-Time Test Results

8.3.1 NOS Results

Figure 8.3 shows the real-time test results of the fault detector module and trip logic module during normal operation. It is noticed that the EFS and IFS output neurons have slightly higher values than in the simulation results shown in Chapter 6. This may be attributed to CT mismatches and noisy current patterns. However, the FNN based fault detector module is still able to accurately identify the state of the generator, Fig. 8.3-a. Also, the averaging scheme of the trip logic module smooths the outputs of all three neurons, Fig. 8.3-b. Finally the NOS condition specified in (5.2) enables the relay to identify a NOS even in the presence of noisy signals and CT mismatches.

8.3.2 EFS Results

The DSP program, Fig. 8.2, allows for an external fault to persist for 30 samples after its detection before it is stopped. In other words, if the DSP board is connected to a circuit breaker, which is not the case, a trip signal will be issued after 30 samples based on the detection of a prolonged external fault. All the results presented in this section are up to the sample the DSP program is stopped. The terms used in the figures captions to indicate the type of fault, phases involved, ...etc are the same as those used in Chapter 6.

The results shown in Figs. 8.4 and 8.5 are for external single phase to ground faults occurring at the machine terminals and at the end of the TL, respectively. The NN based relay clearly indicated the existence of an EFS for the fault at the machine terminals, Fig. 8.4. The performance of the relay for the fault at the end of the TL, Fig. 8.5, is very good considering that this is a light fault and the impedance of the TL, Appendix D, is three

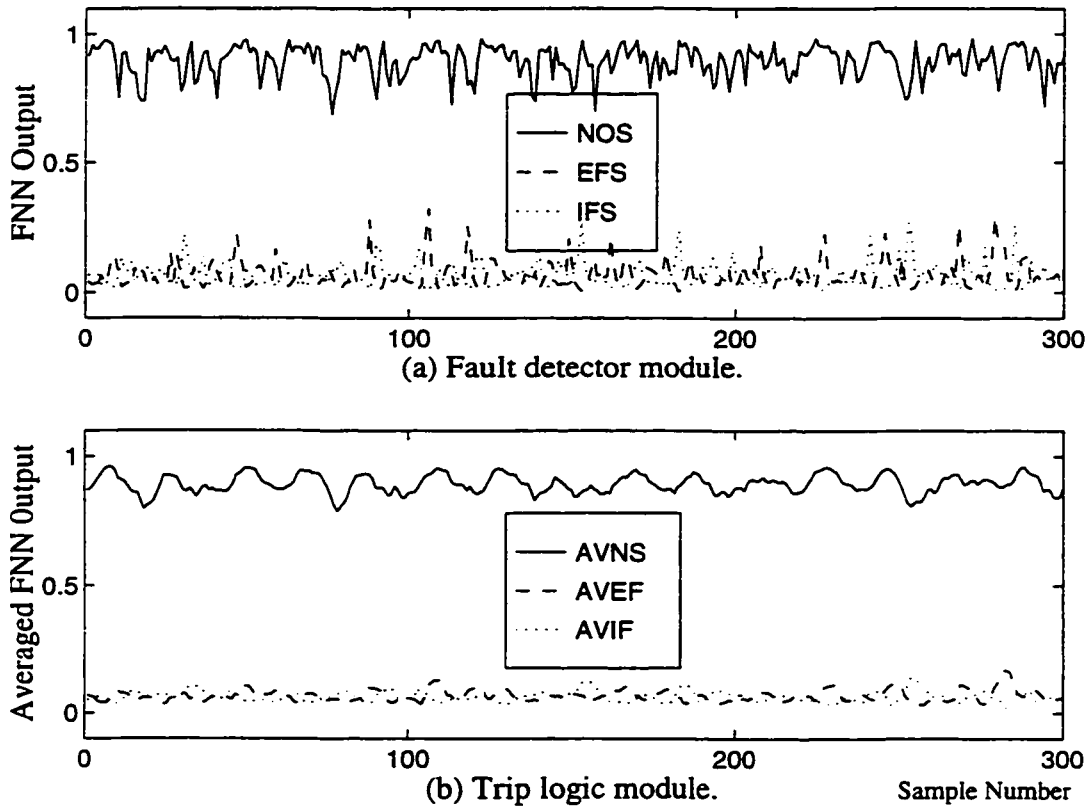

Figure 8.3: NOS, P=0.5 pu and pf=0.85 lag.

times bigger than the one used in the simulation studies, Appendix C.

Current transformer mismatches are more appreciable during external faults involving more than one phase. The response of the NN based relay to a phase to phase fault is shown in Fig. 8.6 and to a two phase to ground fault is shown in Fig. 8.7. It is shown that the relay is not affected by CT mismatches, which can cause a conventional digital differential relay to maloperate.

In this laboratory setup it has been found that a terminal 3 phase fault causes CTs to saturate. Current transformer saturation presents a problem to differential relays in general. The response of the relay to a 3 phase fault at the machine terminals is shown in Fig. 8.8. The relay clearly indicated the existence of an EFS. The only effect of saturation may be the fluctuations occurring, in the EFS and IFS neurons, for a couple of samples. However, the averaging scheme diminished these fluctuations and the tripping speed of the relay has also not been affected, Fig. 8.8-b. In this case also the performance of the NN based relay is better than the conventional digital relay.

8.3.3 IFS Results

For internal faults, the DSP program, Fig. 8.2, detects an internal fault and then activates the fault classifier module to identify the faulted phase(s). The DSP program is stopped after the classification is done. For each internal fault presented in this section the results of the fault detector module, trip logic module, FNN fault classifier and fault classifier confirmation logic are shown.

The results shown in Fig. 8.9 are for an internal single phase to ground fault at 100% of phase *b*, and those in Fig. 8.10 are for a similar fault at 50% of phase *a*. It is noticed that even though the relay has not been exposed to an internal fault at 100% of the winding during the simulation studies, the

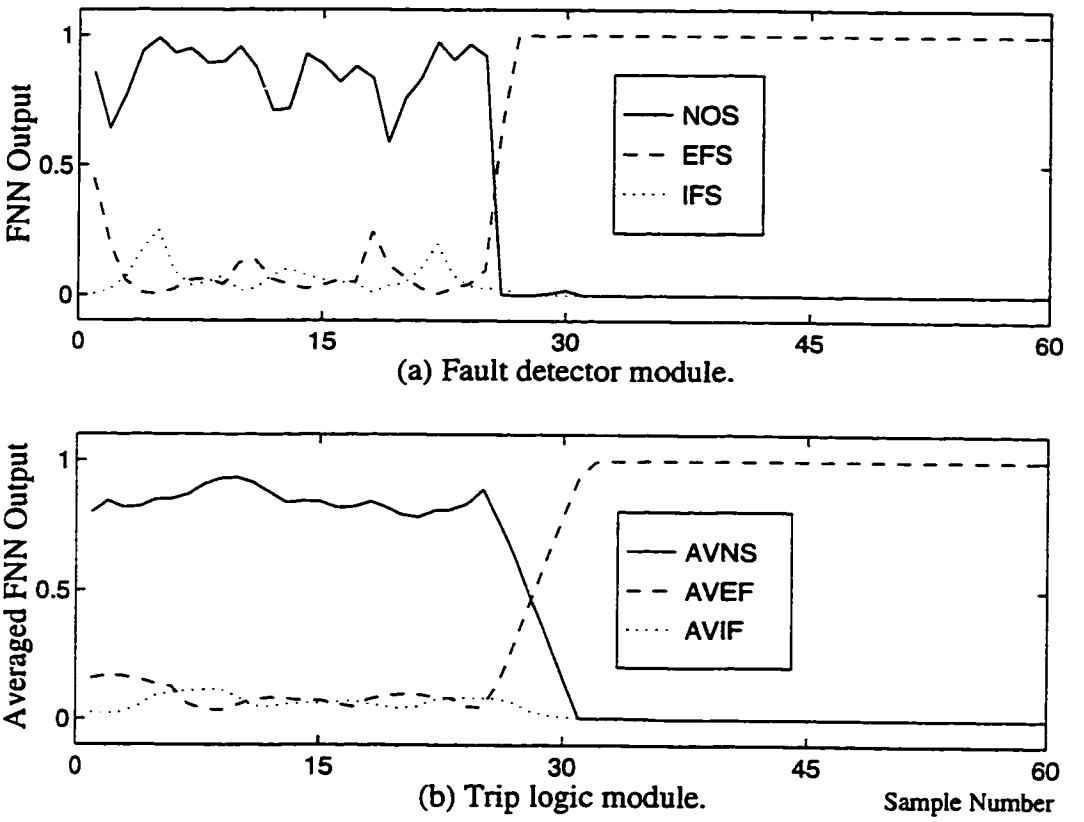

Figure 8.4: EFS, pg *c*, at machine terminals, P=0.76 pu, pf=0.95 lead and FI=25.

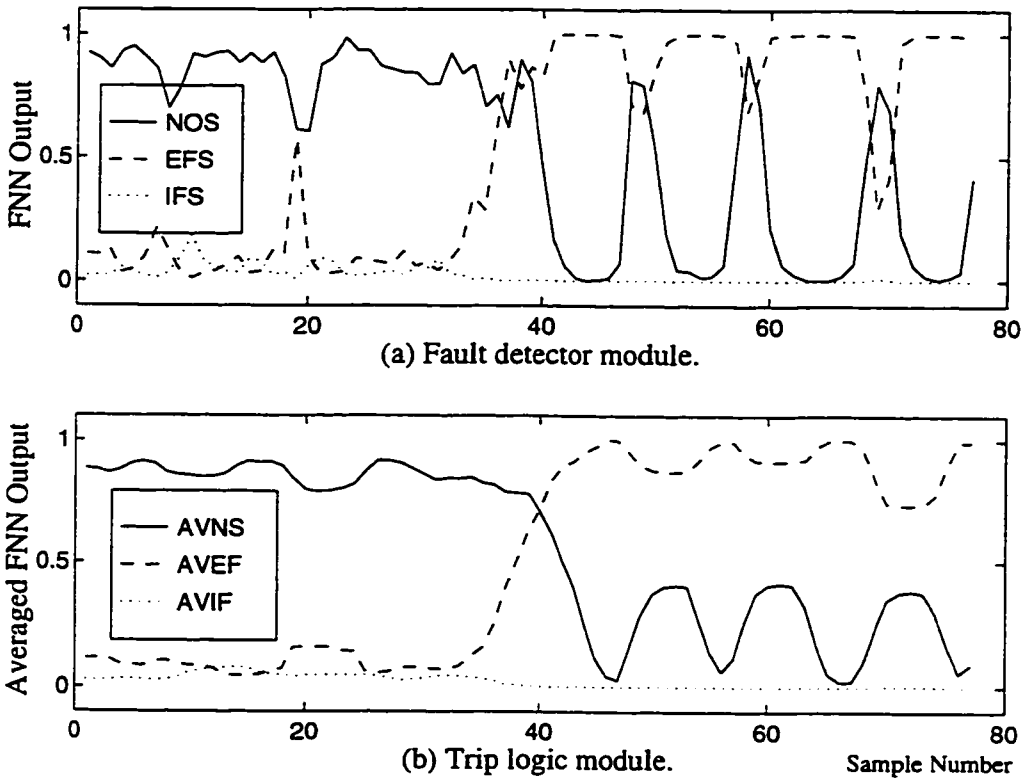

Figure 8.5: EFS, pg a, at end of TL, P=0.73 pu, pf=0.78 lag and FI=34.

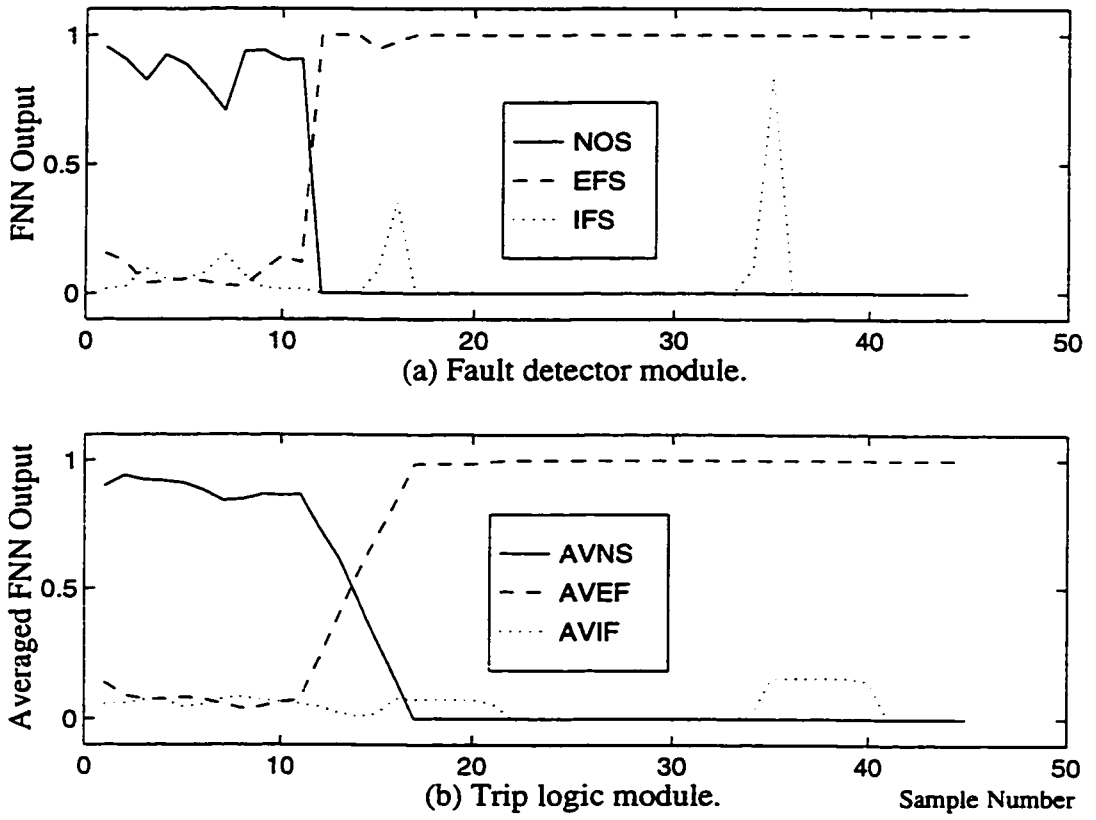

Figure 8.6: EFS, pp a, b, at machine terminals, P=0.47 pu, pf=0.8 lag and FI=11.

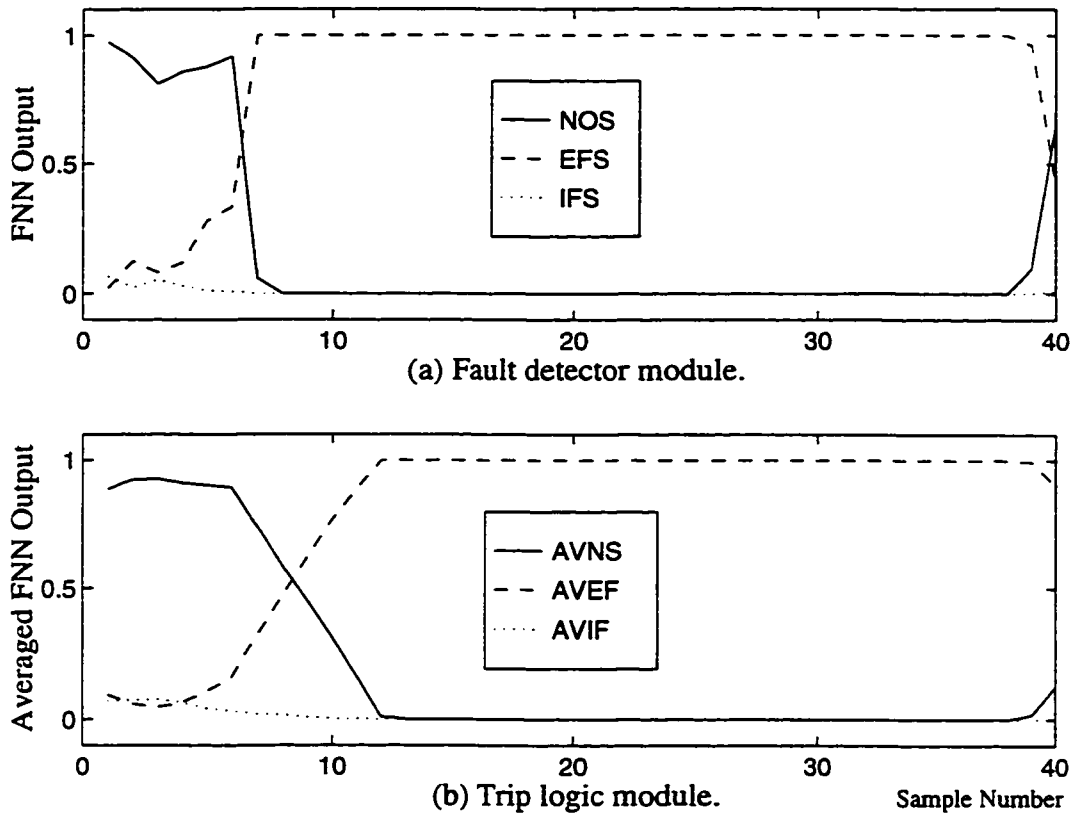

Figure 8.7: EFS, ppg a, c, at end of TL, P=0.8 pu, pf=0.8 lag and FI=4.

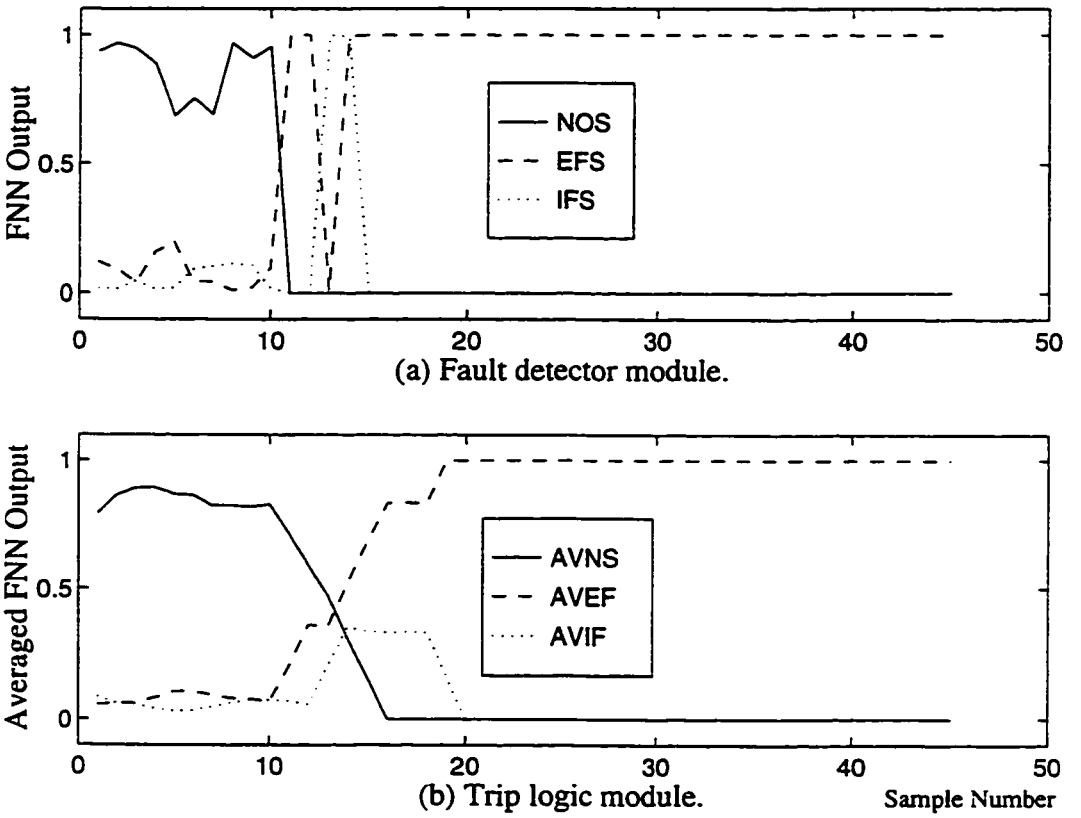

Figure 8.8: EFS, 3 phase at machine terminals with CT saturation, P=0.58 pu, pf=0.92 lag and FI=10.

results of Fig. 8.9 show that the relay performance is very good. The relay tripping time is 8 to 9 samples (less than one half cycle) after fault inception and classification takes 7 samples.

The developed internal faults algorithm, Chapter 3, is not able to simulate phase to phase faults. However, the relay clearly detected and classified internal phase to phase faults, as shown in Figs. 8.11 and 8.12. The response of the relay to an internal two phase to ground fault is shown in Fig. 8.13. It has been shown in Chapter 7 that when the unsaturated parameters of the machine are used in the internal two phase to ground faults algorithm a phase shift occurs between the computed and recorded currents for the healthy phase, Fig. 7.7. Even though the FNNs were trained with current patterns obtained using the unsaturated parameters, the response of the relay is not affected, Fig. 8.13.

8.4 Summary

Implementation of the NN based relay in a laboratory environment and real-time test results on a physical model power system are presented in this chapter. The NN parameters used in the implementation are the same parameters obtained from the off-line training process described in Chapter 5. A sequential implementation method is used to simulate the parallel mechanism of a real multi-layer NN. The relay is implemented in a real-time digital environment by means of a DSP board. The real-time test results done indicate the following:

- The relay is always successful in detecting any of the generator three states. In general, the response of the relay to actual current patterns is similar to its response to simulated patterns, even in terms of tripping time and classification time.

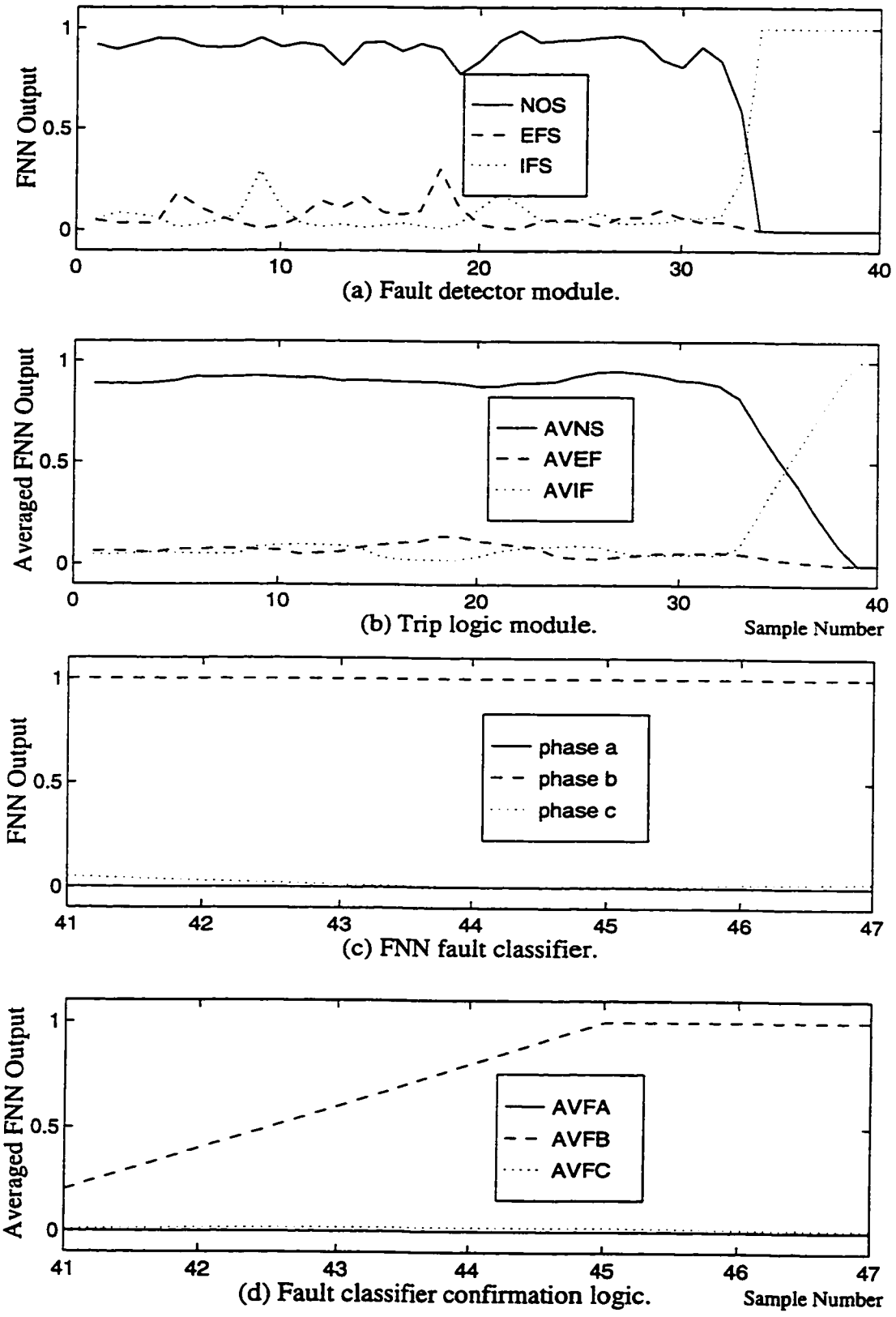

Figure 8.9: IFS, pg at 100% of *b*, P=0.7 pu, pf=0.95 lead and FI=32.

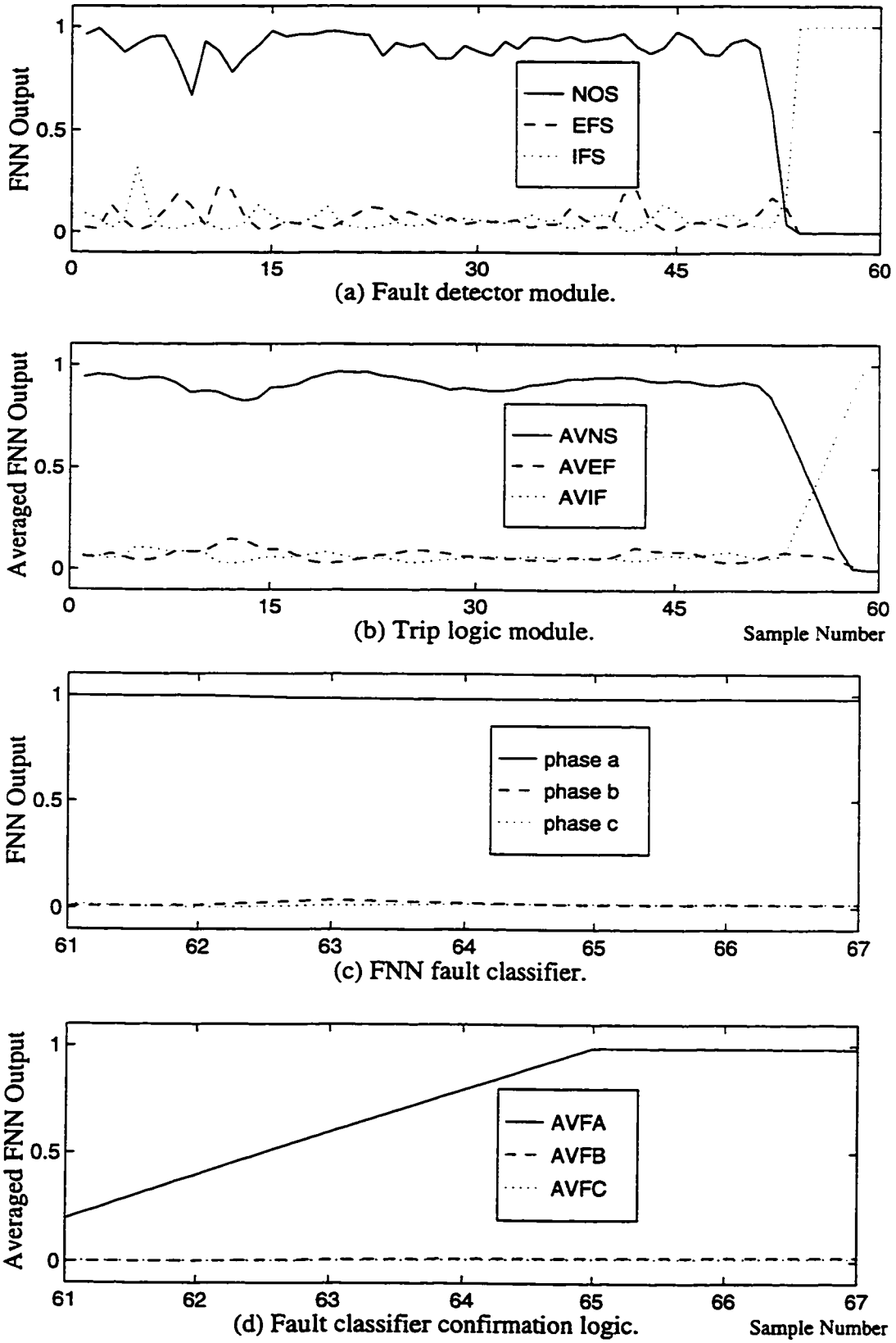

Figure 8.10: IFS, pg at 50% of a, P=0.45 pu, pf=0.91 lead and FI=51.

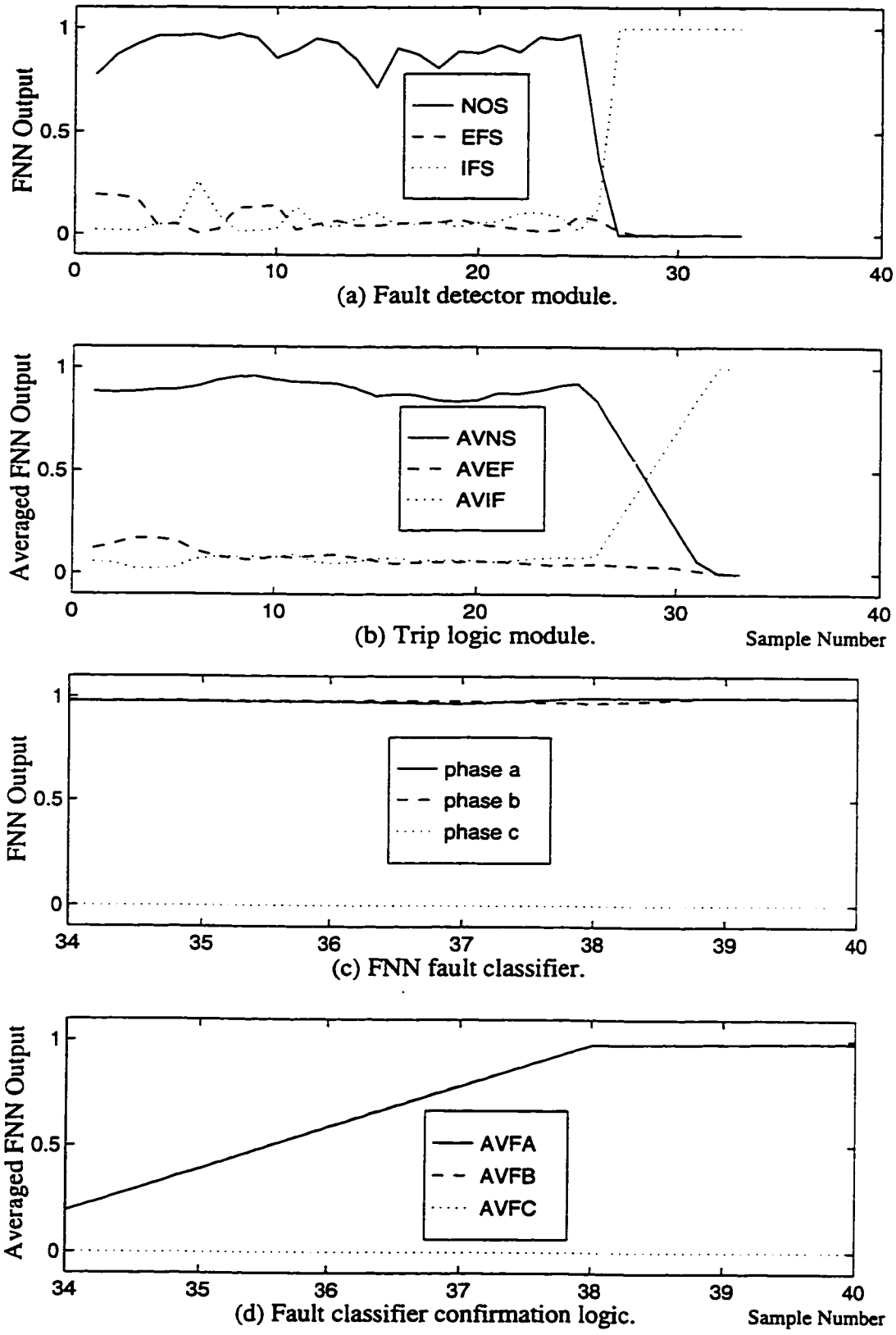

Figure 8.11: IFS, pp at 100% of *a* & 100% of *b*, P=0.4 pu, pf=0.8 lag and FI=25.

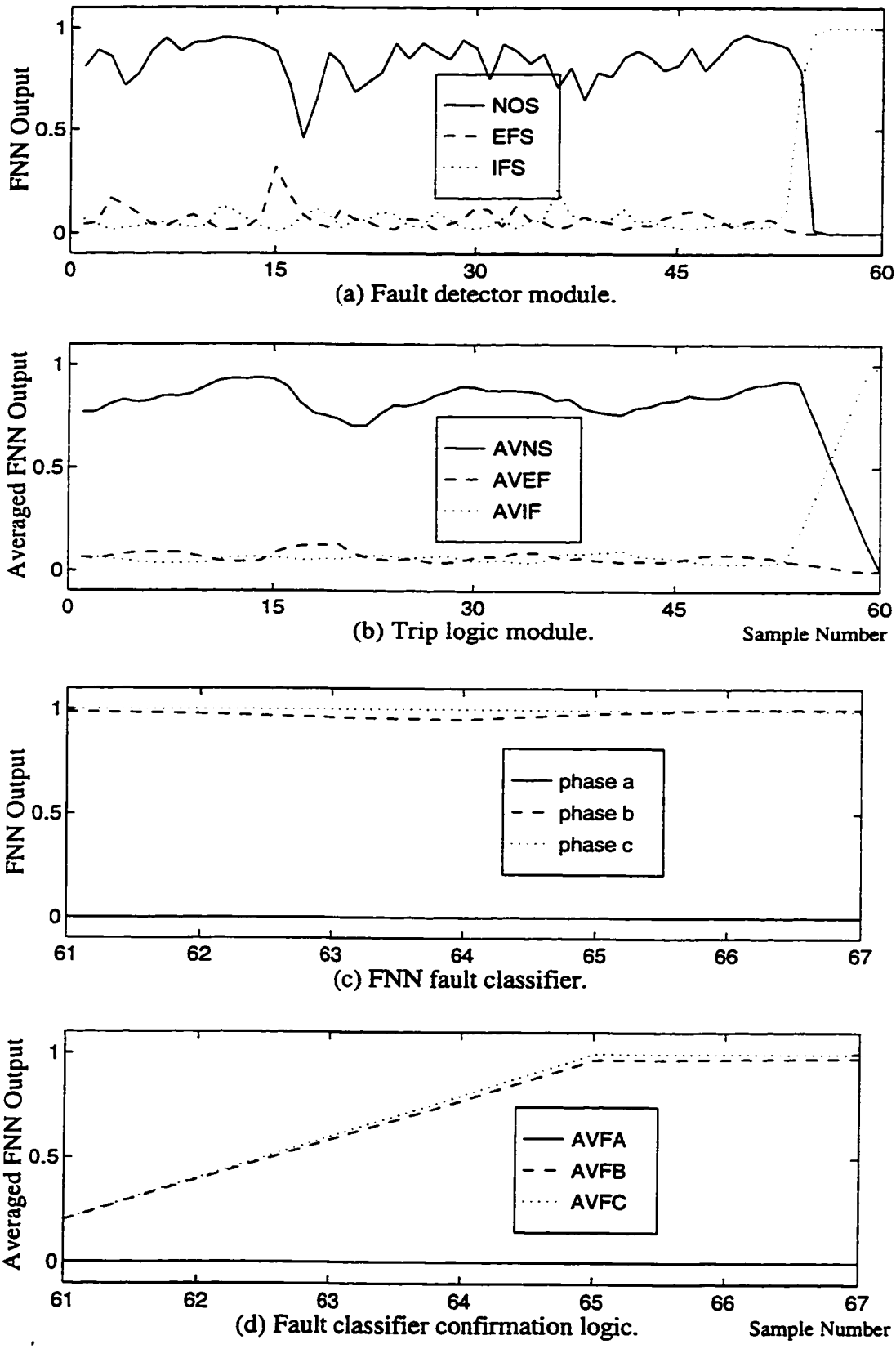

Figure 8.12: IFS, pp at 50% of *b* & 50% of *c*, P=0.7 pu, pf=0.9 lag and FI=52.

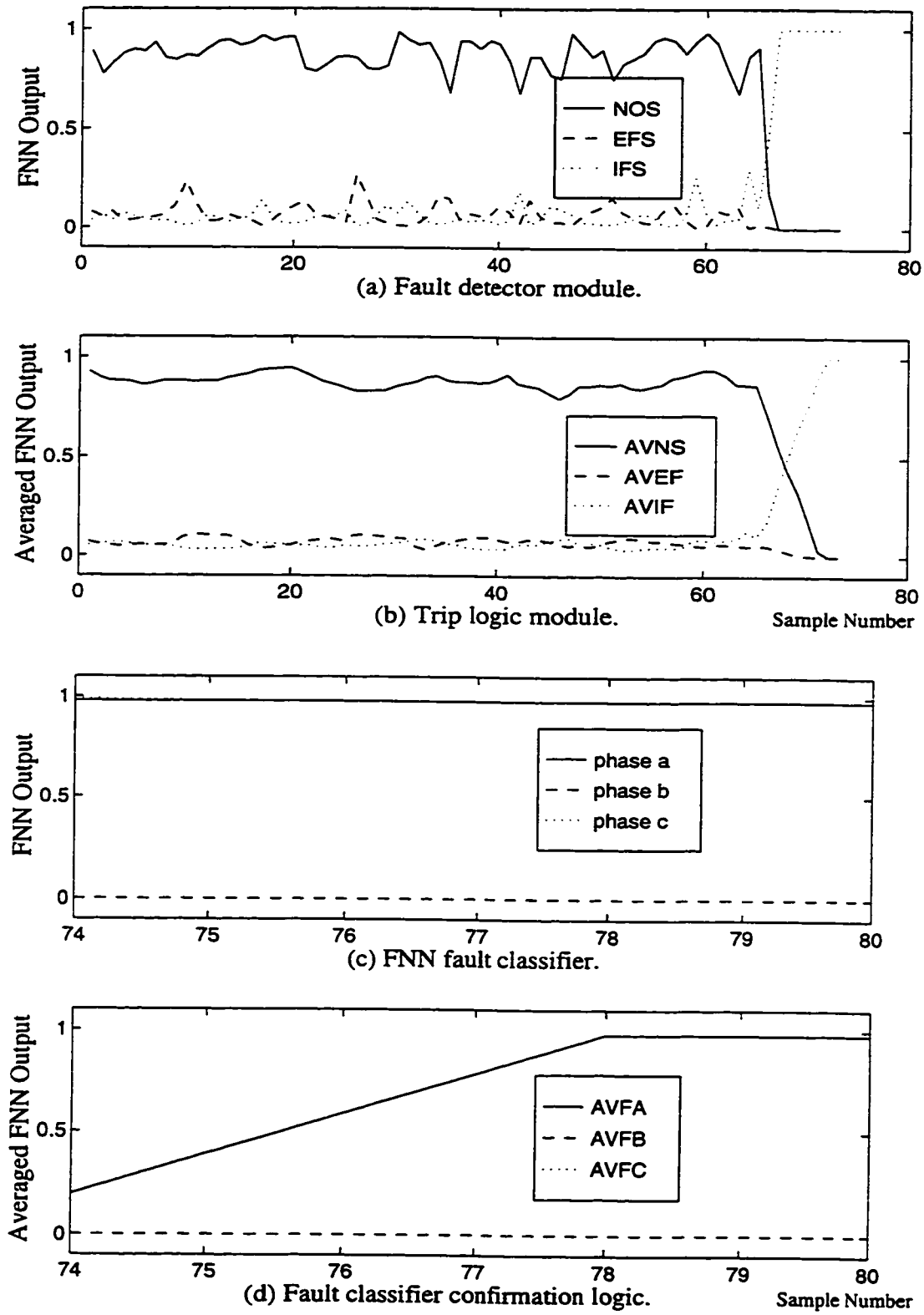

Figure 8.13: IFS, ppg at 50% of a & 50% of c, P=0.86 pu, pf=0.95 lag and FI=65.

- The relay performs very well in the presence of CT mismatches and saturation. These CT problems are likely to make conventional digital differential relays fail.

- The FNN based modules are able to detect and classify internal faults they have not been exposed to during training.

- The relay tripping time (8 to 10 samples) and classification time (7 to 10 samples) are faster than those of conventional digital differential relays.

Chapter 9

Conclusions and Future Work

9.1 Conclusions

A phase fault in a generator stator winding is always considered to be serious because of the high currents encountered and the partial damage to the machine windings as well as to the shafts and couplings. Long repair times for severely damaged machines is very expensive. Minimizing the damage due to stator faults, by using high speed relays, is therefore important.

The design, simulation studies, implementation and real-time test results of a new NN based digital differential relay used for generator stator winding protection are presented in this dissertation. Also, a new method for simulating internal faults in multi-path and single-path synchronous generators is developed and experimentally verified.

This dissertation begins with reviewing existing digital differential techniques that are used in generator differential protection. This review shows that the majority of these techniques are based on fault detection principles that are used in their electro-mechanical counterparts. Moreover, the extensive computations performed to obtain accurate estimates of phasors prevent the relay from taking a quick trip decision. The majority of these

digital techniques take at least one cycle after fault inception to issue a trip signal.

Successful application of NNs in other areas of power engineering has demonstrated that it can be employed as an alternative method for solving certain long standing problems where conventional digital techniques have had difficulty or have not achieved the desired speed, accuracy or efficiency. The ability of MFNNs to learn by training any complex input/output mapping, combined with the availability of data from the power industry, makes the MFNN a viable candidate for solving significant power system protection problems. Hence, the MFNN has been employed to build the proposed neural network based digital differential relay.

In this dissertation accurate estimation of generator 3-phase currents during normal operation, external faults and internal faults is of primary importance. A direct 3-phase model that enables a more exact study of synchronous machine performance is used. This model is capable of simulating normal operation and various kinds of external faults. The use of this model allows a uniform approach to the study of both symmetrical and unsymmetrical external faults, while retaining the generator nonlinear model. Moreover, the parameters used in the 3-phase model are physical values and it is not necessary to go through complex transformations as in other models. In this dissertation a new method for simulating internal faults in a synchronous generator, using the direct phase quantities, is described. The developed method follows the same basic approach as followed in the direct 3-phase model for the simulation of external faults. The method for calculating the self and mutual inductances of the faulted phase of the synchronous machine is explained. The internal faults algorithm is capable of simulating internal single phase to ground faults and internal two phase to ground faults in multi-path and single-path generators [68–70]. The ability of the

developed algorithm to retain the generator nonlinear model and to take into account the variation of speed under transient conditions enhances its accuracy. Grounding the generator through a resistance has the beneficial effect of reducing the fault current and the subsequent fault damage. It is shown that including the ground resistance in the direct 3-phase model only affects the machine terminal voltage equations during a fault.

The function of the NN based relay is to discriminate between three generator states, namely the normal operation state, external fault state and internal fault state. In the case of an internal fault the relay issues a trip signal and identifies the faulted phase or phases. In the case of an external fault the relay acts as a backup relay for the main protection against external faults. The NN based relay is designed using two MFNNs. One MFNN is used by the fault detector module and the other by the fault classifier module. This design uses current samples from the line-side and the neutral-end of the generator in addition to samples from the field current. Fault simulation studies have shown that the field current is distinctive for each generator state. Hence, samples of the field current are used to help the FNN based fault detector module to differentiate between the three states. The back-propagation algorithm is used to train the MFNNs. The structure and training process of each MFNN is described. Also the averaging scheme and the conditions used by the trip logic module and the fault classifier confirmation logic to detect and classify faults are explained.

The ability of the NN based relay to adequately generalize is shown by testing it using a large set of independent test patterns. Fault detection is fast, accurate and reliable even in the presence of current transformer mismatches or system transients. The relay tripping time, for the majority of internal faults, is well within half a cycle. The relay is able to detect internal faults as small as 10% of the winding for phase to ground faults and

4% of each winding for two phase to ground faults. The proposed relay also manages to detect light external faults occurring at the end of the TL. The results of the fault classifier module indicate that it is fast (one half cycle), robust and accurate, even for internal faults involving smaller percentages of the winding [72–74].

To verify the developed internal faults algorithm simulation results, obtained by the developed internal faults algorithm, are compared with actual fault currents. The laboratory physical model, which consists of the power system model and the associated hardware, is described. The model has high accuracy in the case of internal single phase to ground faults. In the case of internal two phase to ground faults, the unsaturated parameters cause a phase shift to occur between the computed and recorded currents for the healthy phase. Saturated steady-state parameters, when used in the internal two phase to ground faults algorithm, produce more accurate results. Saturated steady-state parameters do not affect the internal single phase to ground faults algorithm.

The proposed NN based relay is implemented using a DSP board mounted on an 80486 PC. The NN parameters used in the implementation are the same parameters obtained from the off-line training process, which was done using the simulation model. Real-time experiments have produced results consistent with the simulation studies. The results show that the relay works properly in the presence of CT mismatches and saturation. The relay tripping time (8 to 10 samples) and classification time (7 to 10 samples) are faster than those of conventional digital differential relays.

9.2 Future Work

Based on the work in this dissertation, the following are recommended as further research topics.

- Further improvement in the developed internal faults algorithm, so it can simulate internal phase to phase faults and interturn faults. This can be achieved by only modifying the machine terminal voltage equations.

- Developing a method to compute the inductances of the machine at each calculation step of the internal faults algorithm. In this way the effect of magnetic saturation can be accounted for based on the actual condition of the machine. This approach can further improve the simulation of internal two phase to ground faults. A neural network that uses the currents and voltages obtained in the previous calculation step can give the parameters of the machine to be used in the next step.

- Developing a NN based fault locator module that can classify the phases and locate the fault for three phase synchronous generators with a single-path per phase.

References

[1] The English Electric Company Limited, *Protective Relays Applications Guide*, The English Electric Company Limited, Relay Division, Stafford, 1975.

[2] Walter A. Elmore (Editor), *Protective Relaying Theory and Applications*, ABB Power T & D Company, Inc., Coral Springs, Florida, 1994.

[3] C.J. Mozina (Coordinator), *IEEE Tutorial on the Protection of Synchronous Generators*, IEEE Tutorial Course, IEEE Power Engineering Society Special Publ., no. 95 TP102, 1995.

[4] IEEE committee report, "Survey of experience with generator protection and prospects for improvements using digital computers", *IEEE Trans. on Power Delivery*, vol. 3, no. 4, pp. 1511–1520, Oct. 1988.

[5] R.L. Schlake, G.W. Buckley, and G. McPherson, "Performance of third harmonic ground fault protection schemes for generator stator winding protection", *IEEE Trans. on Power Apparatus and Systems*, vol. PAS-100, no. 2, pp. 3195–3202, July 1981.

[6] C.H. Griffin and J.W. Pope, "Generator ground fault protection using overcurrent, overvoltage and undervoltage relays", *IEEE Trans. on Power Apparatus and Systems*, vol. PAS-101, no. 12, pp. 4490–4501, Dec. 1982.

[7] J.W. Pope, "A comparison of 100% stator ground fault protection schemes for generator stator windings", *IEEE Trans. on Power Apparatus and Systems*, vol. PAS-103, no. 4, pp. 832–840, April 1984.

[8] R.J. Marttila, "Design principles of a new generator stator ground relay for 100% coverage of the stator winding", *IEEE Trans. on Power Delivery*, vol. 1, no. 4, pp. 41–51, Oct. 1986.

[9] M.S. Sachdev (Coordinator), *Computer Relaying*, IEEE Tutorial Course, IEEE Power Engineering Society Special Publ., no. 79 EH0148-7-PWR, 1979.

[10] M.S. Sachdev (Coordinator), *Microprocessor Relays and Protection Systems*, IEEE Tutorial Course Text, IEEE Power Engineering Society Special Publ., no. 88 EH0269-1-PWR, 1988.

[11] M.S. Sachdev (Coordinator), *Advancements in Microprocessor Based Protection and Communication*, IEEE Tutorial Course, IEEE Power Engineering Society Special Publ., no. 97 TP120-0, 1997.

[12] A.G. Phadke and J.S. Thorp, *Computer Relaying for Power Systems*, Research Studies Press, Taunton, England, 1988.

[13] A.T. Johns and S.K. Salman, *Digital Protection for Power Systems*, Peter Peregrinus Ltd. for IEE, London, England, 1995.

[14] G.D. Rockeffeller, "Fault protection with a digital computer", *IEEE Trans. on Power Apparatus and Systems*, vol. PAS-88, no. 4, pp. 438–461, April 1969.

[15] S. Haykin, *Neural Networks: A Comprehensive Foundation*, Macmillan College Publishing Company, New York, 1994.

[16] I. Aleksander and H. Morton, *An Introduction to Neural Computing*, Chapman & Hall, 1990.

[17] S. Grossberg, "Adaptive pattern classification and universal recording: I. parallel development and coding of neural feature detectors", *Biological Cybernetics*, vol. 23, pp. 121–134, 1976.

[18] S. Grossberg, "Adaptive pattern classification and universal recording: Ii. feedback, expectation, olfaction, illusions", *Biological Cybernetics*, vol. 23, pp. 187–202, 1976.

[19] J.J. Hopfield, "Neural networks and physical systems with emergent collective computational abilities", *Proc. of the National Academy of Sciences of the USA*, vol. 79, pp. 2554–2558, 1982.

[20] P.J. Werbos, *Beyond Regression: New Tools for Prediction and Analysis in Behavioral Sciences*, PhD thesis, Harvard University, 1974.

[21] D.E. Rumelhart and J.L. McClelland (Editors), *Parallel Distributed Processing: Explorations in the Microstructure of Cognition*, vol. 1: Foundations, MIT Press, Cambridge, MA, 1986.

[22] R.P. Lippmann, "An introduction to computing with neural nets", *IEEE ASSP Magazine*, vol. 2, pp. 4–22, Apr. 1987.

[23] M.A. El-Sharkawi and D. Niebur (Editors), *A Tutorial Course on Artificial Neural Networks with Applications to Power Systems*, IEEE Tutorial Course, IEEE Power Engineering Society Special Publ., no. 96 TP112-0, 1996.

[24] V.S.S. Vankayala and N.D. Rao, "Artificial neural networks and their application to power system - a bibliographical survey", *Electric Power Systems Research*, vol. 28, pp. 67–79, 1993.

[25] Westinghouse Electric Corporation, *Applied Protective Relaying*, Westinghouse Electric Corporation, Relay-Instrument Division, Newark, 1976.

[26] M.S. Sachdev and D.W. Wind, "Generator differential protection using a hybrid computer", *IEEE Trans. on Power Apparatus and Systems*, vol. PAS-92, no. 6, pp. 2063–2072, Nov./Dec. 1973.

[27] G.S. Hope, P.K. Dash, and O.P. Malik, "Digital differential protection of a generating unit scheme and real-time test results", *IEEE Trans. on Power Apparatus and Systems*, vol. PAS-96, no. 2, pp. 502–512, March/April 1977.

[28] P.K. Dash, O.P. Malik, and G.S. Hope, "Fast generator protection against internal asymmetrical faults", *IEEE Trans. on Power Apparatus and Systems*, vol. PAS-96, no. 5, pp. 1498–1506, Sept./Oct. 1977.

[29] H.K. Verma and K. Soundararajan, "Digital differential relaying for generator protection: development of algorithm and off-line evaluation", *Electric Power Systems Research*, vol. 17, pp. 109–117, 1989.

[30] K. Soundararajan and H.K. Verma, "Microcomputer based digital differential relaying for generator protection: real time test results", *Electric Power Systems Research*, vol. 20, pp. 237–243, 1991.

[31] A.V. Oppenheim and R.W. Schafer, *Discrete-Time Signal Processing*, Prentice-Hall, Inc., Englewood Cliffs, New Jersey, 1989.

[32] R.W. Hamming, *Digital Filters*, Prentice-Hall, Inc., Englewood Cliffs, New Jersey, 1977.

[33] G. Benmouyal, S. Barceloux, and R. Pelletier, "Field experience with a digital relay for synchronous generators", *IEEE Trans. on Power Delivery*, vol. 7, no. 4, pp. 1984–1992, Oct. 1992.

[34] G. Ziegler, "Developments in generator protection - design and application aspects of a new numerical relay range", *IEE 5th International Conference on Developments in Power System Protection*, , no. 368, pp. 111–114, 1993.

[35] H.T. Yip, "An integrated approach to generator protection", *E&0 Division Meeting of Canadian Electrical Association*, , no. 94-SP-25, March 20-24, 1994.

[36] T.S. Sidhu, B. Sunga, and M.S. Sachdev, "A digital technique for stator winding protection of synchronous generators", *Electric Power Systems Research*, vol. 36, pp. 45–55, 1996.

[37] B. Widrow and M.A. Lehr, "30 years of adaptive neural networks: perceptron, madaline and back propagation", *Proc. of the IEEE*, vol. 78, no. 9, pp. 1415–1442, Sep. 1990.

[38] A.F. Sultan, G.W. Swift, and D.J. Fedirchuk, "Detection of high impedance arcing faults using a multi-layer perceptron", *IEEE Trans. on Power Delivery*, vol. 7, no. 4, pp. 1871–1877, Oct. 1992.

[39] T.S. Sidhu, H. Singh, and M.S. Sachdev, "Design, implementation and testing of an artificial neural network based fault direction discriminator for protecting transmission lines", *IEEE Trans. on Power Delivery*, vol. 10, no. 2, pp. 697–706, April 1995.

[40] T. Dalstein, D. Sobajic, B. Kulicke, and Y.H. Pao, "Neural network approach to fault direction identification in electric power systems", *Proc.*

of the IEEE North American Power Symposium, pp. 290–299, Oct. 11-12, 1993.

[41] T. Dalstein and B. Kulicke, "Neural network approach to fault classification for high speed protective relaying", *IEEE Trans. on Power Delivery*, vol. 10, no. 2, pp. 1002–1011, April 1995.

[42] T. Dalstein and B. Kulicke, "Multineural network based fault area estimation for high speed protective relaying", *IEEE Trans. on Power Delivery*, vol. 11, no. 2, pp. 740–747, April 1996.

[43] R.K. Aggarwal, A.T. Johns, Y.H. Song, R.W. Dunn, and D.S. Fitton, "Neural network based adaptive single-pole autoreclosure technique for ehv transmission systems", *IEE Proc. -C*, vol. 141, no. 2, pp. 155–160, March 1994.

[44] Y.H. Song, A.T. Johns, and Q.Y. Xuan, "Artificial neural network based protection scheme for controllable series compensated ehv transmission lines", *IEE Proc. -C*, vol. 143, no. 6, pp. 535–540, Nov. 1996.

[45] Q.Y. Xuan, Y.H. Song, A.T. Johns, R. Morgan, and D. Williams, "Performance of an adaptive protection scheme for series compensated ehv transmission systems using neural networks", *Electric Power Systems Research*, vol. 36, pp. 57–66, 1996.

[46] L.G. Perez, A.J. Flechsig, J.L. Meador, and Z. Obradovic, "Training an artificial neural network to discriminate between magnetizing inrush and internal faults", *IEEE Trans. on Power Delivery*, vol. 9, no. 1, pp. 434–441, Jan. 1994.

[47] J. Pihler, B. Grcar, and D. Dolinar, "Improved operation of power transformer protection using artificial neural network", *IEEE Trans. on Power Delivery*, vol. 12, no. 3, pp. 1128–1136, July 1997.

[48] P. Bastard, M. Meunier, and H. Regal, "Neural network based algorithm for power transformer differential relays", *IEE Proc. -C*, vol. 142, no. 4, pp. 386–392, July 1995.

[49] M. Chow and S.O. Yee, "Methodology for on-line incipient fault detection in single-phase squirrel-cage induction motors using artificial neural networks", *IEEE Trans. on Energy Conversion*, vol. 6, no. 3, pp. 536–545, Sept. 1991.

[50] M. Chow and S.O. Yee, "A neural network approach to real-time condition monitoring of induction motors", *IEEE Trans. on Industrial Electronics*, vol. 38, no. 6, pp. 448–453, Dec. 1991.

[51] M. Chow, R.N. Sharpe, and J.C. Hung, "On the application and design of artificial neural networks for motor fault detection", *IEEE Trans. on Industrial Electronics*, vol. 40, no. 2, pp. 181–188, April 1993.

[52] D.W. Auckland, I.E.D. Pickup, R. Shuttleworth, Y.-T. Wu, and C. Zhou, "Novel approach to alternator field winding interturn fault detection", *IEE Proc. -C*, vol. 142, no. 2, pp. 97–102, March 1995.

[53] M.A. El-Sharkawi, R.J. Marks II, S. Oh, S.J. Huang, I. Kerszenbaum, and A. Rodriguez, "Localization of winding shorts using fuzzified neural networks", *IEEE Trans. on Energy Conversion*, vol. 10, no. 1, pp. 140–144, March 1995.

[54] T. Grigoriu, V.K. Sood, K. Khorasani, and R.V. Patel, "Fault identification in a series compensated ac line using neural networks", *E&O Division Meeting of Canadian Electrical Association*, , no. 93-SP-96, March 29-31, 1993.

[55] M. Kezunovic and I. Rikalo, "Detect and classify faults using neural nets", *IEEE Computer Applications in Power*, vol. 9, no. 4, pp. 42–47, Oct. 1996.

[56] B. Adkins, *The General Theory of Electrical Machines*, Chapman & Hall, 1964.

[57] C. Concordia, *Synchronous Machines: Theory and Performance*, John Wiley & Sons, Inc., New York, 1951.

[58] N.N. Hancock, *Matrix Analysis of Electrical Machinery*, Pergamon Press, Inc., New York, 1974.

[59] H.H. Hwang, "Unbalanced operation of a.c. machines", *IEEE Trans. on Power Apparatus and Systems*, vol. PAS-84, no. 8, pp. 1054–1066, Aug. 1965.

[60] P. Subramaniam and O.P. Malik, "Digital simulation of a synchronous generator in direct-phase quantities", *Proc. IEE*, vol. 118, no. 1, pp. 153–160, Jan. 1971.

[61] Paul C. Krause, *Analysis of Electric Machinery*, McGraw-Hill, Inc., 1986.

[62] V.A. Kinitsky, "Calculation of internal fault currents in synchronous machines", *IEEE Trans. on Power Apparatus and Systems*, vol. PAS-84, no. 5, pp. 381–389, May 1965.

[63] V.A. Kinitsky, "Digital computer calculation of internal fault currents in a synchronous machine", *IEEE Trans. on Power Apparatus and Systems*, vol. PAS-87, no. 8, pp. 1675–1679, Aug. 1968.

[64] X.H. Wang, L.Z. Zhang, W.J. Wang, and Z.H. Yu, "Research and application of protection relay schemes for internal faults in stator windings

of a large hydro-generator with multi branch and distributed arrangement", *IEE 5th International Conference on Developments in Power System Protection*, , no. 368, pp. 51–55, 1993.

[65] V.A. Kinitsky, "Mutual inductances of synchronous machines with damper windings", *IEEE Trans. on Power Apparatus and Systems.* vol. PAS-83, no. 10, pp. 997–1001, Oct. 1964.

[66] V.A. Kinitsky, "Inductances of a portion of the armature winding of synchronous machines", *IEEE Trans. on Power Apparatus and Systems.* vol. PAS-84, no. 5, pp. 389–396, May 1965.

[67] V.A. Kinitsky, "Calculation of synchronous machine constants by a digital computer", *Proc. of the IEEE Power Industry Computer Applications Conference*, pp. 74–90, 1965.

[68] A.I. Megahed and O.P. Malik, "Simulation of internal faults in synchronous generators", *Proc. of the IEEE International Electric Machines and Drives Conference*, pp. TC1 2.1–2.3, Milwaukee, May 18-21, 1997.

[69] A.I. Megahed and O.P. Malik, "Simulation of internal faults in synchronous generators (extended version)", *to be published in an IEEE Power Engineering Society Transaction*, accepted in Oct. 1997.

[70] A.I. Megahed and O.P. Malik, "Synchronous generator internal fault computation and experimental verification", *IEE Proc.*, submitted in Sept. 1997.

[71] H. Demuth and M. Beale, *Neural Network Toolbox: For Use with Matlab*, The Math Works, Inc., 1993.

[72] A.I. Megahed and O.P. Malik, "An artificial neural network based digital differential protection scheme for synchronous generator stator winding protection", *to be published in the IEEE Trans. on Power Delivery*, . no. PE-169-PWRD-0-11-1997, 1997.

[73] A.I. Megahed, "An artificial neural network approach to generator internal fault classification", *Proc. of the Student Paper/Poster Session of the IEEE-PES Power Industry Computer Applications Conference*, pp. 63–66, Columbus, May 11-16, 1997.

[74] A.I. Megahed and O.P. Malik, "Artificial neural network based modules for generator stator winding internal fault classification", *International Journal of Engineering Intelligent Systems*, vol. 5, no. 4, pp. 229–234, Dec. 1997.

[75] G. Shackshaft and P.B. Henser, "Model of generator saturation for use in power system studies", *Proc. IEE*, vol. 126, no. 8, pp. 759–763, Aug. 1979.

[76] F.P. de Mello and L.N. Hannett, "Representation of saturation in synchronous machines", *IEEE Trans. on Power Systems*, vol. 1, no. 4, pp. 8–18, Nov. 1986.

[77] D.W. Auckland, S.M.L. Kabir, and R. Shuttleworth, "Generator model for power system studies", *IEE Proc. -C*, vol. 137, no. 6, pp. 383–390, Nov. 1990.

[78] D.L. Brooks and S.M. Halpin, "An improved fault analysis algorithm including detailed synchronous machine models and magnetic saturation", *Electric Power Systems Research*, vol. 42, pp. 3–9, 1997.

[79] M.R. Zaman and M.A. Rahman, "Experimental testing of the artificial neural network based protection of power transformers", *presented in*

the IEEE Winter Meeting, , no. PE-045-PWRD-0-11-1996, New York, Feb. 1997.

[80] S. Haykin, *Adaptive Filter Theory*, Prentice-Hall, Inc., Englewood Cliffs, New Jersey, 1991.

[81] J.M. Mendel and R.W. McLaren, "Reinforcement-learning control and pattern recognition systems", in *Adaptive, Learning and Pattern Recognition Systems: Theory and Applications.* pp. 287–318, Academic Press, New York, 1970.

[82] T. Kohonen, "The self-organizing map", *Proc. of the IEEE*, vol. 78, no. 9, pp. 1464–1480, Sep. 1990.

Appendix A

Neural Network Structure

A.1 Basic Elements

Neurons are the basis of the neural networks (NNs). A neuron is an information processing unit that is fundamental to the operation of a NN. Figure A.1 shows the model of a neuron. There are three basic elements of the neuron model, as described here:

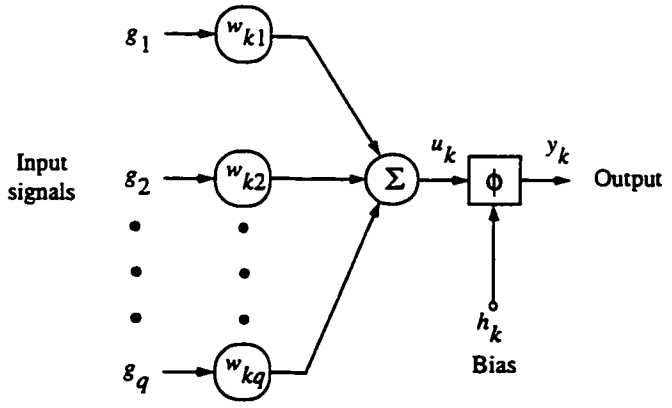

Figure A.1: Nonlinear model of a neuron.

- A set of synapses or connecting links, each of which is characterized by a weight. A signal g_j at the input of the synapse j connected to neuron

k is multiplied by the synaptic weight w_{kj}.

- An adder for summing the input signals, weighted by the respective synapses.

- An activation function for limiting the amplitude of the output of a neuron. This limit usually is in the unit interval [0,1] or [-1,1].

This model also includes an externally applied bias, h_k, that has the effect of increasing the net input of the activation function, Fig. A.1. In mathematical terms, a neuron k can be described by the following equations:

$$u_k = \sum_{j=1}^{q} w_{kj} g_j \tag{A.1}$$

$$v_k = u_k + h_k \tag{A.2}$$

$$y_k = \phi(v_k) \tag{A.3}$$

where $g_1, g_2, ..., g_q$ are the input signals; $w_{k1}, w_{k2}, ..., w_{kq}$ are the synaptic weights of neuron k, u_k is the linear output; h_k is the bias; v_k is the total weighted sum; $\phi(.)$ is the activation function and y_k is the output signal of the neuron. There are three basic types of activation functions:

- *Threshold function:*

$$\phi(v) = \begin{cases} 1 & \text{if} \quad v \geq 0 \\ 0 & \text{if} \quad v < 0 \end{cases} \tag{A.4}$$

- *Piecewise-Linear function:*

$$\phi(v) = \begin{cases} 1 & \text{if} \quad v \geq \frac{1}{2} \\ v & \text{if} \quad \frac{1}{2} > v \geq -\frac{1}{2} \\ 0 & \text{if} \quad v < -\frac{1}{2} \end{cases} \tag{A.5}$$

- *Sigmoid function:*

$$\phi(v) = \frac{1}{1 + exp(-v)} \quad (log - sigmoid) \tag{A.6}$$

$$\phi(v) = \frac{exp(v) - exp(-v)}{exp(v) + exp(-v)} \quad (tan - sigmoid) \tag{A.7}$$

A.2 Network Architectures

The manner in which the neurons of a NN are connected can be classified into four architectures [15]:

- *Single-layer feed-forward networks*

  A layered NN is a network of neurons organized in the form of layers. It has an input layer of source nodes that projects onto an output layer of neurons (computation nodes), but not vice versa. In other words, this network is strictly of a feed-forward type. It is illustrated in Fig. A.2 for the case of four nodes in both the input and output layers. Such a network is called a single-layer network, with the designation *single-layer* referring to the output layer of computation nodes (neurons), i.e. the input layer of source nodes is not counted because no computation is performed there.

  A single-layer feed-forward neural network (FNN) is used for simple cases of pattern classification, as it can only distinguish between two separable classes. In other words, classes that fall on opposite sides of some hyperplane [22].

- *Multi-layer feed-forward networks*

  The second class of a FNN distinguishes itself by the presence of one or more hidden layers of neurons. The function of the hidden neurons

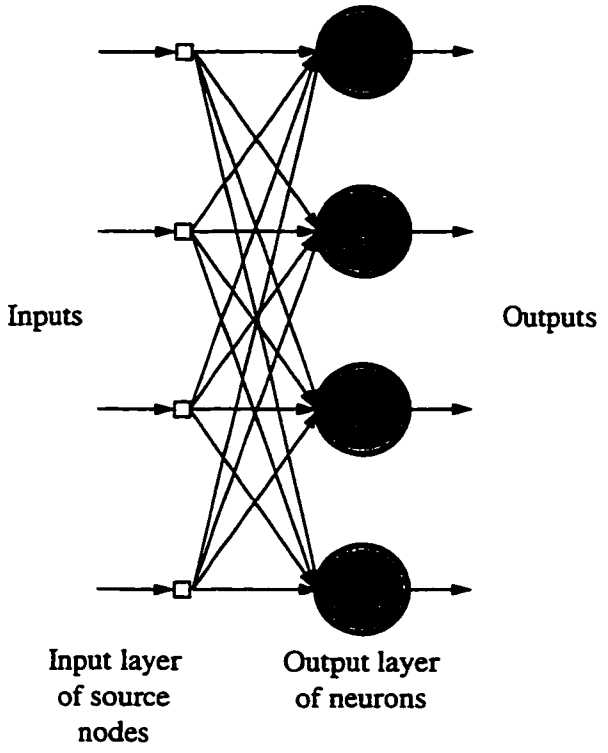

Figure A.2: Single-layer feed-forward network.

is to intervene between the external input and the network output. By adding one or more hidden layers, the network is enabled to extract higher-order statistics, for the network acquires a global perspective despite its local connectivity by virtue of the extra set of synaptic connections and the extra dimension of neural interactions . A two layer FNN can be used to classify inside, convex and open or closed fields, but a three layer FNN can generate arbitrary complex decision regions [22].

A three layer FNN is shown in Fig. A.3. Neurons in the first hidden layer receive the inputs from the source nodes and send the outputs to the second hidden layer. The neurons in the second hidden layer receive the outputs of the first hidden layer as their inputs, and send their outputs to the output layer. Neurons in the output layer get the

outputs from the second hidden layer as the inputs, and the outputs of the output layer are the outputs of the neural network.

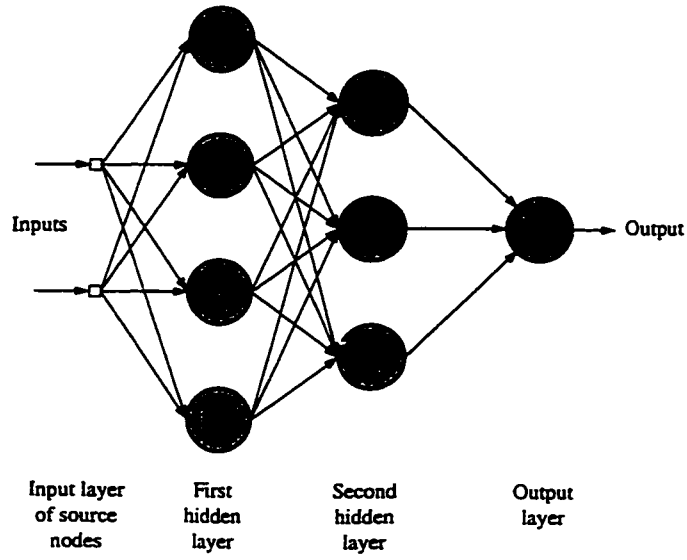

Figure A.3: A three layer feed-forward network.

Each neuron k gets the weighted sum of the outputs of all the neurons j in the previous layer that connect with neuron k through weight w_{kj}, which is given as:

$$v_k = \sum_j w_{kj} y_j + h_k \tag{A.8}$$

If neuron k is in the first layer, the weighted sum is over all of the external inputs q that connect with neuron k as expressed in (A.3). This weighted sum is altered by one of the activation functions given in (A.4-A.7) to produce the output.

- *Recurrent networks*

  The main difference between a recurrent NN and a FNN is that the former has at least one feedback. In Fig. A.4, the recurrent network is shown with feedback loops. This has a profound impact on the learning capability of the network, and on its performance. Moreover,

the feedback loops involve the use of unit delay elements, which result in a nonlinear dynamical behavior by virtue of the nonlinear nature of the neurons.

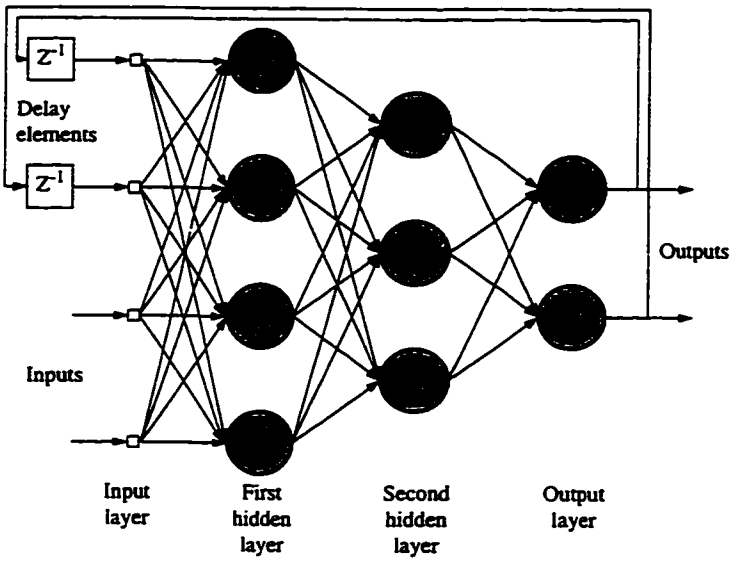

Figure A.4: Recurrent network with hidden neurons.

- *Lattice structures*

  A lattice consists of a one dimensional, two dimensional, or higher dimensional array of neurons with a corresponding set of source nodes that supply the input signals to the array; the dimension of the lattice refers to the number of the dimensions of the space in which the graph lies. The architectural graph of Fig. A.5 depicts a two dimensional lattice of 3-by-2 neurons fed from a layer of 3 source nodes. Each source node is connected to every neuron in the lattice. A lattice network is really a feed-forward network with the output neurons arranged in rows and columns.

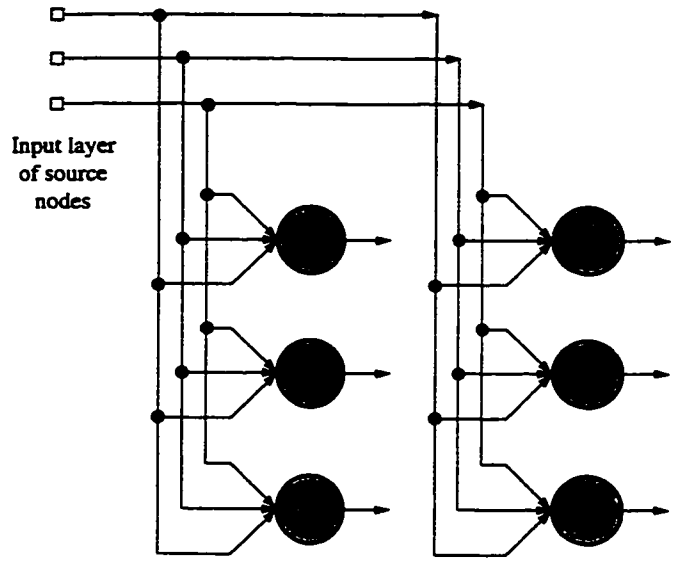

Figure A.5: Two dimensional lattice of 3-by-2 neurons.

A.3 Learning Paradigms

Among the many properties of a neural network, the property that is of primary significance is the ability of the network to learn from training data, and to improve its performance through learning. There are basically three classes of learning paradigms:

- *Supervised learning*

  As it implies, supervised learning is performed under the supervision of an external teacher. The network parameters are adjusted under the combined influence of the training data and error signal; the error signal is defined as the difference between the actual response of the network and the desired response.

  Examples of supervised learning algorithms include the least-mean-square (LMS) algorithm [80] and its generalization known as the back-propagation algorithm [20,21]. The back-propagation algorithm, which is described in Chapter 2, derives its name from the fact that error terms in the algorithm are back-propagated through the network, on a

layer-by-layer basis.

Supervised learning can be performed in an off-line or on-line manner. In the off-line case, once the desired performance is accomplished, the training is frozen, which means the NN operates in a static manner. On the other hand, in on-line training, learning is accomplished in real time, with the result that the NN dynamically adjusts its parameters.

- *Reinforcement learning*

  Reinforcement learning involves the use of a critic that evolves through a trial and error process. Compared to supervised learning, reinforcement learning is done on the basis of the reinforcement received from the environment; there is no teacher to supply gradient information during learning. To obtain information, a reinforcement learning system probes the environment through the combined use of trial and error, and delayed reward. This learning is more suited in less structured situations where it may be possible to improve plant performance over time by means of on-line reinforcement learning [81].

- *Unsupervised learning*

  In unsupervised or self-organized learning there is no external teacher or critic to oversee the learning process. In other words, there are no examples of the function to be learned by the network. Rather, provision is made for a task-independent measure of the quality of representation that the network is required to learn, and the free parameters of the network are optimized with respect to that measure. Once the network has become tuned to the statistical regularities of the input data, it develops the ability to form internal representations for encoding features of the input and thereby create new classes automatically. The two most important unsupervised network architectures are Kohonen Self-Organizing Map [82] and Grossberg's ART network [17,18].

Appendix B

Inductance Matrices Components

B.1 Components of the $\mathbf{L_1}$ Matrix

Formulas of the components of the $\mathbf{L_1}$ inductance matrix in (2.17), which is used to represent the machine inductances during normal operation and external faults, are [60, 61]:

$$
\begin{aligned}
L_a &= -L_{a0} - L_{ma1}\cos(2\theta) \\
M_{ab} = M_{ba} &= -M_{a0} - L_{ma1}\cos(2\theta - \tfrac{2\pi}{3}) \\
M_{ac} = M_{ca} &= -M_{a0} - L_{ma1}\cos(2\theta + \tfrac{2\pi}{3}) \\
M_{af} = -M_{fa} &= M_{ad}\cos(\theta) \\
M_{akd} = -M_{kda} &= M_{ad}\cos(\theta) \\
M_{akq} = -M_{kqa} &= -M_{aq}\sin(\theta) \\
L_b &= -L_{a0} - L_{ma1}\cos(2\theta + \tfrac{2\pi}{3})
\end{aligned}
$$

$$
\begin{aligned}
M_{bc} = M_{cb} &= -M_{a0} - L_{ma1}\cos(2\theta) \\
M_{bf} = -M_{fb} &= M_{ad}\cos(\theta - \tfrac{2\pi}{3}) \\
M_{bkd} = -M_{kdb} &= M_{ad}\cos(\theta - \tfrac{2\pi}{3}) \\
M_{bkq} = -M_{kqb} &= -M_{aq}\sin(\theta - \tfrac{2\pi}{3}) \\
L_c &= -L_{a0} - L_{ma1}\cos(2\theta - \tfrac{2\pi}{3}) \\
M_{cf} = -M_{fc} &= M_{ad}\cos(\theta + \tfrac{2\pi}{3}) \\
M_{ckd} = -M_{kdc} &= M_{ad}\cos(\theta + \tfrac{2\pi}{3}) \\
M_{ckq} = -M_{kqc} &= -M_{aq}\sin(\theta + \tfrac{2\pi}{3}) \\
L_f &= constant \\
M_{fkd} = M_{kdf} &= constant \\
L_{kd} &= constant \\
L_{kq} &= constant
\end{aligned}
$$

where

L_{a0}, L_{ma1}, M_{a0} = inductance coefficients of the stator windings.

M_{ad} = mutual inductance between armature and field winding.

M_{aq} = mutual inductance between armature and quadrature axis damper winding.

B.2 Components of the L_2 Matrix

In this section the formulas of the components of the L_2 inductance matrix in (3.12), which is used to represent the machine inductances during an internal single phase to ground fault in phase a of a multi-path generator, are given.

The formulas for the self and mutual inductances of the healthy windings, i.e. b, c, f, kd and kq windings, are the same as in the $\mathbf{L_1}$ matrix, Section B.1, hence they are not rewritten in this section. So, the formulas given below are only those of the three windings p, m and n of faulty phase a [62,65,66].

$$
\begin{aligned}
L_p &= -L_{a0} - L_{ma1}\cos(2\theta) - \tfrac{L_{la}}{X-1} \\
M_{pm} = M_{mp} &= \tfrac{N}{N_m}[-L_{mam0} - L_{mam1}\cos(2\theta + \delta_{mo})] \\
M_{pn} = M_{np} &= \tfrac{N}{N_n}[-L_{man0} - L_{man1}\cos(2\theta + \delta_{no})] \\
M_{pb} = M_{bp} &= -M_{a0} - L_{ma1}\cos(2\theta - \tfrac{2\pi}{3}) \\
M_{pc} = M_{cp} &= -M_{a0} - L_{ma1}\cos(2\theta + \tfrac{2\pi}{3}) \\
M_{pf} = -M_{fp} &= M_{ad}\cos(\theta) \\
M_{pkd} = -M_{kdp} &= M_{ad}\cos(\theta) \\
M_{pkq} = -M_{kqp} &= -M_{aq}\sin(\theta) \\
L_m &= -L_{m0} - L_{mam1}\cos(2\theta_m) \\
M_{mn} = M_{nm} &= \tfrac{N_n}{N_m}[-L_{mam0} - L_{mam1}\cos(2\theta_{mn})] \\
M_{mb} = M_{bm} &= \tfrac{N_m}{N}[-M_{a0} - L_{ma1}\cos(2\theta + \delta_{mo} - \tfrac{2\pi}{3})] \\
M_{mc} = M_{cm} &= \tfrac{N_m}{N}[-M_{a0} - L_{ma1}\cos(2\theta + \delta_{mo} + \tfrac{2\pi}{3})] \\
M_{mf} = -M_{fm} &= \tfrac{N_m}{N}[M_{ad}\cos(\theta_m)] \\
M_{mkd} = -M_{kdm} &= \tfrac{N_m}{N}[M_{ad}\cos(\theta_m)] \\
M_{mkq} = -M_{kqm} &= \tfrac{N_m}{N}[-M_{aq}\sin(\theta_m)]
\end{aligned}
$$

$$
\begin{aligned}
L_n &= -L_{n0} - L_{man1}\cos(2\theta_n) \\
M_{nb} = M_{bn} &= \tfrac{N_n}{N}[-M_{a0} - L_{ma1}\cos(2\theta + \delta_{no} - \tfrac{2\pi}{3})] \\
M_{nc} = M_{cn} &= \tfrac{N_n}{N}[-M_{a0} - L_{ma1}\cos(2\theta + \delta_{no} + \tfrac{2\pi}{3})] \\
M_{nf} = -M_{fn} &= \tfrac{N_n}{N}[M_{ad}\cos(\theta_n)] \\
M_{nkd} = -M_{kdn} &= \tfrac{N_n}{N}[M_{ad}\cos(\theta_n)] \\
M_{nkq} = -M_{kqn} &= \tfrac{N_n}{N}[-M_{aq}\sin(\theta_n)]
\end{aligned}
$$

where

$L_{a0} = L_{la} + L_{ma0}$

$L_{m0} = L_{lm} + L_{mam0}$

$L_{n0} = L_{ln} + L_{man0}$

$\theta_{mn} = \theta + \frac{\delta_{mo}+\delta_{no}}{2}$

B.3 Components of the L_3 Matrix

The $\mathbf{L_3}$ inductance matrix is used in the flux linkage relationship of (3.39) for the simulation of internal two phase to ground faults in phases a and b of a multi-path machine. The $\mathbf{L_3}$ matrix has many components in common with the $\mathbf{L_1}$ and $\mathbf{L_2}$ matrices. In this section, only the formulas of those components not shared with any of the other matrices are given [62,65,66].

$$
\begin{aligned}
L_z &= -L_{a0} - L_{ma1}\cos(2\theta + \tfrac{2\pi}{3}) - \tfrac{L_{la}}{X-1} \\
L_r &= -L_{ro} - L_{mar1}\cos(2\theta_r + \tfrac{2\pi}{3}) \\
L_s &= -L_{s0} - L_{mas1}\cos(2\theta_s + \tfrac{2\pi}{3}) \\
M_{rs} = M_{sr} &= \tfrac{N_s}{N_r}[-L_{mar0} - L_{mar1}\cos(2\theta_{rs} + \tfrac{2\pi}{3})]
\end{aligned}
$$

$$
\begin{aligned}
M_{mr} = M_{rm} &= \tfrac{N_m N_r}{N^2}[-M_{a0} - L_{ma1}\cos(2\theta_{mr} - \tfrac{2\pi}{3})] \\
M_{ms} = M_{sm} &= \tfrac{N_m N_s}{N^2}[-M_{a0} - L_{ma1}\cos(2\theta_{ms} - \tfrac{2\pi}{3})] \\
M_{nr} = M_{rn} &= \tfrac{N_n N_r}{N^2}[-M_{a0} - L_{ma1}\cos(2\theta_{nr} - \tfrac{2\pi}{3})] \\
M_{ns} = M_{sn} &= \tfrac{N_n N_s}{N^2}[-M_{a0} - L_{ma1}\cos(2\theta_{ns} - \tfrac{2\pi}{3})]
\end{aligned}
$$

where

N_r, N_s = effective number of turns of the r, s windings.

$\theta_r = \theta + \delta_{ro}$, δ_{ro} = displacement angle of the r winding from the original axis of the b winding due to the fault.

$\theta_s = \theta + \delta_{so}$, δ_{so} = displacement angle of the s winding from the original axis of the b winding due to the fault.

$\theta_{rs} = \theta + \frac{\delta_{ro}+\delta_{so}}{2}$

$\theta_{mr} = \theta + \frac{\delta_{mo}+\delta_{ro}}{2}$

$\theta_{ms} = \theta + \frac{\delta_{mo}+\delta_{so}}{2}$

$\theta_{nr} = \theta + \frac{\delta_{no}+\delta_{ro}}{2}$

$\theta_{ns} = \theta + \frac{\delta_{no}+\delta_{so}}{2}$

Appendix C

Simulation Model Parameters

Synchronous Generators

All parameters given in Table C.1, except the ratings (kVA or MVA) and inertia constants (kWs/kVA), are in pu. Each pu generator parameter set is based on its own ratings.

Transmission Line

All parameters presented below are also in pu, and have been fixed throughout the simulation studies.

$$R_{TL} = 0.0075 \quad L_{TL} = 0.15$$

Infinite Bus

$$E_{bus} = 1.414 \quad \omega = 377 rad/s = 1$$

Ground Resistances

$$R_{g1} = 1.5 \quad R_{g2} = 0.8$$

Table C.1: Parameters of the generators.

Parameter	G_1	G_2	G_3	G_4	G_5	G_6
Rating	15 kVA	22 kVA	30 MVA	40 MVA	100 MVA	975 MVA
H	4.75	4.6	4.6	2.7	4.98	3.76
X	1	2	2	2	2	2
R_a	0.0315	0.0165	0.0026	0.0062	0.0035	0.0048
L_{la}	0.1366	0.0969	0.105	0.14	0.075	0.215
L_{ao}	1.4622	0.5834	0.7415	0.6167	0.812	1.222
L_{ma1}	0	0.1833	0.2455	0.1267	0	0.0433
M_{ao}	-0.6628	-0.2906	-0.334	-0.2433	-0.368	-0.5033
M_{ad}	1.3256	0.7014	0.8919	0.6067	0.74	1.05
M_{aq}	1.3256	0.3593	0.4103	0.3533	0.74	0.9633
R_f	0.0057	0.0032	0.00043	0.0005	0.00038	0.00032
L_f	1.3765	0.7367	0.9786	0.7563	0.848	1.1526
R_{kd}	0.0363	0.0276	0.0053	0.0181	0.011	0.0135
L_{kd}	1.3444	0.7367	0.9372	0.8353	0.826	1.12
M_{fkd}	1.3256	0.7014	0.8919	0.6067	0.74	1.05
R_{kq}	0.0450	0.0247	0.0041	0.0141	0.023	0.0485
L_{kq}	1.3571	0.3940	0.4357	0.5147	0.786	1.005

Appendix D

Physical Model Parameters

The parameters, in pu, of the laboratory power system model are as follows:

Synchronous Generator

$$H = 4 \quad X = 1 \quad R_a = 0.037$$
$$L_{la} = 0.075 \quad L_{a0} = 0.659 \quad L_{ma1} = 0.274$$
$$M_{a0} = -0.292 \quad M_{ad} = 0.858 \quad M_{aq} = 0.31$$
$$R_f = 0.00405 \quad L_f = 0.923$$

Transmission Line

$$R_{TL} = 0.0091 \quad L_{TL} = 0.5$$

Infinite Bus

$$E_{bus} = 1.414 \quad \omega = 377 rad/s = 1$$

Ground Resistances

$$R_{g1} = 1.5 \quad R_{g2} = 0.8$$

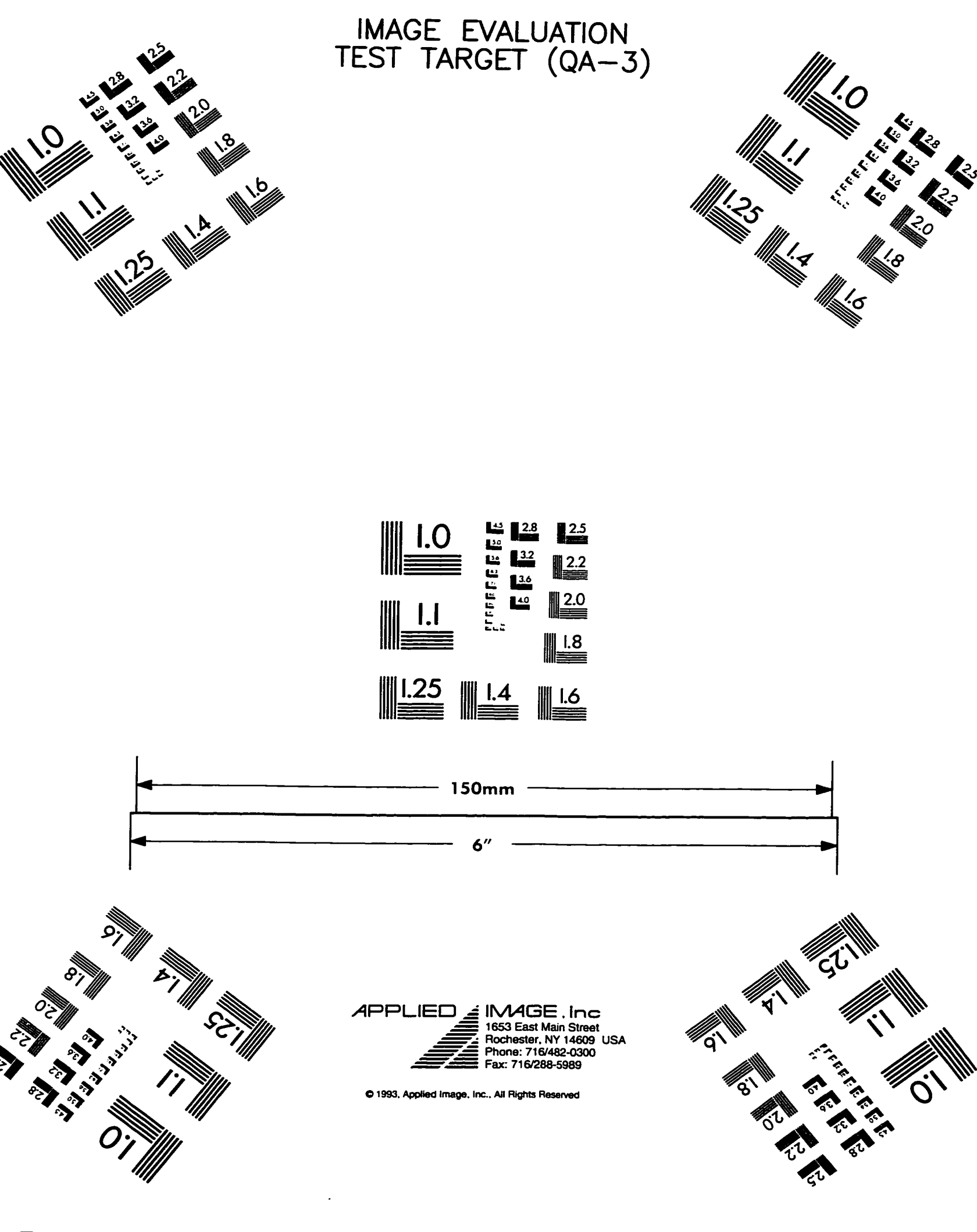
IMAGE EVALUATION
TEST TARGET (QA-3)
1.0
1.1
1.25
1.4
1.6
2.8
2.5
3.2
2.2
3.6
2.0
4.0
1.8
150mm
6"
APPLIED IMAGE, Inc
1653 East Main Street
Rochester, NY 14609 USA
Phone: 716/482-0300
Fax: 716/288-5989
© 1993, Applied Image, Inc., All Rights Reserved